Dynamic processes on networks and higher-order structures

by

Hanlin Sun

A thesis submitted to the University of London for the degree of
Doctor of Philosophy

School of Mathematical Sciences
Queen Mary, University of London
United Kingdom

May 2023

This work was supported by the Chinese Scholarship Council.

TO MY FAMILY

Statement of Originality

I, Hanlin Sun, confirm that the research included within this thesis is my own work or that where it has been carried out in collaboration with, or supported by others, that this is duly acknowledged below and my contribution indicated. Previously published material is also acknowledged below. I attest that I have exercised reasonable care to ensure that the work is original, and does not to the best of my knowledge break any UK law, infringe any third party's copyright or other Intellectual Property Right, or contain any confidential material. I accept that the College has the right to use plagiarism detection software to check the electronic version of the thesis. I confirm that this thesis has not been previously submitted for the award of a degree by this or any other university. The copyright of this thesis rests with the author and no quotation from it or information derived from it may be published without the prior written consent of the author.

Signature: Hanlin Sun

Date: 24th May 2023

Details of collaboration and publications:

[1] Sun, H., Ziff, R. M. & Bianconi, G. Renormalization group theory of percolation on pseudofractal simplicial and cell complexes. *Physical Review E* **102**, 012308 (2020).

[2] Sun, H. & Bianconi, G. Higher-order percolation processes on multiplex hypergraphs. *Physical Review E* **104**, 034306 (2021).

[3] Sun, H., Saad, D. & Lokhov, A. Y. Competition, collaboration, and optimization in multiple interacting spreading processes. *Physical Review X* **11**, 011048 (2021).

[4] St-Onge, G., Sun, H., Allard, A., Hébert-Dufresne, L. & Bianconi, G. Universal nonlinear infection kernel from heterogeneous exposure on higher-order networks.

Physical Review Letters **127**, 158301 (2021).

[5] Bianconi, G., Sun, H., Rapisardi G. & Arenas A. Message-passing approach to epidemic tracing and mitigation with apps. *Physical Review Research* **3**, L012014 (2021).

[6] Sun, H., Kryven, I. & Bianconi, G. Critical time-dependent branching process modelling epidemic spreading with containment measures. *Journal of Physics A: Mathematical and Theoretical* **55**, 224006 (2022).

[7] Sun, H., Radicchi, F. , Kurths, J. & Bianconi, G. The dynamic nature of percolation on networks with triadic interactions. *Nature Communications* **14**, 1308 (2023).

Abstract

Higher-order interactions are increasingly recognized as a critical aspect in the modeling of complex systems. Higher-order networks provide a framework for studying the relationship between the structure of higher-order interactions and the function of the complex system. However, little is known about how higher-order interactions affect dynamic processes. In this thesis, we develop general frameworks of percolation aiming at understanding the interplay between higher-order network structures and the critical properties of dynamics. We reveal that degree correlations strongly affect the percolation threshold on higher-order networks and interestingly, the effect of correlations is different on ordinary percolation and higher-order percolation. We further elucidate the mechanisms responsible for the emergence of discontinuous transitions on higher-order networks. Moreover, we show that triadic regulatory interaction, as a general type of higher-order interaction found widely in nature, can turn percolation into a fully-fledged dynamic process that exhibits period doubling and a route to chaos. As an important example of dynamic processes, we further investigate the role of network topology on epidemic spreading. We show that higher-order interactions can induce a non-linear infection kernel in a pandemic, which results in a discontinuous phase transition, hysteresis, and superexponential spreading. Finally, we propose an epidemic model to evaluate the role of automated contact-and-tracing with mobile apps as a new containment measure to mitigate a pandemic. We reveal the non-linear effect on the reduction of the incidence provided by a certain fraction of app adoption in the population and we propose the optimal strategy to mitigate the pandemic with limited resources.

Altogether, the thesis provides new insights into the interplay between the topology of higher-order networks and their dynamics. The results obtained may shed light on the research in other areas of interest such as brain functions and epidemic spreading.

Acknowledgments

It is still hard for me to believe I am now almost finishing my PhD. I can still clearly recall the first day of my arrival in London and it was like yesterday. Tracing back on these four years, I am grateful to many people. Without them, my PhD life will not be the same.

First of all, I would like to thank my supervisor Prof. Ginestra Bianconi for her immense guidance in my PhD projects, but also for her enduring patience, constant support, and motivating encouragement along this way. For me, Prof. Bianconi is a model scientist with outstanding physics intuition, extraordinary technical skills, and fruitful academic contributions. Her enthusiasm for research deeply motivates me to step on the way into academia. Moreover, I am grateful to Prof. David Saad who gave me advice not only in our collaboration project but also constant care and support during my entire PhD.

I am very fortunate to have had the chance to collaborate with many extraordinary scientists, in addition to those mentioned above– Prof. Alex Arenas, Prof. Antoine Allard, Prof. Laurent Hébert-Dufresne, Prof. Jürgen Kurths, Prof. Ivan Kryven, Prof. Andrey Lokhov, Dr. Giacomo Rapisardi, Prof. Filippo Radicchi, Dr. Guillaume St-Onge and Prof. Robert Ziff. They have contributed in relative ways to this thesis and my other research projects, as well as my personal growth as a researcher. I would also like to thank Prof. Mauricio Barahona and Dr. Omer Bobrowski for agreeing to be my examiners and for their valuable time devoted to reading my thesis.

Furthermore, I would like to thank Annalisa, Gabriele, and Silvia for being the best teammates in organizing the *NetPLACE* seminars. With their passions and ideas, the seminar shapes magically from scratch and still thriving today.

My PhD journey might be a totally different story without the support and companion-

ship of my friends and colleagues from Queen Mary. Specifically, I am deeply thankful to Danilo, Elisa, Evelyn, Gabriele, Lorenzo, Marica, and Tim. The joy they have brought to me supports me through the toughest times. Without them, London might still be an attractive city to me, but I will not call it "home".

I would also like to thank my old friends Jiayu, Lingrui, and Xiaohan. Though thousands of miles apart, they are still the first ones I turn to when I have a tough day. A huge thank you to you all for supporting and motivating me along the path in your way.

In particular, special thanks have to be given to my most trustworthy friend and science pal Zhuan for his support and wise advice. Although I am not sure whether our constant discussions on peculiar science-related problems have contributed to my research, the joy I have gained from these chats is invaluable. Besides, I would also like to thank him for reading my thesis and giving helpful suggestions.

Finally, I want to dedicate this thesis to my family. I will not be here writing this thesis without their unwavering love, unconditional support, and almost blind trust in my decisions.

Table of Contents

Chapter 1

Introduction

Generalized network structures including multilayer networks and higher-order networks are increasingly recognized as the new paradigm for modeling dynamic processes on interacting systems. These generalized network structures allow to distinguish between interactions of different natures and connotations and also allow to capture the higher-order interactions involving two or more elements of a complex system.

Recent research on multilayer and higher-order interactions is dramatically changing and enriching our understanding of the interplay between structures and dynamics of networks. It is well known that network topology strongly affects the dynamics of the network, yet many fundamental questions concerning the role of higher-order interactions are awaiting answers. For instance, while degree correlations on multiplex networks have been shown to play an important role in network robustness, little is known about the effects of correlation on higher-order networks. Ref. [1] studies social contagion processes on hypergraphs and reveals that positive hyperdegree correlations suppress explosive transitions. However, the discussion is restricted to hypergraphs exclusively formed by links and triangles, and the effects of degree correlation on general hypergraphs are still unknown.

Recently, extensive literature has reported the novel dynamic properties of networks

where higher-order interactions are present. For example, the higher-order Kuromoto model defined on simplicial complexes can display an explosive synchronization transition [2]. On spreading processes such as epidemic spreading and social contagion defined on simplicial complexes [3, 4] and hypergraphs [1, 5, 6], phase transitions can become discontinuous. Despite these observations of rich phenomenology of dynamics on higher-order networks, a theoretical understanding of the underlying mechanism that accounts for these phenomena is still a challenge.

In this thesis, we investigate the interplay between structure and the dynamics of generalized network structures. We establish theoretical frameworks of percolation to study dynamic properties and critical phenomena on generalized network structures.

Percolation is a fundamental critical phenomenon defined on networks that predicts the fraction of nodes in the giant component when nodes or links in the network are randomly removed. Indeed, having an extensive number of nodes in the giant component is the minimum requirement for dynamic processes such as epidemic spreading, social contagion, and diffusion to take place on the network. Therefore, percolation does not only reveal the robustness of a network, but it is also fundamental for the study of a large variety of other dynamic processes.

Epidemic spreading, as an important dynamic process on networks, has been shown to be mappable to the link percolation problem on the same network [7, 8]. Thus, the percolation theory can be used to determine the epidemic threshold on a given network topology. The study of real pandemics greatly benefits from insights provided by the percolation theory.

Percolation has been extensively studied on pairwise networks. Mathematically, nodes or links are randomly damaged with probability $1 - p$, and the fraction of nodes in the giant component R is studied as a function of p to characterize how macroscopic connectivity of the network is affected by the increasing entity of random damage. At the percolation threshold $p = p_c$, the giant component vanishes, indicating the dysfunc-

tioning of the network. It is well known that the topology of networks strongly affects the critical threshold in the infinite network size limit [9, 10]. For instance, on scale-free networks, the critical threshold vanishes, *i.e.*, $p_c = 0$, indicating that scale-free networks are robust to random damages. The recent developments of percolation on multilayer networks provide exciting new insights into the interplay between the dynamic and topology of networks. The percolation threshold on multilayer networks is strongly affected by the structure of interlayer dependency [11–13], degree correlation [14, 15], and link overlap [16, 17].

Apart from multilayer networks, another important generalization of networks is higher-order networks. Refs. [18–22] study percolation on hyperbolic simplicial complexes using the real-space renormalization group theory and the percolation threshold is obtained analytically. Novel critical phenomena such as discontinuous phase transition for simple link percolation [18] and unusual critical scaling [22] are observed. For percolation on random higher-order networks that do not display a hyperbolic network geometry, fewer results are known and the higher-order network structure being explored is very restricted [23, 24].

Other dynamical processes such as diffusion have also been investigated on multilayer networks [25, 26] and higher-order networks [27–29]. Ref. [25] shows that the 2-layer multiplex network structure speeds up the diffusion on the less diffusive layers and under specific conditions, super-diffusion can emerge. Ref. [26] generalizes the analysis of the spectrum of graph Laplacian on multiplex networks with an arbitrary number of layers. On higher-order networks, on the other hand, the graph Laplacian that determines the properties of diffusion processes is generalized to Hodge Laplacian on simplicial complexes [28]. Spectrum properties of generalized higher-order Laplacian are studied on a framework called *Network Geometry with Flavor* [27]. It is shown that higher-order up and down Laplacian can have a finite spectrum dimension that strongly affects the return-time probability of the diffusion process [29].

Besides, in a large variety of complex systems, such as brain networks and climate

networks, the functional connectivity in the network changes over time. Ordinary percolation is unsuitable to describe such systems. Typically, indeed some cascading processes are associated with percolation. For instance, for interdependent percolation on multilayer networks, the damage propagates back and forth among the layers reaching a steady state at the end of the cascading process [11], resulting in the network connectivity changes over time. An important open question is whether percolation can capture even more general time-dependent variations in the connectivity of a network.

In this thesis, we fill the gaps discussed above by providing general frameworks for understanding percolation and epidemic spreading on networks and their generalization. In order to generalize the percolation on systems with time-dependent connectivity, we focus on a general type of higher-order interaction named triadic interactions which occur when a node regulates the interaction between two other nodes. By introducing signed triadic interaction, we define triadic percolation. We show that triadic percolation is a fully-fledged dynamic process that the order parameter exhibits period doubling and a route to chaos. Triadic percolation is dramatically different from ordinary percolation on networks. Percolation on pairwise networks displays a second-order continuous phase transition while the phase diagram of triadic percolation is much richer and becomes an orbit diagram. The results obtained radically change our understanding of percolation and shed light on the study of real systems such as brain networks and climate networks.

To study the effects and degree correlation on higher-order networks and investigate the mechanism behind the discontinuous phase transition, we propose a novel hypergraph model called *Multiplex Random Hypergraph* that distinguishes hyperedges of different cardinality in different layers. As such we can define generalized hyperdegrees that represent the number of hyperedges of different cardinality that incidents to a node and the multiplex hypergraph is characterized by correlations between generalized hyperdegrees. Moreover, the multiplex hypergraph model allows for defining and exploring simple and higher-order percolation processes. We show that these percolation processes display rich phenomenology including discontinuous hybrid transitions and multiple percolation

transitions. These results elucidate the mechanisms responsible for the emergence of discontinuous transition.

We further investigate the interplay between network structure and dynamics by studying examples of epidemic models. We propose an epidemic model on hypergraphs where hyperedges account for the effect of higher-order interactions in epidemic spreading due to the colocation of individuals in different environments. We find that the higher-order interactions together with heterogeneous participation time in different environments induce non-linear infection kernels, which lead to discontinuous phase transition, hysteresis, and superexponential spreading.

Finally, motivated by the recent COVID-19 pandemic, we propose a theoretical framework based on link percolation to study the role of automated contact-and-tracing with mobile apps in mitigating a pandemic. On uncorrelated networks, we derive the epidemic threshold analytically as a function of the distribution of the tracing app in the population. We show that in general the more the app is diffused among the population, the higher is the value of the epidemic threshold, meaning that the endemic state is more likely to be achieved. Moreover, we propose the optimal strategy to mitigate the pandemic when the app coverage in the population is limited by the resources available. These results provide important quantitative insights into the level of adoption needed for contact-tracing apps to be effective in mitigating an epidemic.

The thesis is structured as follows. In Chapter 2, a general introduction to networks and their generalization, including multilayer networks and higher-order networks, as well as critical phenomena studied on these structures is provided. This chapter also provides technical preparations for the following chapters including the percolation theory and message-passing approaches. In Chapter 3, the percolation theory on Networks with Triadic Interactions is discussed. We provide a general theory for triadic percolation which accurately predicts the full phase diagram on random graphs as confirmed by extensive numerical simulations. We find that triadic percolation on real network topologies reveals a similar phenomenology. In Chapter 4, we focus on the percolation

theory on the multiplex random hypergraph model and we explore higher-order percolation processes and the effects of correlation within this framework. Chapter 5 is devoted to a mean-field theory of the SIS-type epidemic model on hypergraphs. In Chapter 6, we discuss the epidemic spreading model on a contact network with mobile apps for contact-and-tracing, and we provide an optimal strategy to distribute the mobile apps. Finally, in Chapter 7 we reflect on the thesis and discuss some future perspectives.

Chapter 2

Networks and Dynamics

2.1 Networks and their generalizations

In the last three decades, Network Science has blossomed and become the new paradigm for the study of complex systems. This interdisciplinary research area has greatly benefited from tools and theories in mathematics, physics, and computer science. In return, Network Science has influenced numerous fields such as quantum physics [30, 31], ecology [32–35], biology [36–39], climate science [40, 41], brain study [42–44], sociology [45], and epidemiology [8, 46]. Indeed, pairwise interactions in a complex system can be mathematically described by as a network $G(V, E)$ formed by a set of nodes V representing elements of the system and a set E representing the interactions among them. The network can be constructed from real data that one wants to investigate, or it can also be modeled using statistical mechanics approaches. The network approach to study complex systems provides a powerful tool for understanding not only its underlying structure but also its dynamics, such as epidemic spreading [8], synchronization [47], and diffusion [48].

Nevertheless, networks have intrinsic limitations. Indeed, real systems are rarely formed exclusively by single networks with links of equivalent meaning [49]. For in-

stance, in social networks, the links representing human interactions within a group can be distinguished depending on the several different social ties that they represent such as friends, relatives, colleagues *etc*. Similarly, in transport networks, the nodes might represent cities and links can be categorized as different means of transport (trains, cars, planes, *etc*) between them. The need to distinguish between links of different types has prompted scientists to define and study *multilayer* networks. A multilayer network is formed by aggregating several interacting networks. Multilayer network formalism has been introduced in social science for more than 30 years [50] but has been extensively studied only very recently. Mathematically, a multilayer network $\mathcal{M}$ is formed by a set of layers $Y = \{\alpha | \alpha \in \{1, 2, \cdots, M\}\}$, a set of networks in each layer $\mathbf{G} = (G_1, G_2, \cdots, G_M)$, as well as the interlayer interactions $\mathcal{G}$ characterized by *interlayer links* $E_{\alpha,\beta}$ between two node sets V_α and V_β. There are several most commonly studied multilayer network models, depending on the characters one would like to include, such as multiplex networks [11], multi-slice networks [51, 52], and networks of networks [53–55]. Multiplex networks are multilayer networks that deserve special attention. In multiplex networks, there is a one-to-one correspondence between nodes (called *replica nodes*) in different layers, and interlinks exist exclusively between replica nodes. A typical example of a multiplex network is a transport network: replica nodes are cities while links in different layers represent different means of transport among these cities. The multilayer network formalism has been extensively applied in social networks [56–60], complex infrastructures [61–63], economic and financial networks [64, 65], molecular networks [66], brain networks [67], ecological networks [68–71], climate networks [72, 73], *etc*.

Another class of generalized networks that are gaining increasing attention recently is higher-order networks. In many complex systems in nature, such as biological, neural, ecological, and social systems, the elements of a complex system are interacting in *groups* and cannot simply be decomposed into a collection of pairwise interactions [74]. For instance, in a scientific collaboration network, one wants to distinguish between the scenarios in which three scientists coauthor a paper and the one in which each pair of

the same three authors is coauthoring a paper. Empirical results in real systems such as neural networks have shown that higher-order interactions have both topological and statistical effects [75], while theoretical advances has revealed that higher-order interactions strongly affect critical phenomena such as percolation [19, 21, 76, 77], epidemic spreading [78, 79], synchronization [2, 80–82], and social processes [1, 3, 5].

Higher-order interactions are commonly studied using either simplicial complexes or hypergraphs. Both structures are formed by a set of nodes $v \in \{1, 2, \cdots, N\}$ and a set of higher-order interactions where each higher-order interaction α involves two or more nodes, *i.e.*, $\alpha = [v_1, v_2, \cdots, v_n]$ [83]. In hypergraphs, the higher-order interactions are encoded in *hyperedges*. The number of nodes that incident to one hyperedge is called the *cardinality* of this hyperedge. While in simplicial complexes, the interactions are represented by *simplices*. The number of nodes involved in a many-body interaction is characterized by the *dimension* of a simplex. A $d-$dimensional simplex contains $d+1$ nodes and hence represents a $(d+1)$-body interaction. The difference between hypergraphs and simplicial complexes is that, in simplicial complexes, if a simplex $\alpha = [v_1, v_2, \cdots, v_n]$ is included, all of its faces, *i.e.*, nonvoid proper subsets of α of also need to be included, while in hypergraphs this restriction does not hold. Although simplicial complexes are more constrained, they are convenient to apply the powerful tools of topology to investigate higher-order network structures [84]. Interestingly, by considering weighted simplicial complexes [85], the dichotomy between simplicial complexes and hypergraphs can be addressed as weighted simplicial complexes are a more flexible and therefore more powerful representation of higher-order networks. In practice, the choice of either hypergraphs or simplicial complexes in modeling higher-order interactions is usually motivated by technical convenience yet a recent study shows this choice may affect the higher-order dynamics [86]. In addition to hypergraphs and simplicial complexes, higher-order networks include also *Networks with Triadic Interactions*. In Ref. [87], we propose these networks to study the effect of signed triadic regulations, which can be found generally in real complex systems, such as brain networks and ecological networks. This model

will be discussed in Chapter 3.

The study of higher-order networks is still in its infancy, and the investigation of higher-order interactions will shed light on numerous areas of interest such as brain study, climate science, ecology, *etc*

It is well known that the network structure strongly affects the dynamic processes that take place on the network. For instance, on scale-free networks, the percolation threshold vanishes [9], indicating that if an infectious disease spreads on this network, it will always develop into a pandemic in which a finite fraction of the population is infected; on the interdependent multiplex network that can be a good candidate of modeling transportation networks and power grid networks, the damage of nodes can cause a cascading failure which leads to a discontinuous percolation transition at criticality [11], indicating that multiplex networks are more fragile than single networks and the failure can be more abrupt and less predictable; higher-order interactions can lead to abrupt outbreaks, bistable regimes, and hysteresis in an epidemic spreading process [3, 78]. In this thesis, we will focus on investigating the interplay between network topologies and their dynamic properties. In particular, we will study the percolation theory and epidemic spreading models on networks and their generalizations.

2.2 Critical phenomena on networks

Percolation is one of the most important and most studied critical phenomena defined on networks [9, 10, 88–90]. Percolation quantifies the network robustness, *i.e.*, how the random removal of nodes or links affects the macroscopic connectivity of the network. It is widely accepted that the macroscopic connectivity of a network is a prerequisite for dynamic processes taking place on the network, such as epidemic spreading, diffusion, social process, and so on. Thus, the percolation is widely used to evaluate the robustness of networks when nodes or links are randomly damaged [10, 91]. Moreover, percolation is closely related to epidemic spreading. We will discuss their relationship and differences

later in this section.

It is convenient for the following discussion to briefly introduce the percolation theory first. The macroscopic connectivity, which is a minimum requirement for the functioning of a network, is characterized by an extensive number of nodes in the *giant component*. Mathematically, a giant component is characterized by a non-zero fraction largest connected component in the network, at the infinite network limit. The relative size of the giant component is thus defined as

$$R = \lim_{N \to \infty} \frac{N_L}{N} \tag{2.1}$$

where N_L is the number of nodes in the largest connected component and N is the total number of nodes in the network. The percolation theory studies the relationship between the fraction of nodes in the giant component R, namely the *order parameter*, and the probability p that a node or a link is retained (or the probability $1 - p$ that a node or a link is damaged), namely the *control parameter* accounting for the random removal of nodes or links. In the infinite network limit, a phase transition is observed. The transition is characterized by a critical value of p, denoted as p_c, such that for $p < p_c$, the order parameter $R = 0$ and $p > p_c$, $R > 0$. The critical value p_c is called the *critical threshold* and it separates the percolation process into the percolating phase ($p > p_c$) and non-percolating phase ($p < p_c$). Thus, the value of the critical threshold is an important indicator of the robustness of a network under random damage: a network with a smaller critical threshold p_c is more robust, as the network is still relatively well-connected under a serious random attack.

The percolation transition is well captured by the statistical mechanic theory of critical phenomena. This includes the critical behaviors characterized by the critical exponents and the onset of a macroscopically ordered phase [46]. For Network Science applications, the critical threshold p_c is one of the key objects of study. Fortunately, percolation problems have been studied for decades by statistical physicists. The initial

investigation mainly focused on percolation on regular lattices [92–94] and important results had been obtained both analytically and numerically [95, 96]. It is rigorously proven that the percolation on $d-$dimensional hypercubes with $d \geq 2$ displays a phase transition at a critical p_c characterized by an infinite connected component [97]. Ref. [98, 99] further shows that in the subcritical regime $p < p_c$, the typical size of the largest connected components scales with $\log N$ where N is the size of the lattice system. While in the supercritical regime $p > p_c$, the infinite connected component is unique on a large variety of lattices [100, 101].

In the last two decades, percolation theory on complex networks has attracted great attention. The locally tree-like structure of sparse random networks allows for studying the critical properties from another approach. The critical threshold of random networks with a given degree distribution was given for the first time in Ref. [102] and the behavior of the system near the critical threshold was further characterized in Ref. [103]. Moreover, the critical properties are found to be strongly affected by the topological structures. For instance, the critical threshold vanishes on scale-free networks, where the second moment of the degree distribution diverges [9]. In the meantime, a formal connection between percolation and network robustness was established, from both experimental and theoretical perspectives [10, 91]. Until today, the percolation theory has been extensively developed beyond random networks. For instance, percolation on directed networks [104] and spatial networks [105, 106]; the effect of network geometries on percolation [18, 21, 22, 77]; the effect of degree correlation on percolation threshold [14, 107–109]; percolation on other generalized network structures such as multilayer networks [11, 49, 110, 111], hypergraphs [23, 76], simplicial complexes [19, 22, 77], *etc.* New percolation rules have also been proposed, for instance, k-core percolation [112–114], explosive percolation [115–118], weak percolation [119] and homological percolation [120, 121], *etc*, and new critical phenomena have been reported such as discontinuous phase transitions [112], multiple phase transitions [20, 76], tricritical points [12, 122, 123], unusual critical exponents [22, 116].

In the following sections, we will focus on the percolation theory on networks and their generalization, including multilayer networks and higher-order networks. we will illustrate in detail how critical behaviors of percolation transition are affected by the topological structures of the networks.

2.2.1 Percolation on networks

Percolation has been well-studied on random pairwise networks. In Ref. [102], the authors first gave the criterion for a giant component emerging in a random network with a given degree distribution. Here we can use an equivalent approach to obtain the critical threshold on an uncorrelated random network, as an introduction for the discussions in the following chapters.

Consider an uncorrelated random network with degree distribution $P(k)$ and let us consider the node percolation, *i.e.*, all the nodes are retained with probability p. Here we note that the link percolation has the same critical threshold [49]. Let us define S as the probability that following a random link in the network, one can find a node in the giant component. First, by following a random link, one can find a node that has degree k and is undamaged with probability $pkP(k)/\langle k\rangle$, where $\langle k\rangle$ denotes the average degree of nodes. This is because the network is uncorrelated, the probability of finding a node with degree k following a random link is independent of the degree of the node on the other end of the link and is proportional to k. If this node with degree k is in the giant component, it indicates that at least one of its other $k-1$ neighbors is in the giant component. Thus, with the tree-like approximation which is true on sparse random networks [124], the probability S satisfies the following self-consistent equation at the infinite network size limit:

$$S = p\sum_{k}\frac{kP(k)}{\langle k\rangle}\left[1-(1-S)^{k-1}\right]. \tag{2.2}$$

Similarly, if a node with degree k is in the giant component, it indicates that at least one of its k neighbors is in the giant component. Thus the order parameter R that the

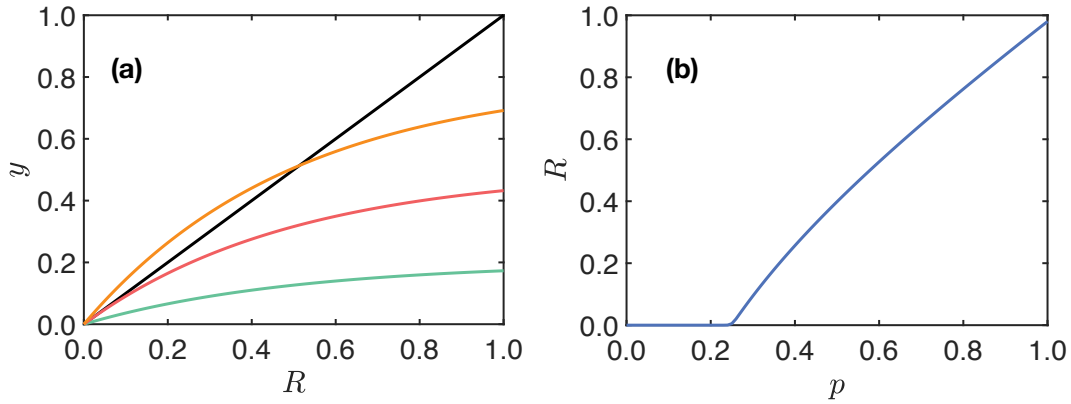

Figure 2.1: Demonstration of the percolation transition on networks. In panel (a), the black line refers to the left-hand side of Eq. 2.2 $y = S$ and the orange, red, and green lines refer to the right-hand side with different values of p. At a lower p, Eq. 2.2 only has a trivial solution $S = 0$ (the green line), while at a higher p, a non-trivial solution emerges (the orange line). At the critical p value, two lines should be tangent at $S = 0$ (the red line). The non-trivial solution emerges continuously from $S = 0$ hence the transition is continuous. In panel (b), the corresponding phase diagram is shown.

fraction of nodes in the giant component, or equivalently, the probability that a random node is in the giant component can be obtained by

$$R = p \sum_k P(k) \left[1 - (1 - S)^k\right]. \tag{2.3}$$

Observing Eq. 2.2 and Eq. 2.3, one will notice that $S = 0$ and thus $R = 0$ are trivial solutions. The critical threshold p_c indicates a point where a non-trivial solution of R (equivalently a non-trivial solution of S) emerges. The critical condition for such a non-trivial solution emerging is (see Figure 2.1)

$$\left.\frac{\mathrm{d}S}{\mathrm{d}S}\right|_{S=0} = \left.\frac{\mathrm{d}}{\mathrm{d}S} p_c \sum_k \frac{kP(k)}{\langle k \rangle} \left[1 - (1 - S)^{k-1}\right]\right|_{S=0} \tag{2.4}$$

Thus, the critical threshold p_c satisfies [9, 10]

$$p_c = \frac{\langle k \rangle}{\langle k(k-1) \rangle} = \frac{\langle k \rangle}{\langle k^2 \rangle - \langle k \rangle}. \tag{2.5}$$

If we let $p_c = 1$, indicating the nodes are not damaged, we obtained the structural requirement for the emergence of a giant component in an uncorrelated random network, *i.e.*, the Molley-Reed criterion [102]

$$\frac{\langle k^2 \rangle}{\langle k \rangle} = 2. \tag{2.6}$$

From Eq. 2.5, we see the critical threshold of a random uncorrelated network is dominated by the first and second moment of the degree distribution $P(k)$. For an Erdös-Rényi network $G(N, c/N)$, the degree distribution is given, in the infinite network limit $N \to \infty$, by a Poisson distribution $P(k) = \frac{c^k e^{-c}}{k!}$ with an average c, thus

$$\langle k \rangle = c, \quad \langle k^2 \rangle = c + c^2. \tag{2.7}$$

The critical threshold is hence

$$p_c = \frac{1}{c}. \tag{2.8}$$

On the other hand, for a scale-free network with a power-law degree distribution

$$P(k) = \frac{1}{\zeta(\beta)} k^{-\beta}, \quad 2 < \beta < 3, \tag{2.9}$$

the second moment $\langle k^2 \rangle$ diverges. Thus we recover the well-known result of the robustness of scale-free networks [9, 10]

$$p_c = 0. \tag{2.10}$$

Moreover, to characterize the nature of the phase transition, it is useful to investigate

the behavior of the order parameter R at criticality. In statistical physics, this behavior is characterized by the critical exponent β. *i.e.*,

$$R \sim (p - p_c)^{\beta}, \quad \text{for} \quad p - p_c \ll 1. \tag{2.11}$$

Let us first derive here the critical exponent β of the percolation transition on a random Poisson network with average degree c. For convenience let us rewrite Eq. 2.2 and Eq. 2.3 here as

$$\begin{aligned} S &= p\,(1 - G_1(1 - S)) \equiv h(S) \\ R &= p\,(1 - G_0(1 - S)) \end{aligned} \tag{2.12}$$

where $G_0(x)$ and $G_1(x)$ are generating functions defined as

$$\begin{aligned} G_0(x) &= \sum_k P(k) x^k, \\ G_1(x) &= \sum_k \frac{kP(k)}{\langle k \rangle} x^{k-1} \end{aligned} \tag{2.13}$$

It is known that for Poisson distribution, $G_0(1-S) = G_1(1-S) = e^{-cS}$. Thus, Eq. 2.12 is reduced to

$$R = p\left(1 - e^{-cR}\right) \tag{2.14}$$

In the vicinity of critical threshold, $p \simeq p_c$ and $R \ll 1$ thus we can expand the right-hand side of Eq. 2.14 as

$$R = pcR - p\frac{c^2R^2}{2} + o(R^3) = \frac{p}{p_c}R - \frac{p}{p_c}\frac{cR^2}{2} + o(R^3) \tag{2.15}$$

By truncating the expansion at the second order, we obtain

$$R = \frac{2}{c}\frac{p - p_c}{p} \propto (p - p_c)^{\beta} \tag{2.16}$$

where

$$\beta = 1. \tag{2.17}$$

It can be shown that as long as the first, second, and third moments of the degree distribution are converging, the critical threshold $\beta = 1$ is universal [49]. This critical exponent also confirms that the percolation transition on random networks is a continuous phase transition.

2.2.2 Percolation on generalized network structures

As generalized network structures such as multilayer networks, hypergraphs, and simplicial complexes have been introduced to capture the interactions beyond pairwise, the percolation theory has also been developed to study critical phenomena defined on these structures. In Ref. [11], Buldyrev *et al.* first defined interdependent percolation on multiplex networks. This generalization of percolation theory provides a fundamental tool for analyzing the robustness of an interdependent multiplex network and deeply enriches our understanding of the response of interdependent systems to random damage.

The robustness of an interdependent multiplex network is characterized by the relative size of *Mutually Connected Giant Component* (MCGC). On an interdependent multiplex network, the damage of a node implies the damage of its replica nodes in all other layers. Therefore, the functional region should only contain nodes that are in the giant component in *all* layers. Thus the equations for interdependent percolation can be derived as follows. Let us denote by S_α the probability that following a random link in layer α we reach a node in MCGC. If this node is in MCGC, it should also be found in MCGC in all other layers. Thus, the self-consistent equations read

$$S_\alpha = p \sum_{k_\alpha} \frac{k_\alpha P_\alpha(k_\alpha)}{\langle k_\alpha \rangle} \left[1 - (1 - S_\alpha)^{k_\alpha - 1}\right] \prod_{\beta \neq \alpha} \sum_{k_\beta} P_\beta(k_\beta) \left[1 - (1 - S_\beta)^{k_\beta}\right] \tag{2.18}$$

where $P_\alpha(k_\alpha)$ indicates the degree distribution in layer α (for simplicity we limit the

discussion to multiplex networks in which there is no correlation between degrees of a node in different layers) and p denotes the probability of retaining a node. The order parameter R that denotes here the fraction of nodes in the MCGC satisfies

$$R = p \prod_{\alpha} \sum_{k_\alpha} P_\alpha(k_\alpha) \left[1 - (1 - S_\alpha)^{k_\alpha} \right] \tag{2.19}$$

If all layers have Poisson degree distribution with the same average degree c, the self-consistent equations are greatly simplified as

$$S_\alpha = S = R = p \left(1 - e^{-cR} \right)^M \tag{2.20}$$

where M is the number of layers in the multiplex network.

The interdependent multiplex network is found to be more fragile than its single-layer counterpart with the same degree distribution. Moreover, at criticality, the percolation transition is discontinuous (see Figure 2.2), characterized by large avalanches of node failures that propagate back and forth across different layers of the network [11, 49]. Interestingly, in a multiplex network formed by Poissonian layers with the same average, the phase transition is found to be hybrid [88, 108, 125, 126], *i.e.*, near criticality,

$$R \propto (p - p_c)^{1/2}. \tag{2.21}$$

Beyond the interdependent percolation, various percolation processes have been defined on general multilayer networks, such as interdependent percolation with partial dependencies [12, 122] and redundant dependencies [13]; percolation on networks of networks with replica nodes [55] and without replica nodes [53, 127]; percolation on general multilayer networks without replica nodes [54], *etc.*

In comparison, the study of percolation on higher-order networks is still in its infancy. The percolation process on higher-order networks was first investigated on hyperbolic simplicial complexes [18–22]. Thanks to the real-space renormalization group method

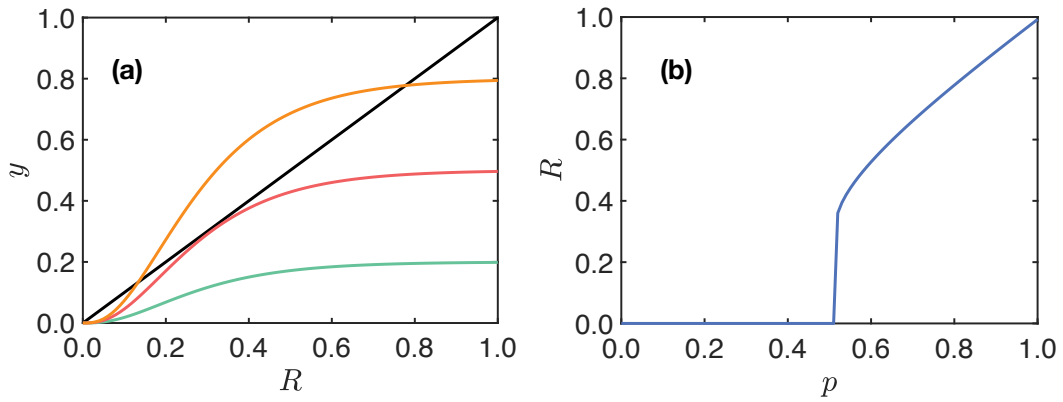

Figure 2.2: Demonstration of the percolation transition on interdependent multiplex networks. In panel (a), the black line refers to the left-hand side of Eq. 2.20 $y = S$ and the orange, red, and green lines refer to the right-hand side with different values of p. At a lower p, Eq. 2.20 only has a trivial solution $S = 0$ (the green line), while at a higher p, non-trivial solutions emerge (the orange line, only the largest one is stable). At the critical p value, two lines are tangent at a non-zero $S = S_c$ (the red line). The non-trivial solution emerges discontinuously from $S = 0$ hence the transition is discontinuous. In panel (b), the corresponding phase diagram is shown.

[128], the percolation threshold on these higher-order structures can be exactly solved. Rich critical phenomena have been observed including discontinuous phase transition for simple link percolation [18] and unusual critical exponents [22]. Moreover, homological percolation [120, 121] has been defined on simplicial complexes to characterize the emergence of topological features.

For percolation on general hypergraphs, there are fewer results [23, 24], mainly focusing on very restricted scenarios where the cardinality of hyperedges is fixed. In Ref. [76], we proposed a general framework for simple and higher-order percolation processes on hypergraphs. This framework also allows for defining degree correlations and exploring their effects on critical phenomena. This will be discussed in detail in Chapter 4.

The study of percolation processes on higher-order networks is developing rapidly. The investigation of the interplay between the structure of higher-order networks and the dynamic defined on them will deepen our understanding of higher-order interactions

and shed light on the study in related areas such as brain networks and social interactions.

2.2.3 Epidemic spreading and percolation theory

Epidemic spreading processes are one of the most studied examples of dynamic processes on networks [8, 46]. The epidemic-spreading processes studied are not limited to the transmission of infectious diseases, but also their analogs such as the spread of rumors and misinformation among social media [129], the spread of computer viruses [130], the diffusion of political opinions *etc.* One of the most important questions in the context of epidemic spreading is predicting the outbreak of a pandemic, and proposing strategies to control the pandemic accordingly. More precisely, how do the infectivity and the topology of the underlying network where the pandemic happens affect the onset and the size of a pandemic? Whether the outbreak of a pandemic is a continuous process or an abrupt event? What is the best immunization strategy to contain a pandemic? Thanks to the mapping between the epidemic model and the percolation process, the percolation theory can provide answers to these important questions.

One of the most famous and important epidemic-spreading models is the susceptible-infected-recovered (SIR) model [131]. In the model, three different states of individuals in the population are considered: Susceptible (S), Infected (I), and Recovered (R). A susceptible individual can be infected at a given rate by contacting infected individuals, and an infected individual will recover at a constant rate. A recovered individual will not be infected anymore in the subsequent spreading process. This process can be written as follows:

$$S + I \xrightarrow{\beta} I + I \quad \text{and} \quad I \xrightarrow{\mu} R \tag{2.22}$$

where β and μ are the rates of infection and recovery, respectively.

The SIR model on a homogeneously mixed population has been very well-understood. In a well-mixed population, every individual in the population is considered to be able

to contact all other individuals. Under these assumptions, the epidemic will grow exponentially if the spreading rate $\lambda \equiv \beta/\mu > 1$ and die out exponentially if $\lambda < 1$.

The SIR model has also been extensively studied on networks as human contact is usually heterogeneous. Consider a network $G = (V, E)$ formed by $|V| = N$ individuals and contacts among them, denoted in the set E. The infection can only happen between neighbors on the network, *i.e.*,

$$S_i + I_j \xrightarrow{\beta} I_i + I_j, \quad \text{if} \ \ (i,j) \in E. \tag{2.23}$$

while the recovery process is not affected:

$$I_i \xrightarrow{\mu} R_i. \tag{2.24}$$

Let us show the SIR model on a network can be mapped to a link percolation problem on the same network [7].

Considering a continuous SIR model with a constant spread rate β and a constant recover rate μ, *i.e.*, in a short time interval δt, an infected individual will infect his/her neighbor with probability $\beta\delta t$ and recover with probability $\mu\delta t$. First, let us determine the distribution of the infectious period. The cumulative distribution $\tilde{P}(\tau' < \tau)$ that the infectious period is shorter than τ is given by

$$\tilde{P}(\tau' < \tau) = 1 - \lim_{\delta \to 0} (1 - \mu\delta t)^{\tau/\delta t} = 1 - e^{-\mu\tau} \tag{2.25}$$

Therefore the distribution of the infectious period is given by an exponential distribution

$$\tilde{P}(\tau) = \frac{\mathrm{d}\tilde{P}(\tau' < \tau))}{\mathrm{d}\tau} = \mu e^{-\mu\tau}. \tag{2.26}$$

Similarly, an infected individual can infect his/her neighbor with the probability

$$\tilde{T}(\tau' < \tau) = 1 - \lim_{\delta \to 0} (1 - \beta \delta t)^{\tau/\delta t} = 1 - e^{-\beta \tau} \tag{2.27}$$

Let us denote by S the probability that following a random link one reaches an infected node. This node has degree k with a probability $kP(k)/\langle k \rangle$ where $P(k)$ is the degree distribution of the network and $\langle k \rangle$ is the average degree. On a locally tree-like network, the infection caused by different neighbors is independent. Thus S satisfies a self-consistent equation as follows:

$$S = \sum_k \frac{kP(k)}{\langle k \rangle} \left[1 - \left(1 - S \int_0^\infty \mathrm{d}\tau \tilde{P}(\tau) \tilde{T}(\tau' < \tau) \right)^{k-1} \right]. \tag{2.28}$$

Similar to the percolation problem, the fraction of infected individuals, denoted by R, reads

$$R = \sum_k P(k) \left[1 - \left(1 - S \int_0^\infty \mathrm{d}\tau \tilde{P}(\tau) \tilde{T}(\tau' < \tau) \right)^{k} \right]. \tag{2.29}$$

Defining the *transmissibility* T as

$$T = \int_0^\infty \mathrm{d}\tau \tilde{P}(\tau) \tilde{T}(\tau' < \tau) \tag{2.30}$$

Eq. 2.28 and Eq. 2.29 reduce to the equations for link percolation where links are retained with probability T (for instance, See Ref. [88]).

Here we show that the critical threshold of the SIR model on networks can be obtained by studying link percolation on the same network. It is worth noting that the epidemic-spreading process is not equivalent to the percolation process. The percolation theory predicts the *equilibrium state* of the dynamic while in epidemic-spreading processes, time-dependent quantities such as the number of infections at a given time are usually of interest as well.

2.3 Message passing approach

We have shown in the previous sections a mean-field approach to the percolation threshold on an uncorrelated network ensemble. However, real networks are usually characterized by the degree correlations thus the critical threshold obtained by the mean-field approach will deviate from reality. To address this concern, message-passing approaches are extensively used. Message passing approaches are a class of algorithms on graphs involving probabilities defined on links, called *messages*, that follow a recursive set of equations [49]. Each equation only requires local messages to update, resulting in a kind of "distributed computation". Statistical quantities of interest are obtained by iteratively evaluating the set of message-passing equations until convergence. Rooted in *Belief Propagation* [132–134], a series of message-passing algorithms have been developed and shown wide applicability in various hard computational problems in statistical mechanics [132], as well as inference [135, 136] and optimization problems [129, 137] on networks. As for the dynamic processes on networks and their generalization, message-passing approaches have also been shown powerful on epidemic spreading problems and percolation on single networks [138–141] and multilayer networks [13, 16].

The key idea behind message-passing approaches is that if the network is a tree (or effectively locally tree-like), then when a node is removed, the network will be decomposed into several *independent* branches rooted in this node. Following this principle, in general, the message defined on a link $i \to j$, let us denote by $\sigma_{i\to j}$ here, refers to a marginal probability of interest defined on node i on a *cavity network* where node j (and all links associated with it) is removed. Thus, messages $\sigma_{i\to j}$ for all nodes i that are neighbors of j are independent. On auxiliary cavity networks, correlations between nodes are reduced, which leads to a great simplification of the calculation of marginal probabilities of interest.

Due to the principle explained above, the message-passing algorithms are exact only on trees. However, they have been shown to be robust and widely applicable on networks with loops [142–144]. In this section, we will discuss the application of message-passing

approaches to percolation problems on networks and show that it is consistent with the mean-field derivation shown in Section 2.2.1.

2.3.1 Message passing approach to percolation

The message-passing technique provides a possible approach to the critical threshold p_c when the network structure deviates from the uncorrelated random network with a given degree distribution, as long as the network structure is explicitly known. Let us denote $\sigma_{i\to j}$ as the probability that node j is connected to the giant component via node i, or equivalently, node i is in the giant component on the cavity graph where node j is removed. Node i will be in the giant component only if at least one of its *other* neighbors except j is in the giant components. Thus $\sigma_{i\to j}$ satisfies

$$\sigma_{i\to j} = p\left[1 - \prod_{k\in N(i)\backslash j}(1-\sigma_{k\to i})\right] \tag{2.31}$$

The marginal probability σ_i that a node i is in the giant component hence reads

$$\sigma_i = p\left[1 - \prod_{k\in N(i)}(1-\sigma_{k\to i})\right]. \tag{2.32}$$

Finally, the order parameter R that the fraction of nodes in the giant component is obtained by averaging σ_i

$$R = \frac{1}{N}\sum_{i=1}^{N}\sigma_i. \tag{2.33}$$

Alternatively, this result can be derived via a general approach starting from the size distribution of the connected component [140]. Let us denote by $\pi_{i\to j}(s)$ the probability that node i is in a connected component of size s, on a cavity graph in which its neighbor node j is removed. Let us still consider the node percolation problem. Given that node i is not damaged and belongs to a component of size s, all of its neighbors $k_1, k_2, \cdots, k_m$ except node j should be found in a connected component of size s_m on a cavity graph

in which node i is removed and $s_1, s_2, \cdots, s_m$ can be related to s via

$$s = \sum_{m'} s_{m'} + 1. \tag{2.34}$$

Otherwise, if node i is damaged, it will be included in a component of size 0. Thus $\pi_{i\to j}$ satisfies

$$\pi_{i\to j}(s) = (1-p)\delta(s,0) + p \sum_{s_1,\cdots,s_m} \prod_{m'} \pi_{k_{m'}\to i}(s_{m'})\delta\left(s, \sum_{m'} s_{m'} + 1\right) \tag{2.35}$$

where $\delta(x,y)$ is the Kronecker delta. Due to the existence of the giant component, the distribution $\pi_{i\to j}(s)$ is not normalized. The probability $\sigma_{i\to j}$ that node i is in the giant component on the cavity graph in which node j is removed is given by

$$\sigma_{i\to j} = 1 - \sum_{s=1}^{\infty} \pi_{i\to j}(s). \tag{2.36}$$

The problem can be solved using the generating function method. Defining the generating function $H_{i\to j}(x)$ as

$$H_{i\to j}(x) = \sum_{s} \pi_{i\to j}(s) x^s \tag{2.37}$$

hence Eq. 2.35 can be rewritten as

$$\begin{aligned}
H_{i\to j}(x) &= 1 - p + p \sum_{s} \sum_{s_1,\cdots,s_m} \prod_{m'} \pi_{k_{m'}\to i}(s_{m'})\delta\left(\sum_{m'} s_{m'} + 1, s\right) x^s \\
&= 1 - p + p \sum_{s_1,\cdots,s_m} \prod_{m'} \pi_{k_{m'}\to i}(s_{m'}) \left[\sum_{s} \delta\left(\sum_{m'} s_{m'} + 1, s\right) x^s\right] \\
&= 1 - p + px \prod_{m'} \sum_{s_{m'}} \pi_{k_{m'}\to i}(s_{m'}) x^{s_{m'}} \\
&= 1 - p + px \prod_{m'} H_{k_{m'}\to i}(x)
\end{aligned} \tag{2.38}$$

Comparing Eq. 2.35 and Eq. 2.37 we observe

$$\sigma_{i\to j} = 1 - H_{i\to j}(1) \tag{2.39}$$

Thus we recover the self-consistent equation Eq. 2.31. On a given network, starting with a random initialization $\{\sigma_{i\to j}\}_{(i,j)\in E}$, Eq. 2.31 can be solved numerically by iterating until converges. Similar to the mean-field calculation in Section 2.2.1, the message-passing approach is also exact only on infinite trees. Nevertheless, it is known to be robust on networks with loops, as long as the iterative process converges [142].

The derivation above provides a concrete numerical approach to the order parameter. The critical threshold p_c can be obtained from Eq. 2.31 by evaluating the dominating eigenvalue of the corresponding non-backtracking matrix [140].

Observing Eq. 2.31 and Eq. 2.32, $\{\sigma_{i\to j}\}_{(i,j)\in E} = 0$ are trivial solutions. Similar to the mean-field calculation on uncorrelated network ensemble discussed in Section 2.2.1, the giant component emerges only when non-trivial solutions for $\{\sigma_{i\to j}\}_{(i,j)\in E}$ emerge. The critical condition can be found via a linear expansion. Near the critical threshold, $\sigma_{i\to j} \ll 1$, Eq. 2.31 can be linearized as

$$\sigma_{i\to j} = p \sum_{k\in N(i)\setminus j} \sigma_{k\to i}. \tag{2.40}$$

This linear equation can be written as a matrix form

$$\vec{\sigma} = p\mathbf{B}\vec{\sigma} \tag{2.41}$$

where $\mathbf{B}$ formed by entries $\mathbf{B}_{i\to j,k\to \ell} = \delta_{jk}(1-\delta_{i\ell})$ is called *non-backtracking matrix* [140, 145], where δ is the Kronecker delta. The trivial solutions are no longer stable when $p_c\Lambda = 1$, where Λ is the dominating eigenvalue of matrix $\mathbf{B}$. Thus we obtain the expression of the critical threshold.

2.3.2 Averaged message passing approach

The above message-passing algorithm provides an alternative approach to evaluate the critical threshold p_c of percolation on a given network. Here we can demonstrate the mean-field approach (Eq. 2.2 and Eq. 2.3) can be obtained from the message passing equations Eq. 2.31 and Eq. 2.32 by averaging over the uncorrelated network ensemble [146].

Let us define S as the averaged message over the uncorrelated network ensemble. A network G is chosen with probability

$$P(G) = \frac{1}{Z}\prod_{i=1}^{N}\delta\left(k_1, \sum_{j=1}^{N} A_{ij}\right). \tag{2.42}$$

where δ is the Kronecker delta and A is the adjacency matrix. The degree sequence is sampled from the distribution $P(k)$.

$$\langle\sigma_{i\to j}\rangle = S = \sum_{G} P(G)\sigma_{i\to j}. \tag{2.43}$$

Taking into account the tree-like approximation, Eq. 2.31 is rewritten as

$$\begin{aligned} S &= p\left[1 - \prod_{k\in N(i)\setminus j}(1 - \langle\sigma_{k\to i}\rangle)\right] = p\left[1 - \prod_{k\in N(i)\setminus j}(1 - S)\right] \\ &= p\left[1 - \sum_{k}\frac{kP(k)}{\langle k\rangle}(1-S)^{k-1}\right] \end{aligned} \tag{2.44}$$

Therefore, we recover the mean-field equation 2.2.

2.4 Percolation and one-dimensional maps

In this thesis, we will establish a new connection between percolation and dynamical processes, in particular the dynamics of one-dimensional maps. The one-dimensional map is an important class of dynamical systems that emerges naturally from dynamic

processes defined on discrete time steps. Mathematically, a one-dimensional map is in general defined in the form $x_{n+1} = f(x_n)$. By iteratively evaluating the function f, interesting results emerge such as periodic oscillation, *i.e.*, x oscillates among some values periodically, or chaos, indicating the map exhibit aperiodic outputs. A paradigmatic one-dimensional map is the logistic map. The logistic map is defined by a quadratic function

$$x_{n+1} = f_r(x_n) \equiv r x_n(1 - x_n). \tag{2.45}$$

As the parameter r varies, the map exhibits steady fixed points, periodic oscillation, and chaos. *Period doubling* bifurcation is also observed, meaning that at some critical values of r, the trajectory $\{x_n\}$ bifurcates and the new trajectory doubles the period of the original one. Interestingly, a large class of dynamics exhibits some universal quantitative characters that are independent of the detailed recursive function [147]. For instance, if we denote r_n as the critical value where oscillations with period 2^n emerge, the values $\{r_1, r_2, \cdots, r_n, \cdots\}$ satisfy

$$\lim_{n\to\infty} \frac{r_{n+1} - r_n}{r_n - r_{n-1}} = \delta \tag{2.46}$$

where δ is an universal quantity called *Feigenbaum constant*. If the recursive function is smooth and has a unique maximum, the constant δ depends only on the behavior of the function near its maximum [147]. For example, for functions that have a quadratic structure near the maximum such as the logistic map and triadic percolation [87], *i.e.*,

$$f(x) - f(x_{\max}) \sim |x - x_{\max}|^2, \tag{2.47}$$

the Feigenbaum constant $\delta = 4.669201609103\cdots$. This is a new mathematical constant and has been observed not only theoretically but also in experiments on real dynamic systems [148].

The relationship between percolation and the one-dimensional map will be discussed in detail in Chapter 3.

Chapter 3

The dynamic nature of percolation on networks with triadic interactions

In the previous chapters, we have shown that ordinary percolation displays a second-order continuous phase transition, while on multiplex networks and hypergraphs, generalized percolation gives rise to a variety of critical phenomena such as discontinuous hybrid transitions and tricritical points, *etc.* In this chapter, we investigate percolation on a novel higher-order network called *Network with Triadic Interactions* which includes signed triadic interactions formed by a node that regulates the interaction between two other nodes, either positively or negatively. We reveal that the triadic interactions can turn percolation into a fully-fledged dynamical process that we call here *triadic percolation*. The order parameter of triadic percolation undergoes a period-doubling and a route to chaos. We provide a general percolation theory for triadic percolation that is confirmed by extensive numerical simulations. This model provides a general framework for studying real systems in which the functional connectivity of networks changes in time dynamically and non-trivially such as brain and climate networks. The results

presented in this chapter are published in [87].

3.1 Introduction

Percolation is one of the most fundamental critical phenomena defined on networks. By predicting the size of the giant component (GC) of a network when links or nodes are randomly damaged, percolation theory can be used for the establishment of the minimal requirements that a structural network should satisfy in order to allow any type of interactive process to happen. Despite the great success of percolation, the ordinary percolation theory is unsuitable to describe real-world situations that occur in neuronal and climate networks when the connectivity of these networks changes over time.

Typically, the dynamics associated with percolation is a cascading process where an initial failure propagates over a network, possibly affecting the macroscopic connectedness. In the last decade, the generalized percolation problems that capture cascades of failure events on multilayer networks have been extensively studied in the literature [11, 13, 108, 149]. In the context of multilayer networks, the damage can propagate back and forth among the layers, reaching a steady state at the end of the cascading process [49, 110]. Besides, in duplex networks, period-two oscillations can be observed in the presence of antagonistic interactions [150] among different layers of the network. However, this phenomenon seems to be restricted to duplex networks. Furthermore, in damage and recovery models on multilayer networks aiming at getting insights into robustness for complex critical infrastructures and financial systems, more than two coexisting stable configurations of percolation have been observed [151, 152].

Despite the progress made in understanding the dynamics associated with percolation, a crucial question remains unanswered: can percolation capture more general time-dependent variations in the connectivity of a network? In this chapter, we provide a positive answer to this question and we show that a general type of higher-order interaction, namely the *triadic interaction*, can turn percolation into a fully-fledged dy-

namical process in which the order parameter undergoes period doubling and a route to chaos.

Recently, higher-order interactions have attracted much attention in the community of network science. Higher-order networks, including hypergraphs and simplicial complexes, are becoming a new paradigm to study brain activities, biochemical reaction networks, and climate networks. It has been revealed that higher-order interactions could profoundly change the critical properties of dynamical processes compared to those displayed by the same process occurring on pairwise networks. Examples include synchronization, random walk, contagion dynamics, and game theory, and novel critical behaviors have been reported including discontinuous phase transition, multiple phase transitions, tricritical points, and bistability *etc.* However, the study of percolation theory on higher-order networks is still in its infancy and little is known about the critical behaviors so far.

In this paper, we study a paradigmatic type of higher-order interaction, *i.e.*, the triadic interaction, which occurs when a node regulates the interaction between two other nodes. Regulation can be either positive or negative, representing the node facilitates or inhibits the interaction. Triadic interactions are general in interacting systems in nature, such as ecosystems, neuronal networks, climate networks, and biochemical reaction networks. In ecosystems, the competition between two species can be affected by the presence of a third species, either positively or negatively [32–34]. In neuronal networks, the interactions among neurons and glia are known to be triadic in the sense that the glia is able to modulate the synaptic interaction between neurons [153]. In climate networks of extreme rainfall events, triadic interactions can be used to explain the situations in which the links of the network are modulated by large-scale patterns, such as Rossby waves, which have a regulatory activity on climate, inducing long-range synchronization of rainfall between Europe, Central Asia, and East Asia [40]. In biochemical reaction networks, generalized triadic interactions could model the action of enzymes as biological catalysts of biochemical reactions. While triadic interactions have received great atten-

tion in ecology and neuroscience, theoretical studies of triadic interactions have been only focused on small ecological systems [32–34].

In this chapter, combining both perspectives of percolation on higher-order networks and percolation theory on networks with time-dependent connectivity, we study the role of triadic interactions in shaping macroscopic network properties. Specifically, we investigate how triadic interaction can change the critical and dynamical properties of percolation. We combine the percolation theory with the theory of dynamical systems to define triadic percolation, *i.e.*, the percolation in the presence of signed triadic interactions. We show that in triadic percolation, the size of the GC of the network is time-dependent and displays a highly non-trivial dynamic characterized by period doubling and a route to chaos. We propose a general theory to reveal that the phase diagram of triadic percolation is fundamentally different from the phase diagram of ordinary percolation: ordinary percolation displays a second-order phase transition while the phase diagram of triadic percolation is much richer and can be interpreted as an orbit diagram of the order parameter. The theory is confirmed by extensive numerical simulations on both synthetic and real-world networks. These results reveal the dynamic nature of triadic percolation and radically change our understanding of percolation.

3.2 Triadic interaction

Triadic interactions are higher-order interactions between nodes and links (see Figure 3.1). The regulator node can affect the interaction between two other nodes in a either positive or negative way, *i.e.*, the regulator can either facilitate or inhibits the interaction. Triadic interactions are a general type of interaction in nature. For instance, in ecological networks, the presence of a third species can enhance or suppress the interaction between two other species; in neural networks, glia can favor or inhibit the synaptic interactions between two neurons. The triadic interactions can be added not only on simple structural networks but also on multilayer networks or hypergraphs. For instance, biochemical reactions in cells can be modeled with hypergraphs, as chemical reactions always involve

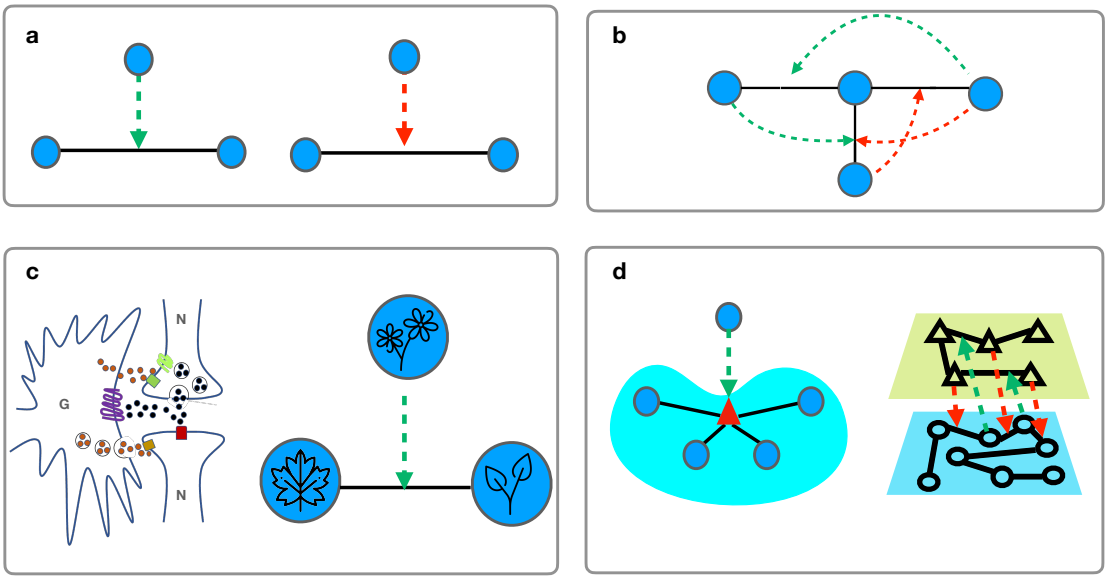

Figure 3.1: Triadic interactions. Triadic interactions occur when a node regulates the interactions between two other nodes. Triadic interactions can be signed with one node either favoring (green dashed link) or inhibiting (red dashed link) the interactions between the other two nodes (panel a). The simplest network including triadic interactions (panel b) is formed by a structural network between nodes and (solid line) structural links and a regulatory network including the regulatory interactions (dashed lines) between nodes and structural links. Examples of triadic interactions (panel c) include glia/neuron interactions and interactions between species in ecosystems. Triadic interactions can be extended to hypergraphs and multiplex networks (panel d). In hypergraphs the triadic interactions can regulate the presence or the activity of a hyper-edge, in multiplex networks, triadic interactions can be used to establish inter-layer interactions between nodes in one layer and links in the other layer.

more than two reactors, and an enzyme can be regarded as a node that regulates a hyperedge representing chemical reactions; a network of glia and a network of neurons can form a multilayer network and two layers interact via interlayer triadic interactions.

Based on the above observations, let us formulate the simplest higher-order networks with triadic interactions built on simple structural networks. This higher-order network can be constructed as the composition of two networks: a simple structural network $\mathcal{A}$ and a regulatory network $\mathcal{B}$. The structural network is $\mathcal{A} = (V, E)$ formed by the set of

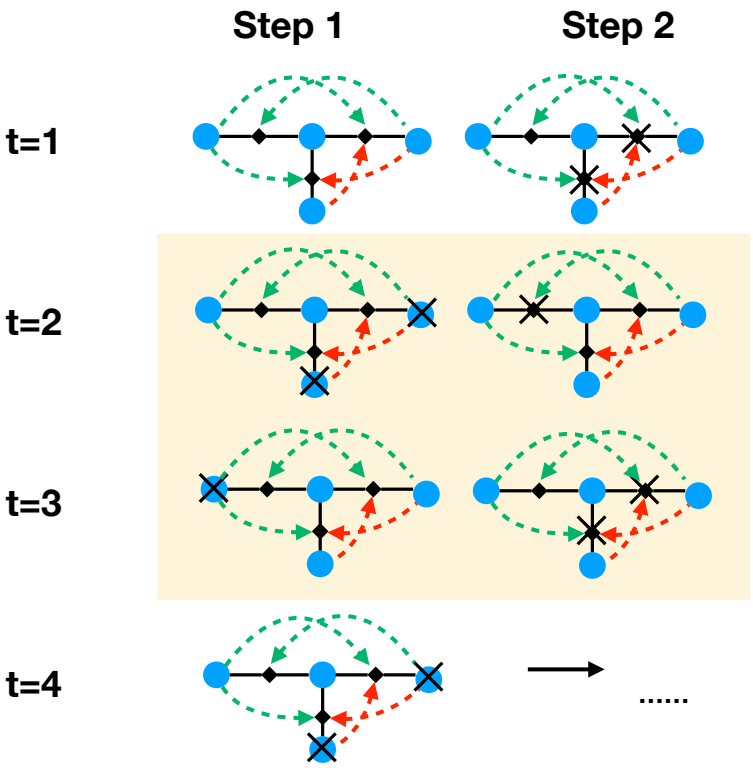

Figure 3.2: Sketch of triadic percolation. Solid lines represent structural links, dashed curves denote regulatory interactions (green stands for positive regulation, red for negative). Blue-filled circles indicate structural nodes and black diamonds indicate triadic interactions. For simplicity, we consider the deterministic bond-percolation model for $p = p_0 = 1$. At each stage, t of the dynamics, bond percolation is applied to the network, and then the effect of the regulatory activity is established. The illustration shows how the dynamics set into a periodic pattern with the giant component of the network "blinking" in time. The periodic pattern is highlighted in yellow. At the time $t = 1$, all links are active and all nodes are part of the giant component (GC). Their regulatory activity causes some links to become inactive (crossed links in the figure). As a consequence, at time $t = 2$, some nodes are no longer part of the GC and become inactive (crossed nodes in the figure). However, this change leads to changes in the activity of some links, which in turn affect the activity of the nodes at time $t = 3, 4$, etc. The final configuration reached at time $t = 3$ is identical to one observed at the end of stage $t = 1$. Due to the determinism of the model, the pattern repeats with period $T = 2$. The relative size R of the GC oscillation switches between $2/4$ and $3/4$.

nodes V connected by the structural links in the set E, and the regulatory network $\mathcal{B} = (V, E, W)$ is a bipartite and signed network between structural nodes V and structural links E, with nodes in V regulating links in E either positively or negatively, specified in the set W. Given a regulated link, a node that regulates this link is called a *positive regulator* if the regulatory interaction is positive and a *negative regulator* if the regulatory interaction is negative. We note that the sign is a property of the regulatory interaction and not an intrinsic property of nodes that act as regulators.

In the following sessions of this chapter, we will focus on the percolation on this network proposed above, however, these results can be easily extended to hypergraphs or multilayer networks with triadic interactions.

3.3 Triadic percolation

The triadic percolation model is defined in the way that the activity of structural links is regulated by the sign of triadic interactions and the activity of their regulator nodes. The activity of nodes is determined by the connectivity of the resulting network after considering only the active links via the percolation process, *i.e.*, only nodes in the giant component are active. In particular, we assume the activity of nodes and links change in time, leading to the following *triadic percolation* process.

- At time $t = 0$, every structural link is active with probability p_0.
- When $t \geq 1$, the activity of nodes and links are determined by the following 2-step iterative process:
  - Step 1: Given the activity of structural links at time $t-1$, one can determine a structural network by considering only active links. We define each node as active if the node belongs to the GC of this structural network.
  - Step 2: Given all the active nodes obtained in Step 1, links that are connected to at least one active negative regulator node and/or that are not connected

to any active positive regulator node are deactivated. All the remaining links are deactivated with probability $q = 1 - p$.

Here we note that for $p = p_0 = 1$, this model is deterministic and the dynamic is fully determined by the structural network and the regulatory network. However, for $p < 1$ (and $p_0 < 1$), the model is stochastic, *i.e.*, the activity of links is not uniquely determined by the activity of the regulator nodes, but also by the random failure with probability $1 - p$.

In the proposed triadic percolation model, links and nodes can be turned on and off dynamically by the regulatory interactions and the percolation process, which makes it distinct from classic percolation models. This model only makes minimal and justifiable assumptions while remaining general. The assumption that only nodes in the GC are active/functioning is well accepted in the context of network robustness [88]. Meanwhile, the regulatory rules for turning on/off links are a minimum assumption that treats both positive and negative regulations in a symmetric way: if a link is solely regulated by one regulator, then the activation of this single positive regulator or deactivation of a single negative regulator can both activate this link. The annealed stochastic effects are considered in this model as well, indicated by $p < 1$ (and $p_0 < 1$), representing the unavoidable stochasticity that can affect the activation of the structural links in real scenarios.

Triadic percolation can lead to a highly non-trivial dynamic of network connectivity. Figure 3.2 illustrates the phenomenon of network "blinking" with nodes and links of the network turning on or off periodically (or chaotically), forming GCs with different sizes.

3.4 Theory of triadic percolation

Here we establish the theoretical framework of triadic percolation that is able to predict the phase diagram (or orbit diagram) of the model on random networks with triadic interactions. The structural network can be generated via the configuration model, given

a degree sequence sampled from the degree distribution $\pi(k)$. We assume the structural network $\mathcal{A}$ contains N nodes and has the averaged degree $\langle k \rangle = c$. The structural degree of a node i is denoted as k_i.

In order to generate the regulatory network $\mathcal{B}$, we assign each node i two other degree values, *i.e.*, the number of links that it regulates positively κ_i^+ and negatively κ_i^-. Similarly, each structural link ℓ is assigned the degree values $\hat{\kappa}_\ell^+$ and $\hat{\kappa}_\ell^-$, indicating the number of its positive regulators and negative regulators. We assume the links' degrees are sampled from the distribution $\hat{P}(\hat{\kappa}^+, \hat{\kappa}^-)$ here taken to be independent $\hat{P}(\hat{\kappa}^+, \hat{\kappa}^-) = \hat{P}_\pm(\hat{\kappa}^+)\hat{P}_\pm(\hat{\kappa}^-)$, and the nodes' degrees are sampled from the distribution $\tilde{P}(k, \kappa^+, \kappa^-)$. Once the degrees of nodes and links have been assigned, one can establish the positive (+) and negative (-) regulatory interaction between the structural link ℓ and the node i with probability

$$p_{\ell,i}^\pm = \frac{\kappa_i^\pm \hat{\kappa}_\ell^\pm}{\langle \kappa^\pm \rangle N} \tag{3.1}$$

where $\langle \kappa^\pm \rangle = c^\pm$ denotes the average of $\kappa^\pm$ over all nodes in the network. We note that when creating the regulatory interactions, a regulator node is prohibited from regulating one structural link positively *and* negatively at the same time. As long as the network $\mathcal{B}$ is large and sparse, this consideration will not induce significant correlations.

The percolation theory on networks with triadic interactions can be derived by combining the classic percolation theory and the theory of dynamical systems. Let us denote $S^{(t)}$ as the probability that a node at the end of a random structural link is in the GC at time t and $\hat{S}^{(t)\pm}$ as the probability that a node regulating (either positively or negatively) a random structural link is in the GC at time t. Moreover, we define with $p_L^{(t)}$ the probability that structural links are active at time t. By putting $p_L^{(0)} = p_0$ indicating the probability that a structural link is active at time $t = 0$, we have that for all $t > 0$,

as long as the network is locally tree-like, $S^{(t)}$, $\hat{S}^{(t)\pm}$ and $p_L^{(t)}$ are updated as

$$\begin{aligned} S^{(t)} &= 1 - G_1\left(1 - S^{(t)} p_L^{(t-1)}\right) \\ \hat{S}^{(t)\pm} &= 1 - \mathcal{G}^{\pm}\left(1 - S^{(t)} p_L^{(t-1)}\right) \\ p_L^{(t)} &= p G_0^{-}\left(1 - \hat{S}^{(t)-}\right)\left[1 - G_0^{+}\left(1 - \hat{S}^{(t)+}\right)\right] \end{aligned} \tag{3.2}$$

where the first two equations implement Step 1 and the third equation implements Step 2, *i.e.*, the regulation process of links. The generating functions are given by

$$\begin{aligned} G_1(x) &= \sum_{k,\kappa^+,\kappa^-} \tilde{P}\left(k,\kappa^+,\kappa^-\right) \frac{k}{\langle k \rangle} x^{k-1}, \\ G_0^{\pm}(x) &= \sum_{\kappa_\pm} \hat{P}_\pm\left(\hat{\kappa}^\pm\right) x^{\hat{\kappa}^\pm}, \\ \mathcal{G}^{\pm}(x) &= \sum_{k,\kappa^+,\kappa^-} \tilde{P}\left(k,\kappa^+,\kappa^-\right) \frac{\kappa^\pm}{\langle \kappa^\pm \rangle} x^{k}. \end{aligned} \tag{3.3}$$

The order parameter R, *i.e.*, the probability that a node is in the GC is given by

$$R^{(t)} = 1 - G_0\left(1 - S^{(t)} p_L^{(t-1)}\right), \tag{3.4}$$

where

$$G_0(x) = \sum_{k,\kappa^+,\kappa^-} \tilde{P}(k,\kappa^+,\kappa^-) x^k. \tag{3.5}$$

For simplicity, we will consider in the following sections the case in which both κ_i^+ and κ_i^- are chosen independently of the structural degree, *i.e.*,

$$\tilde{P}(k,\kappa^+,\kappa^-) = \pi(k) P(\kappa^+,\kappa^-), \tag{3.6}$$

the equations above can be reduced to

$$
\begin{aligned}
S^{(t)} &= 1 - G_1\left(1 - S^{(t)} p_L^{(t-1)}\right) && (3.7)\\
R^{(t)} &= 1 - G_0\left(1 - S^{(t)} p_L^{(t-1)}\right) && (3.8)\\
p_L^{(t)} &= p G_0^{-}\left(1 - R^{(t)}\right)\left[1 - G_0^{+}\left(1 - R^{(t)}\right)\right] && (3.9)
\end{aligned}
$$

where

$$
\begin{aligned}
G_0(x) &= \sum_k \pi(k) x^k,\\
G_1(x) &= \sum_k \pi(k) \frac{k}{\langle k \rangle} x^{k-1},\\
G_0^{\pm}(x) &= \sum_{\kappa_\pm} \hat{P}_\pm\left(\hat{\kappa}^\pm\right) x^{\hat{\kappa}^\pm} \qquad (3.10)
\end{aligned}
$$

Eqs. 3.7, 3.8, 3.9 for the triadic percolation model can be simply written as a one-dimensional map as:

$$
R^{(t)} = f\left(p_L^{(t-1)}\right), \quad p_L^{(t)} = g_p\left(R^{(t)}\right) \qquad (3.11)
$$

which can be further reduced to

$$
R^{(t)} = h\left(R^{(t-1)}\right). \qquad (3.12)
$$

The theoretical prediction of triadic percolation defined on structural networks generated by the configuration model can be made through Eqs. 3.7, 3.8, 3.9 (or equivalently Eq. 3.11). This model is of mean-field nature: the percolation equations (Eq. 3.7 and Eq. 3.8) are averaged over uncorrelated network ensemble while the regulation equation (Eq. 3.9) is averaged over the random failure of links with probability $1 - p$. Yet, as we will see, despite this mean-field approximation, the proposed theoretical approach provides an accurate prediction of the behavior of triadic percolation.

3.5 Results

In presence of negative regulatory interactions, the order parameter R representing the fraction of active nodes in the network becomes a time-dependent variable. The order parameter R undergoes period-doubling and a route to chaos as a function of parameter p which indicates the probability of activating a link while all the regulatory conditions that allow the link to be active are fulfilled. The dynamics is in the same universality class as the logistic map, for structural networks with arbitrary degree distribution $\pi(k)$ and regulatory connectivity generated by Poisson distributions $P(\hat{\kappa}^{\pm})$. Detailed proof of the universality class is given in Appendix A.

Triadic percolation has non-trivial dynamical behaviors. It displays the emergence of both "blinking" oscillations and chaotic patterns of the giant component (see Figure 3.3). "Blinking" refers to the intermittent switching on and off of sets involving two more nodes periodically, which leads to periodic oscillations of the order parameter. While chaos indicates that at each time, a different group and number of nodes are activated. The one-dimensional map defined in Eq. 3.11 can be illustrated graphically in the Cobweb plot, and it captures the nature of the dynamic. The combination of positive and negative regulations in triadic percolation leads to a richer phase diagram compared with ordinary percolation without triadic interactions. More specifically, the ordinary percolation transition on networks is second-order, while the triadic percolation with positive and negative regulatory interactions can display, with different parameters, a first-order hybrid transition, an orbit diagram rather than the phase diagram (see Figure 3.4), *i.e.*, the fraction of active nodes R in the network with a given probability p indicating the probability that a link is active when all the regulatory conditions are satisfied is no longer a fixed value but can take multiple possible values. Note that in the triadic percolation model, we obtain the novel and unexpected result that the phase diagram of the model coincides with the orbit diagram of the map equations (Eq. 3.7-3.9). This result is at the core of the change of paradigm that triadic percolation entails for the critical behavior of the model with respect to standard percolation.

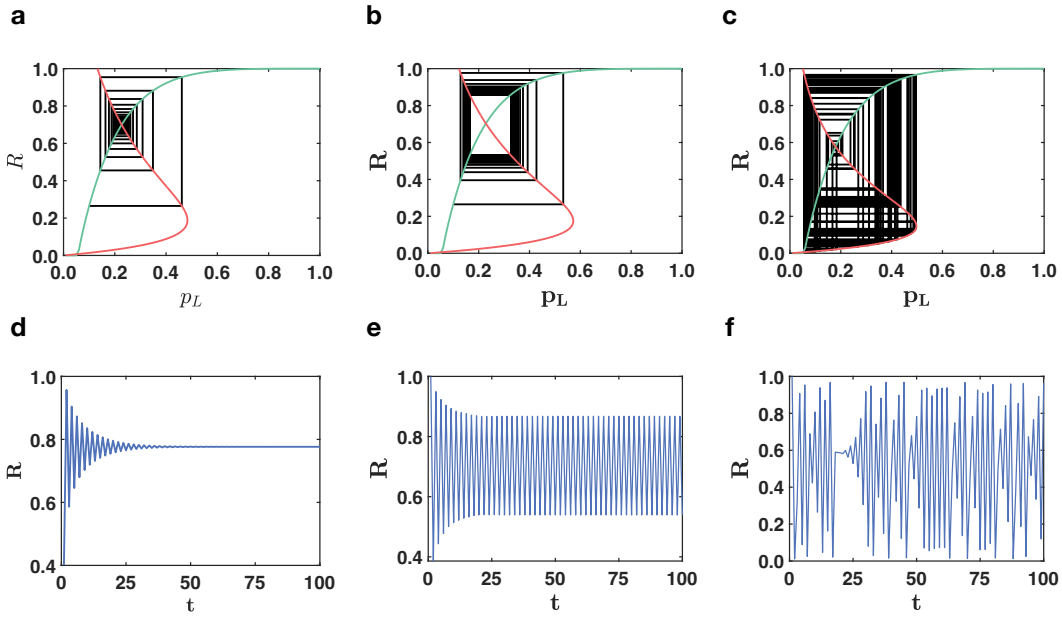

Figure 3.3: Time dependence of the order parameter of triadic percolation. In triadic percolation, the order parameter R can have non-trivial dynamics. Here we demonstrate with theory and simulations the non-trivial dynamics of R for parameter values in which the dynamics reach a steady state (panels a, d), period-two oscillations (panels b, e), and chaotic dynamics (panels c, f). This behavior is predicted by the theory which can be schematically represented by cobweb plots (panels a-c) corresponding to the map Eq. (3.11) with the function f indicated in green and the function g_p in red. Results of Monte Carlo simulations for R as a function of time t (panels d-f) are in excellent agreement (MC) with the theory. The structural network has a power-law degree distribution $\pi(k) \sim k^{-\gamma}$, with minimum degree $m = 4$, maximum degree $K = 100$, and degree exponent $\gamma = 2.5$. The degrees $\hat{\kappa}^+$ and $\hat{\kappa}^-$ of the regulatory network obey Poisson distributions with average c^+ and c^-. The links are activated with probability $p = 0.8$. The parameters $c^+, c-$ are $c^+ = 10$, $c^- = 1.8$ (panel a, d), $c^+ = 10, c^- = 2.1$ (panel b, e). The MC simulations are performed on networks of $N = 10^4$ nodes.

The theoretical predictions from Eq. 3.11 are validated by extensive Monte Carlo simulations (see Figure 3.3 and Figure 3.4). The mean-field theory allows for a good approximation of the dynamical behavior of triadic percolation for both random Poisson and scale-free structural networks.

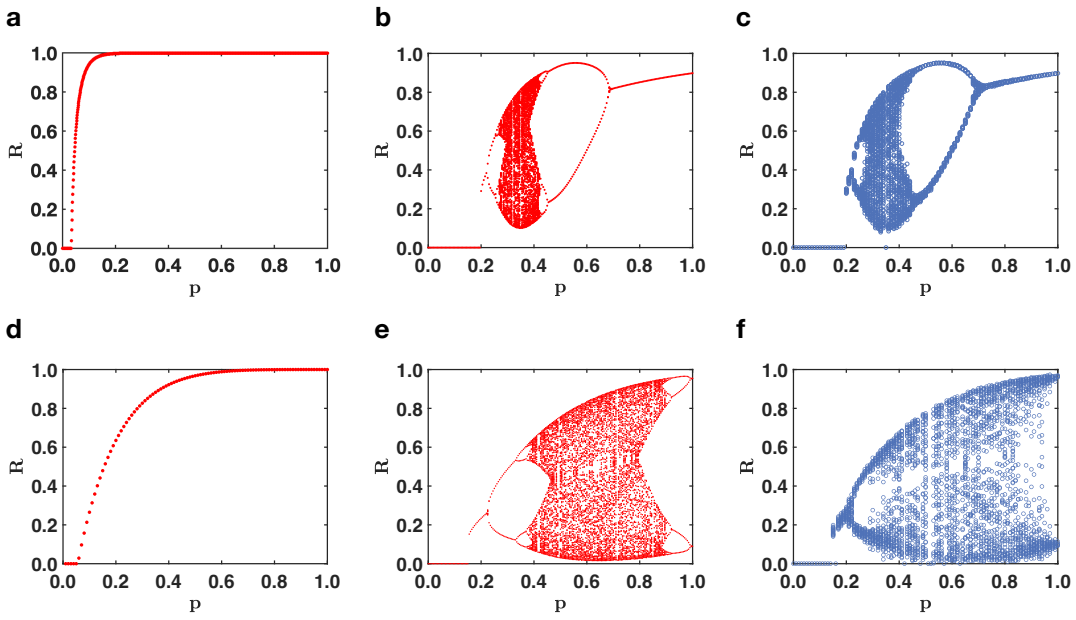

Figure 3.4: Phase diagram of triadic percolation on Poisson and scale-free structural networks. The phase diagram of triadic percolation (panels b, c, e, f) is radically different from the phase diagram of ordinary percolation (panels a, d) for both Poisson (panels a-c) and scale-free structural networks (panels d-f). Ordinary percolation reveals a second-order phase transition (theoretical prediction, panels a, d) while the phase diagram of triadic percolation reveals that the order parameter R displays period doubling and a route to chaos (panels b, c, e, f). The theoretical predictions of the phase diagram obtained from Eqs. 3.7, 3.8, 3.9 are in very good agreement with the phase diagram obtained from extensive Monte Carlo (MC) simulations (panels e, f). In panels (a-c) the structural network is Poisson with average degree $c = 30$; the regulatory network is also Poisson with averages $c^+ = 1.8$ and $c^- = 2.5$. In panels (d-e) the scale-free structural network has degree exponent $\gamma = 2.5$, minimum degree $m = 4$, and maximum degree $K = 100$; the regulatory network is Poisson with $c^+ = 10$ and $c^- = 2.8$. The MC simulations are obtained from networks of size $N = 2 \times 10^5$ (panel e) and $N = 10^4$ (panel f). Here points represent all R values observed in the time range $150 \leq t \leq 200$.

In order to further understand the effects of positive and negative regulatory interactions, we consider two limiting scenarios, *i.e.*, the limit that the average degree of negative regulation $\langle \hat{\kappa}^- \rangle \to 0$, in which the model includes only positive regulatory interactions and the other limit that average degree of positive regulation $\langle \hat{\kappa}^+ \rangle \to \infty$, indicating that

the requirement of activating a link from positive regulators is always satisfied hence the role of positive regulators becomes negligible. In Figure 3.5 and Figure 3.6, we show the theoretical orbit diagrams of triadic percolation for a Poisson structural network and a scale-free structural network respectively. Both networks are formed by the structural networks and regulatory networks with the Poisson distribution of the regulatory degrees. We observe that in absence of negative regulations, *i.e.*, $\langle \hat{\kappa}^- \rangle = c^- \to 0$, the percolation transition is discontinuous for both the Poisson structure network and the scale-free structural network. For $\langle \hat{\kappa}^+ \rangle = c^+ \to \infty$, on the other hand, we observe the period-2 oscillations in both cases of Poisson and scale-free structural networks. Finally, chaos only emerges when both positive and negative regulatory interactions are present.

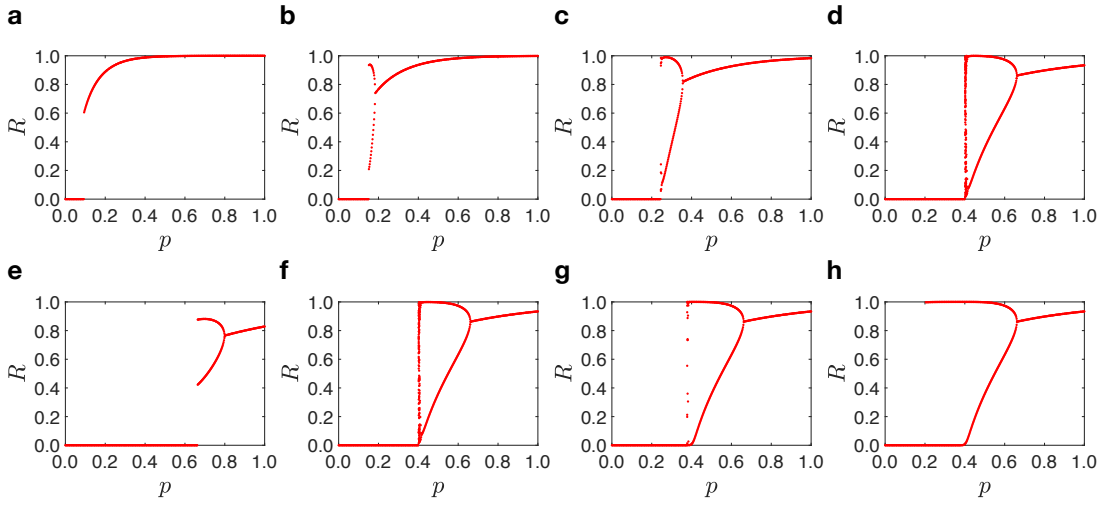

Figure 3.5: Theoretically obtained orbit diagrams for the Poisson structural network with average degree $c = 30$ and uncorrelated structural and regulatory degrees of the nodes. In the first row, $c^+ = 10$, from the left to the right we increase the c^- that $c^- = 1.0$ (a), $c^- = 1.5$ (b), $c^- = 2.0$ (c), $c^- = 2.5$ (d). In the second row, $c^- = 2.5$, from the left to the right we increase the c^+ that $c^+ = 1$ (e), $c^+ = 10$ (f), $c^+ = 1000$ (g), $c^+ = \infty$ (h). For all panels $c^\pm$ indicates the average degree of the Poisson distribution $\hat{P}_\pm(\hat{\kappa}^\pm)$. All figures are obtained by setting the initial condition $p_L^{(0)} = 0.1$.

In the end, in order to show the periodic and chaotic patterns are not artifacts of

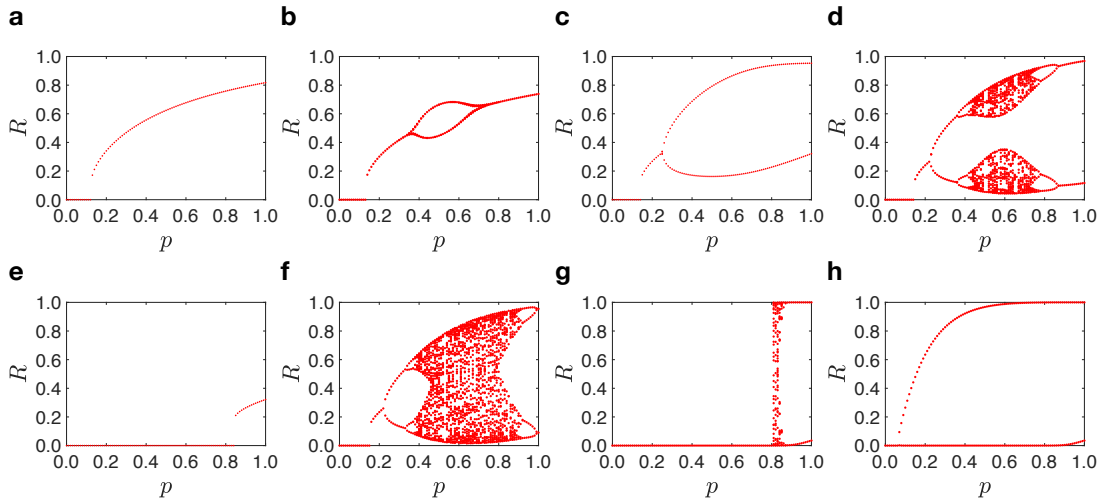

Figure 3.6: Theoretically obtained orbit diagrams of the scale-free structural network with minimum degree $m = 4$, power-law exponent $\gamma = 2.5$, maximum degree $K = 100$, and uncorrelated structural and regulatory degrees of the nodes. In the first row, $c^+ = 10$, from the left to the right we increase the c^- that $c^- = 1.5$ (a), $c^- = 1.9$ (b), $c^- = 2.3$ (c), $c^- = 2.7$ (d). In the second row, $c^- = 2.8$, from the left to the right we increase the c^+ that $c^+ = 1$ (e),$c^+ = 10$ (f), $c^+ = 1000$ (g), $c^+ = \infty$ (h). In all the panels $c^\pm$ indicate the average degree of the Poisson distribution $\hat{P}_\pm(\hat{\kappa}^\pm)$. All figures are obtained by setting the initial condition to $p_L^{(0)} = 0.1$.

synthetic networks, we simulate the dynamic on structural networks which are taken from the real world. In particular, we consider the structural networks constructed from the empirical data collected in the repository [154]. The higher-order networks are constructed by combining real-world structural networks and synthetic regulatory networks. In Figure 3.7, we show the orbit diagram for these topologies revealing the non-trivial dynamics with noisy periodic oscillation in certain regimes and chaotic oscillations in other regimes. More details of the datasets used here can be found in Appendix B.

In the scenario with the absence of negative regulations, however, we find that the dynamics always reach a stationary state. In Figure 3.8(a) we show an example of the time series for the order parameter $R^{(t)}$ converges to its stationary state $R^{(t)} = R^*$. Moreover, in Figure 3.8(b) we show the dependency of the stationary point R^* with the probability p. The theoretical predictions are also confirmed by extensive Monte

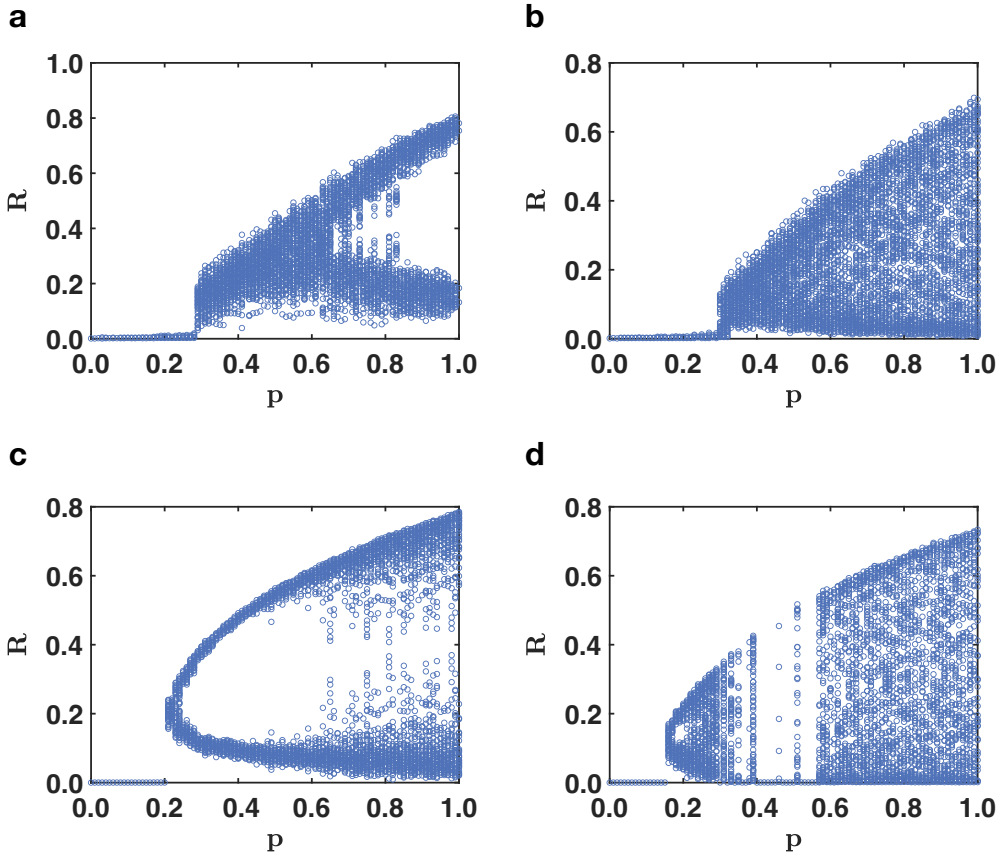

Figure 3.7: Phase diagram of triadic percolation for real-world structural network topologies. The phase diagram of triadic interaction displaying the fraction of nodes R in the GC as a function of p is shown for real-world structural networks obtained from the repository [154]: the mouse brain network (panel a, b) the Human bio grid network (panel c, d). The phase diagrams are obtained by MC simulations with Poisson regulatory networks with parameters $c^+ = 20, c^- = 2$ (panel a), $c^+ = 20, c^- = 4$ (panel b); $c^+ = 20, c^- = 4$ (panel c). $c^+ = 20, c^- = 6$ (panel d). All orbit diagrams are obtained with an initial condition $p_L^{(0)} = 0.1$.

Carlo simulations. Interestingly, the exclusive positive regulation induces a discontinuous hybrid percolation transition. We will further characterize the nature of the phase transitions and oscillations reported above theoretically in the following chapter.

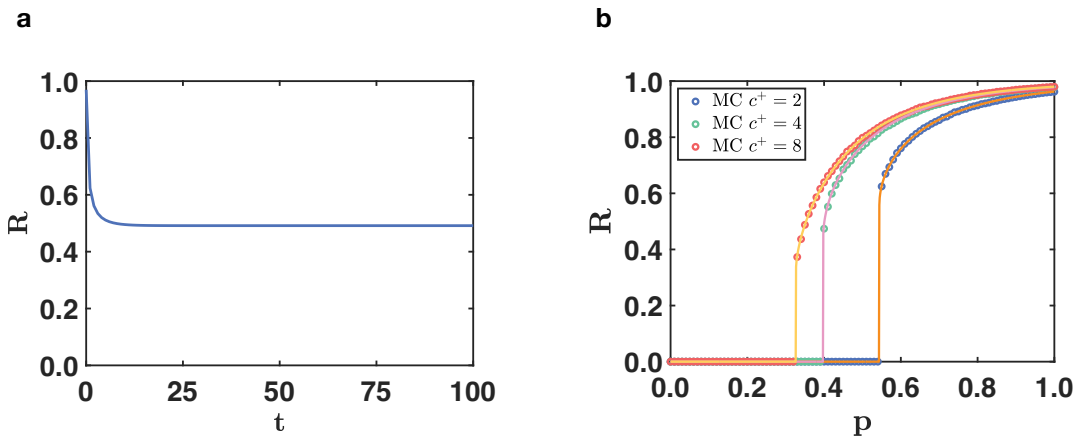

Figure 3.8: Triadic percolation in absence of negative triadic interactions. In the absence of negative triadic interactions the order parameter R of triadic percolations always reaches a stationary state for sufficiently long times (panel a). Moreover, the phase diagram, indicating the stationary solution of R as a function of p displays a discontinuous hybrid transition (panel b). In panel b the results obtained from MC simulations (symbols) over networks of $N = 10^4$ nodes are compared to theoretical expectations (solid curves). In both plots, the Poisson structural network has an average degree $c = 4$, and the Poisson regulatory network including exclusively positive regulations has an average degree c^+. In panel(a) the results are shown for $p = 0.4$ and $c^+ = 4$.

3.6 Investigation into the one-dimensional map

The dynamic properties of triadic percolation can be fully captured by the map Eq. 3.11 or equivalently Eq. 3.12. Thanks to the theory of dynamic systems and the linear stability analysis method, we are able to theoretically characterize the critical behaviors in this dynamic, including discontinuous phase transition, bifurcation, and chaos. These analyses provide a clear picture of the nature of the dynamical triadic percolation processes.

3.6.1 Stability analysis

Here let us restrict our discussion to the case that structural and regulatory degrees of nodes are uncorrelated, *i.e.*, Eq. 3.4 holds, and the one-dimensional map can be written

as Eq. 3.11 or Eq. 3.12. Let us rewrite Eq. 3.12 here as

$$R^{(t)} = h_p\left(R^{(t-1)}\right) = f\left(g_p\left(R^{(t-1)}\right)\right). \tag{3.13}$$

The stationary solution $R^{(t)} = R^*$ of this map satisfies:

$$R^* = h_p\left(R^*\right). \tag{3.14}$$

This stationary solution becomes unstable as soon as

$$|J| = 1 \tag{3.15}$$

where

$$J = h_p'\left(R^*\right) = \left.\frac{\mathrm{d}f}{\mathrm{d}p_L}\right|_{p_L=p_L^\star} \left.\frac{\mathrm{d}g_p}{\mathrm{d}R}\right|_{R=R^\star} \tag{3.16}$$

Interestingly, while the critical condition $J = 1$ indicates a discontinuous and hybrid transition, $J = -1$ indicates the onset of period-2 oscillations.

Let us first show that $J = 1$ indicates a discontinuous and hybrid transition. Let us denote the value of p when $J = 1$ is achieved as p_c and we consider a small perturbation $\delta p = p - p_c \ll 1$. We indicate the corresponding change in the stationary solution R^* with $\delta R = R^*(p) - R^*(p_c)$. Since both $R^*(p)$ and $R^*(p_c)$ satisfy the stationary equation Eq. 3.14, assuming, without loss of generality, that $h_p(R^*)$ is twice differentiable at $R^*(p_c) = R_c > 0$, we can expand the latter equation in terms of δp and δR^*:

$$\delta R = h_{p_c}'\left(R_c\right)\delta R + \frac{1}{2}h_{p_c}''\left(R_c\right)\left(\delta R\right)^2 + \frac{\partial h_{p_c}\left(R_c\right)}{\partial p}\delta p. \tag{3.17}$$

Since $J = h_{p_c}'(R_c) = 1$, this equation reduces to

$$\frac{1}{2}h_{p_c}''\left(R_c\right)\left(\delta R\right)^2 + \frac{\partial h_{p_c}\left(R_c\right)}{\partial p}\delta p = 0, \tag{3.18}$$

from which we can immediately derive the scaling relation

$$\delta R \propto (\delta p)^{1/2} \tag{3.19}$$

as long as $h''_{p_c}(R_c)$ and $\partial h_{p_c}(R_c)/\partial p$ have finite values and opposite sign. Therefore we obtain that

$$R^*(p) - R_c \propto (p - p_c)^{1/2} \tag{3.20}$$

which proves the transition is discontinuous and hybrid.

Now let us discuss the case of $J = -1$, with the help of a concrete example (for instance see Figure 3.11). When J passes the critical point $J = -1$, two solutions R_1 and R_2 emerge. Thus they still satisfy Eq. 3.12, *i.e.*,

$$R_1 = h_p(R_2),\ R_2 = h_p(R_1). \tag{3.21}$$

In other words, R_1 and R_2 are fixed points of the *second-iterate* [155] of h_p, *i.e.*

$$R_1 = h_p\left(h_p\left(R_1\right)\right),\ R_2 = h_p\left(h_p\left(R_2\right)\right), \tag{3.22}$$

and the stability of fixed points R_1 and R_2 can be determined in a similar way by calculating the derivative of the second iterate of h_p.

$$\left.\frac{\mathrm{d}h_p\left(h_p\left(R\right)\right)}{\mathrm{d}R}\right|_{R=R_1} = \left.\frac{\mathrm{d}h_p(R)}{R}\right|_{R=R_1} \left.\frac{\mathrm{d}h_p(R)}{R}\right|_{R=R_2} = \left.\frac{\mathrm{d}h_p\left(h_p\left(R\right)\right)}{\mathrm{d}R}\right|_{R=R_2} \tag{3.23}$$

This equality indicates that both fixed points R_1 and R_2 always have the same stability and at $h'_p(R) = -1$, $h_p(h_p(R))' = 1$. Thus, as long as $|h_p(h_p(R))'| < 1$, both fixed points of the second-iterate map are stable, and the stable 2-cycle emerges.

The dynamic of the one-dimensional map can be graphically illustrated by a cobweb plot. In Figure 3.9 we show the cobweb plot when only positive regulatory interactions

are present, *i.e.*, when Eq. 3.9 is substituted by

$$p_L^{(t)} = p\left[1 - G_0^+\left(1 - R^{(t)}\right)\right]. \tag{3.24}$$

In Figure 3.10 we show the cobweb plot when only the negative regulatory interactions are present and positive interactions do not play a role, *i.e.*, when Eq. 3.9 is substituted by

$$p_L^{(t)} = pG_0^-\left(1 - R^{(t)}\right). \tag{3.25}$$

Eq. 3.16 implies that since $\mathrm{d}f/\mathrm{d}p_L \geq 0$, the onset of the period-2 oscillations can take place only if $g_p(R)$ has a negative slope, which happens only when negative regulatory interactions are present (see Eq. 3.9). Thus, we conclude that the presence of negative regulations is a requisite of period-2 oscillations.

3.6.2 Triadic percolation on uncorrelated Poisson structural networks

In this section, we investigate the stability of the stationary solution in a specific case of a Poisson structural network with an average degree c in which the structural and regulatory degrees of the nodes are uncorrelated, *i.e.*,

$$\tilde{P}\left(k, \kappa^+, \kappa^-\right) = \pi(k) P\left(\kappa^+, \kappa^-\right) \tag{3.26}$$

with

$$\pi(k) = \frac{1}{k!} c^k e^{-c}. \tag{3.27}$$

Additionally, we assume that the positive and negative regulatory degree of a link $\hat{\kappa}^+$ and $\hat{\kappa}^-$ are drawn from Poisson distributions with average degree c^+ and c^- respectively,

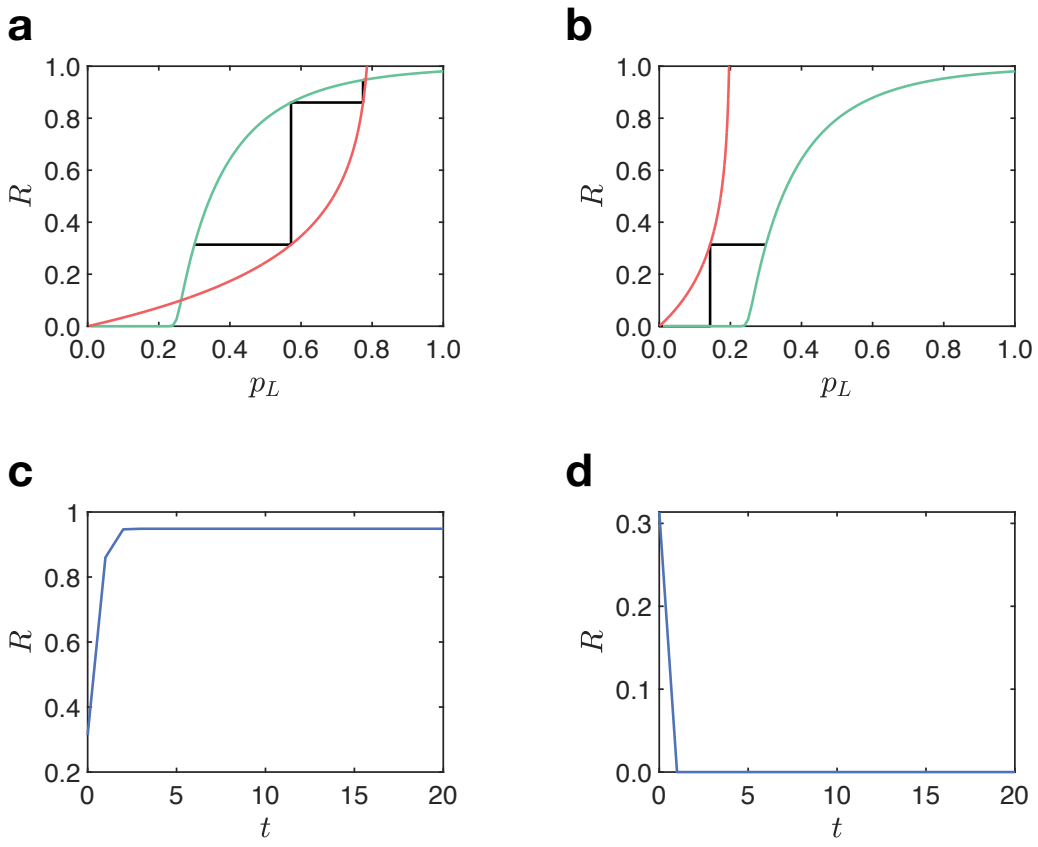

Figure 3.9: The theoretical cobweb plot (panel (a), (b)) and the corresponding dependence of the order parameter R on time t (panel (c), (d)) is shown when regulatory interactions are exclusively positive. The structural network is a Poisson network with average degree $c = 4$, and Poisson distribution $\hat{P}_{\pm}(\hat{\kappa}_{\pm})$ with average degrees $c^{+} = 4$ and $c^{-} = 0$ respectively. In panel (a) and (c) $p = 0.8 > p_c$; in panel (b) and (d) $p = 0.2 < p_c$. The results are obtained with an initial condition $p_L^{(0)} = 0.3$.

i.e.,

$$\hat{P}_{\pm}(\hat{\kappa}^{\pm}) = \frac{1}{\hat{\kappa}^{\pm}!}(c^{\pm})^{\hat{\kappa}^{\pm}} e^{-c^{\pm}}. \tag{3.28}$$

Now Eqs. 3.7, 3.8, 3.9 for the triadic percolation reduce to

$$\begin{aligned} R^{(t)} &= 1 - e^{-cp_L^{(t-1)}R^{(t)}} \\ p_L^{(t)} &= p\left(1 - e^{-c^{+}R^{(t)}}\right) e^{-c^{-}R^{(t)}}. \end{aligned} \tag{3.29}$$

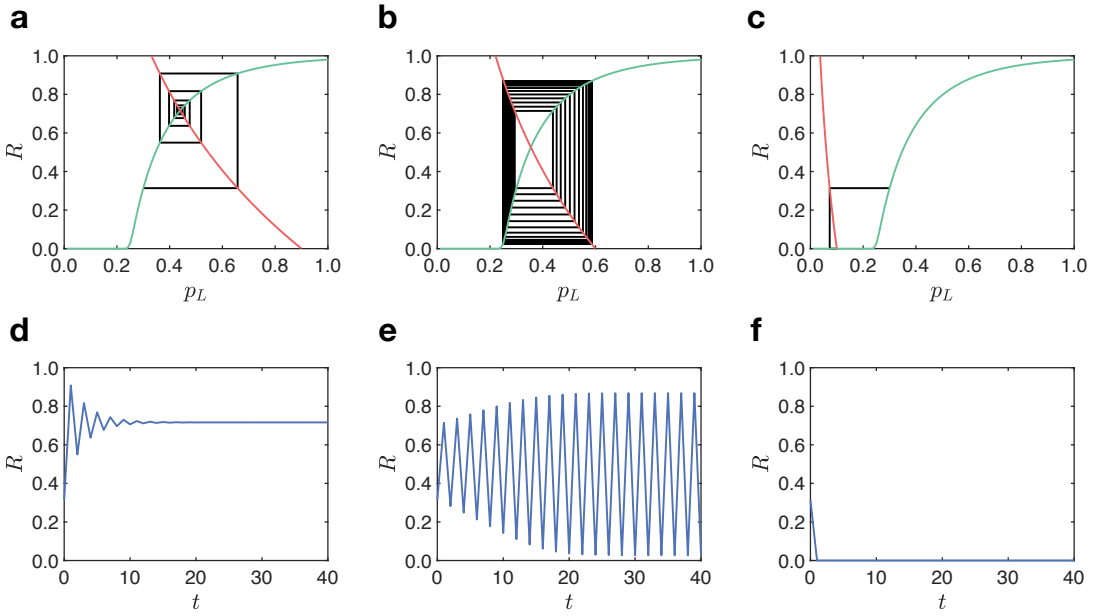

Figure 3.10: The theoretical cobweb plot (panel (a), (b), (c)) and the corresponding dependence of the order parameter R on time t (panel (d), (e), (f)) is shown when regulatory interactions are exclusively negative. The structural network is a Poisson network with average degree $c = 4$, and Poisson distribution $\hat{P}_{\pm}(\hat{\kappa}_{\pm})$ with average degrees $c^{+} = 4$ and $c^{+} = \infty$ respectively. In panel (a) and (d) $p = 0.9$; in panel (b) and (e) $p = 0.6$; in panel (c) and (f) $p = 0.1$. The results are obtained with an initial condition $p_L^{(0)} = 0.3$.

The first equation can be expressed as a map between $p_L^{(t-1)}$ and $R^{(t)}$, while the second equation can be expressed as a map between $R^{(t)}$ and $p_L^{(t)}$, i.e.,

$$R^{(t)} = f\left(p_L^{(t-1)}\right), \quad p_L^{(t)} = g_p\left(R^{(t)}\right). \tag{3.30}$$

Both equations can be combined in the single map

$$R^{(t)} = h_p\left(R^{(t-1)}\right) = f\left(g_p\left(R^{(t-1)}\right)\right). \tag{3.31}$$

Let us denote the stationary solution for R and p_L as R^* and p_L^* respectively. The stationary equations read

$$\begin{aligned} R^\star &= 1 - e^{-cp_L^\star R^\star}, \\ p_L^\star &= p\left(1 - e^{-c^+ R^\star}\right) e^{-c^- R^\star}. \end{aligned} \tag{3.32}$$

and these equations can be merged into one single equation

$$R^\star = h_p(R^\star) = f(g_p(R^\star)), \tag{3.33}$$

The Jacobian reads

$$J = h_p'(R^*) = \frac{\mathrm{d}f(g_p(R^*))}{\mathrm{d}R^*} = f'(p_L^*)g_p'(R^*) \tag{3.34}$$

and the stationary solution becomes unstable at

$$|J| = 1. \tag{3.35}$$

f' and g' are given by

$$\begin{aligned} f'(p_L^\star) &= -\frac{cR^\star}{cp_L^\star - e^{cp_L^\star R^\star}}, \\ g_p'(R^\star) &= p(c^+ + c^-)e^{-(c^- + c^+)R^\star} - c^- p e^{-c^- R^\star}. \end{aligned} \tag{3.36}$$

By solving Eqs. 3.32 and Eq. 3.35 numerically, we obtain the manifold for the onset of period-2 oscillations of the order parameter $R^{(t)}$.

In Figure 3.11, we illustrate graphically the difference between the two types of possible instabilities of the stationary solution. When $J = 1$, we observe the discontinuous emergence of a non-trivial stationary solution $R^* > 0$ while when $J = -1$ we observe the onset of period-2 oscillations of the order parameter.

In Figure 3.12 we show the critical manifolds for the onset of period-2 oscillations of

the order parameters and for the onset of discontinuous hybrid transitions. Note that for any given structural and regulatory networks, the critical point of the onset of the discontinuous hybrid transition is unique, if such transition exists. However, the onset of the period-2 oscillations can occur for different values of p (examples can be observed in Figure 3.6). In Figure 3.12 we plot exclusively the largest and the smallest critical points for the onset of period-2 oscillation if they exist.

3.7 Triadic percolation with time delays

In order to exclude the possibility that the observed periodic and chaotic behavior of triadic percolation is an artifact of the particular choice of the dynamic, we propose generalized versions of the model, taking into account the time-delayed regulatory interactions, where each regulatory link is assigned with a time delay τ. More specifically, Step 1 in the triadic percolation process keep unchanged and Step 2 is replaced by:

- Step 2' Given the set of active nodes obtained in Step 1, each structural link is deactivated

  (a) if no positive regulator of the link is active at time $t - \tau$ and/or

  (b) if the link is connected to at least one negative regulator that is active at time $t - \tau$.

  (c) if the structural link is not deactivated according to conditions (a) and (b), it can still be deactivated due to stochastic events which occur with probability $q = 1 - p$.

Here we consider two different methods to construct the time delay which depends on the choice of the probability distribution for time delays of structural links (see the illustrations in Figure 3.13):

Method 1 Each regulatory interaction is associated with a time delay drawn independently from the distribution $\tilde{p}(\tau)$;

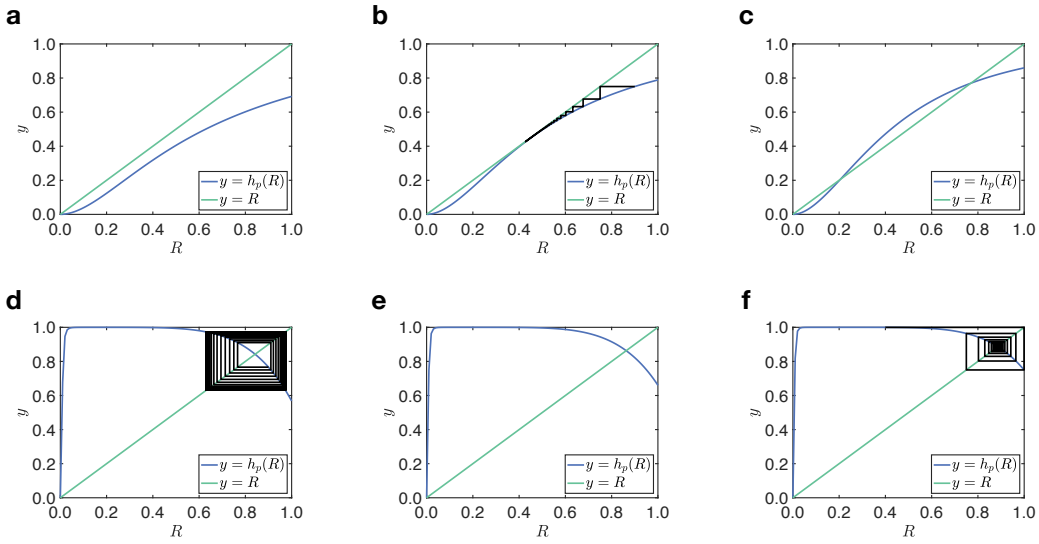

Figure 3.11: The figures show the two different modalities for the onset of the instability of the stable solution of the iterative map $R^{(t)} = h_p(R^{(t-1)})$ for a Poisson network with triadic interactions corresponding to the crossing of the curves $y = h_p(R)$ and $y = R$. In panels (a),(b), and (c) we show the emergence of the discontinuous transition at $p = 0.392$ (panel (b)) on a Poisson network with average degree $c = 4$, and Poisson distribution s $\hat{P}^{\pm}(\hat{\kappa}^{\pm})$ with average degrees $c^{+} = 4$ and $c^{-} = 0$ respectively. Panels (a) and (c) show the functions $y = h_p(R)$ and $y = R$ for $p = 0.30$ (below the transition) and $p = 0.50$ (above the transition). Note that in panel (b) the function $y = h(R)$ and the function $y = R$ are tangent to each other at their non-trivial intersection indicating that the non-trivial solution disappears as soon as $p < 0.392$. In panels (d),(e),(f) we show the emergence of 2-cycle at $p = 0.665$ (panel (e)) for a Poisson network with average degree $c = 30$, and Poisson distributions $\hat{P}^{\pm}(\hat{\kappa}^{\pm})$ with average degree $c^{+} = 10$ and $c^{-} = 2.5$ respectively. Panels (d) and (f) show the functions $y = h(R)$ and $y = R$ for $p = 0.60$ (below the transition) and $p = 0.8$ (above the transition) respectively. Note that in panel (e) the function $y = h_p(R)$ displays a derivative -1 leading to the emergence of the 2-limit cycle observed for $p \leq 0.665$. The relative cobweb is shown only for panels (b), (d), and (f) to improve the readability of the figure.

Method 2 The regulatory interactions associated with each structural link has the same time delay τ, with the delay τ drawn from the distribution $\tilde{p}(\tau)$.

Let us discuss how Method 1 and Method 2 modify the map of triadic percolation. For

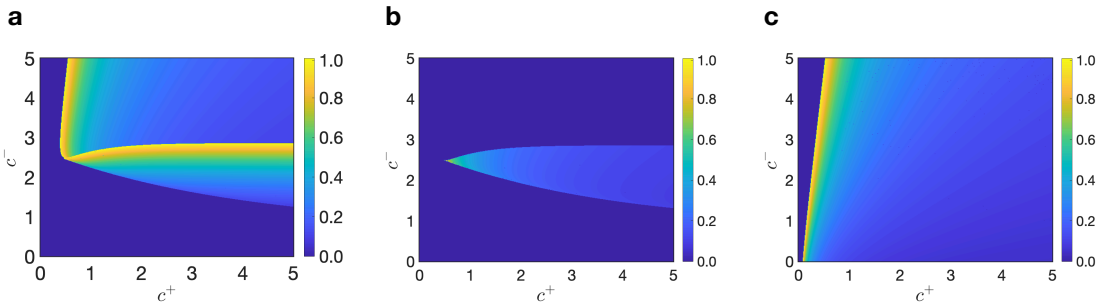

Figure 3.12: The upper critical point p_c^u (panel a) and the lower critical point p_c^l (panel b) determining the onset of period-2 oscillations are plotted plane (c^+, c^-). Panel c represents the critical point p_c at which the discontinuous hybrid transition is observed in the plane (c^+, c^-). In all panels, the structural network has a Poisson degree distribution with degree $c = 30$ the regulatory network has also a Poisson degree distribution with c^+ and c^- indicating the average positive and negative degrees respectively.

simplicity, let us focus on the case of uncorrelated structural network and regulatory degree of the nodes with Poisson distribution $\hat{P}(\hat{\kappa}^{\pm})$.

In the case of Method 1, each regulatory interaction is associated with a delay τ with probability $\tilde{p}(\tau)$. Therefore, among the regulators of a link, the probability that n_i regulatory links are associated with a delay τ_i follows a multinomial distribution

$$\Pi(\{n_i\}_{i=1,2,\cdots,d}|\hat{\kappa}^{\pm}, \tilde{\mathbf{p}}) = \frac{\hat{\kappa}^{\pm}!}{\prod_{i=1}^{d} n_i!} \prod_{i=1}^{d} [\tilde{p}(\tau_i)]^{n_i}, \tag{3.37}$$

with $\tilde{\mathbf{p}} = (\tilde{p}(\tau_1), \tilde{p}(\tau_2), \ldots, \tilde{p}(\tau_d))$ and such that $\sum_{i=1}^{d} \tilde{p}(\tau_i) = 1$. Thus, Eq. 3.9 for triadic percolation is modified to

$$p_L^{(t)} = p \exp\left(-c^- \sum_{\tau_i} \tilde{p}(\tau_i) R^{(t+1-\tau_i)}\right) \left[1 - \exp\left(-c^+ \sum_{\tau_i} \tilde{p}(\tau_i) R^{(t+1-\tau_i)}\right)\right]. \tag{3.38}$$

In the case of Method 2, Eq. 3.7 and Eq. 3.8 remain unchanged while Eq. 3.9 is

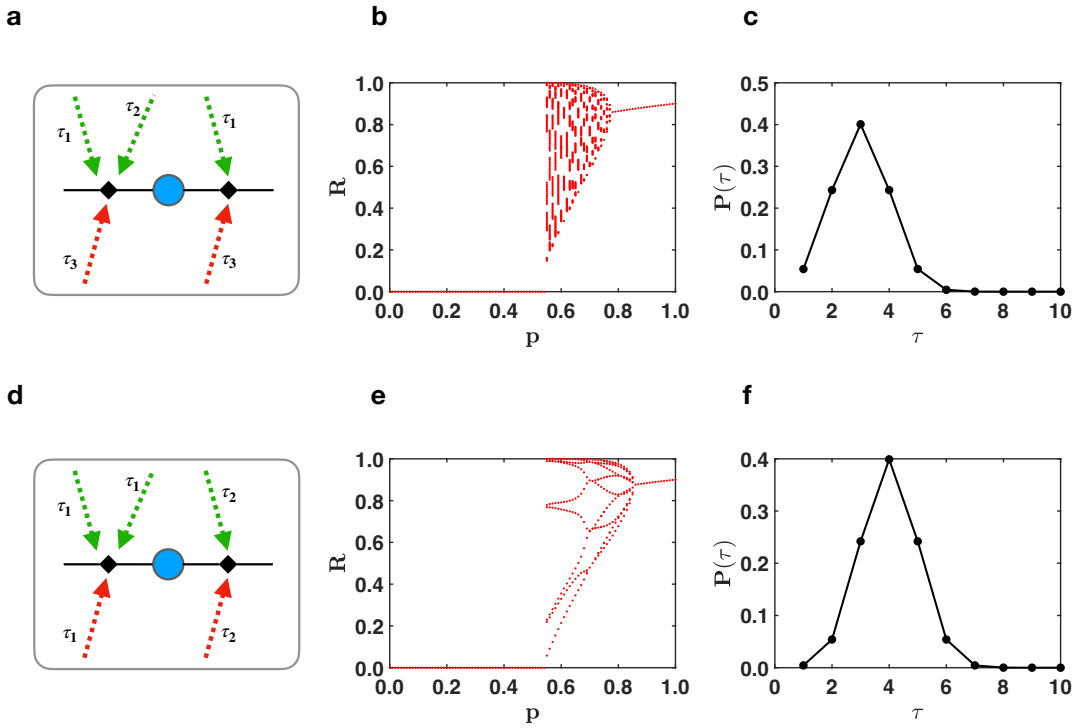

Figure 3.13: **Triadic percolation with time delays.** Method 1 and Method 2 of triadic percolation with delays are illustrated in panel (a) and (d) respectively. The corresponding phase diagrams for the structural Poisson network are shown in panel (b) for Model 1 and in panel (d) for Model 2. The orbit diagrams in panels (b) and (e) are obtained for the $\tilde{p}(\tau)$ distribution of delays shown in panel (c) and (f) respectively. The two orbit diagrams are obtained from the same structural and regulatory network. The structural network is a Poisson network with an average degree $c = 50$ and the regulator network has a Poisson degree distribution with average degree $c_+ = 10$ and $c_- = 3.3$.

modified as

$$p_L^{(t)} = p \sum_{\tau=1}^{d} \tilde{p}(\tau) e^{-c^- R^{(t+1-\tau)}} \left[1 - e^{-c^+ R^{(t+1-\tau)}}\right] \tag{3.39}$$

Both methods reduce to the triadic percolation shown in Eq. 3.9 without delays when $\tilde{p}(\tau) = \delta_{\tau,1}$ where δ is the Kronecker delta.

Interestingly, both methods lead to a route to chaos in the presence of a non-trivial

time delay distribution. This observation demonstrates that the route to chaos is a robust feature of the triadic percolation model.

3.8 Conclusion

In this chapter, we provide a general framework to study the macroscopic properties of networks in the presence of triadic regulatory interactions. By introducing signed triadic interactions on top of the structural network, and assuming that the triadic interactions regulate the links in the structural network, we define triadic percolation. We find that the triadic interactions turn percolation to a fully-fledged dynamical process where the order parameter undergoes period-doubling and a route to chaos when both positive and negative regulations are present.

The signed interactions are known to affect statistical mechanics problems in non-trivial ways. For instance, introducing signed interactions in the Ising model changes the critical properties and the phase diagram of the model dramatically. It gives rise to spin glasses with a complex free-energy landscape which displays a very different structure of equilibrium configurations with respect to the Ising model [132]. Moreover, signed antagonistic interactions induce bistability [156]. In the triadic percolation model, the period-doubling and the route to chaos of the order parameter imply that triadic percolation is drastically different from ordinary percolation. This significant effect of triadic interaction on percolation is captured by the difference between the phase diagram of ordinary percolation and the phase diagram of triadic percolation. While the phase diagram of ordinary percolation displays a second-order phase transition, the phase diagram of triadic percolation is an orbit diagram in the presence of both positive and negative triadic interactions. Furthermore, the order parameter of triadic percolation always converges to a steady state in the absence of negative regulations and the phase diagram displays a discontinuous hybrid phase transition. Our triadic percolation theory gives accurate predictions of the dynamic by comparing with extensive Monte Carlo simulation despite the mean-field nature of the model, while numerical simulations on

real networks indicate that the dynamic nature of the triadic percolation is general and robust.

Periodic and chaotic oscillations, as well as the route to chaos have been observed in different dynamical models including deterministic cellular automata under certain regulatory rules [157] and simple boolean networks [158, 159]. However, triadic percolation is distinct from these models. In triadic percolation, it is the topology of the higher-order network itself that fluctuates in time. In order words, triadic percolation is not just a dynamical model that displays chaos, rather it combines tools coming from dynamical systems with the theory of critical phenomena in order to formulate a novel percolation process in which the giant component becomes a time-varying variable displaying periodic as well as chaotic dynamics.

These results radically change our understanding of percolation on networks. The insights from the theory can shed light on the study of real systems in which the functional connectivity of the network is changing over time, for instance in brain networks and climate networks. There are some promising future directions for the application of this triadic percolation model. Taking into account the spatial features of the structural networks and regulatory networks, the model might be used to understand patterns of activation in brain networks. Moreover, applying this framework to modeling extreme rainfall events could also lead to substantial improvement in their forecasting.

Chapter 4

Higher-order percolation processes on multiplex hypergraphs

In this chapter, we propose a general framework for percolation processes on hypergraphs. In particular, we consider random multiplex hypergraphs, in which each layer is associated with hyperedges of a certain cardinality. We reveal the connections among higher-order percolation processes on multiplex hypergraphs, interdependent percolation on multiplex networks, and K-core percolation processes. Thanks to the multiplex structure of the proposed hypergraph model, we highlight the strong effect of degree correlations on the critical properties of the percolation process. The wide range of critical behaviors observed in higher-order percolation processes on multiplex hypergraphs elucidates the mechanisms responsible for the emergence of discontinuous transitions and uncovers interesting critical properties which can be applied to the study of epidemic spreading and contagion processes on higher-order networks. The results presented in this chapter are published in [76].

4.1 Introduction

Both higher-order networks and multilayer networks are generalized network structures that take into account the topology beyond the single pairwise network framework of complex systems. Higher-order networks include both hypergraphs and simplicial complexes. They encode higher-order interactions present in different systems such as social networks [160], ecological networks [33], and brain networks [42]. While multilayer networks represent complex systems in which interactions of different natures and connotations can exist simultaneously, forming networks of networks. As such multilayer networks and in particular, multiplex networks are becoming a new paradigm to describe social, financial, and biological networks [49, 161].

Meanwhile, both higher-order networks and multilayer networks display a rich interplay between their topological structures and the dynamic processes defined on these structures. Notably, on multilayer networks, correlations display significant effects on the critical properties of the dynamic processes, while on higher-order networks, it is known that the dynamical processes reveal unexpected phenomena in the context of synchronization transitions, diffusion processes, and spreading processes [2, 3, 162, 163].

In this chapter, we investigate the interplay between structure and dynamics of higher-order networks and we provide a comprehensive multilayer framework to study the effects of correlation and higher-order percolation processes on hypergraphs.

Percolation is a fundamental dynamical process defined on networks that predicts the fraction of nodes in the giant component of the network. It is widely accepted that having a non-zero fraction of nodes in the giant component is the minimum requisite for observing collective phenomena emerging from epidemic spreading, diffusion, and opinion dynamics. Therefore, the study of percolation models plays a significant role in investigating the properties of dynamical processes defined on networks.

In the early era of Network Science, node percolation and link percolation have been extensively studied on simple networks [88, 89]. On a given random network with arbi-

trary degree distribution, nodes (or links) are randomly damaged with probability $1-p$. We study the fraction of nodes in the giant component R as a function of the probability of retaining a node (link) p, to show the robustness of the network with a given entity of the random damage on nodes (or links). It is well-known [10] that the network topology can significantly affect the critical properties of the percolation transition. For degree distributions with finite second moments, the critical threshold p_c is finite, while for degree distributions with diverging second moments (for instance scale-free networks), the critical threshold vanishes. Moreover, while both node and link percolation transition are continuous second-order phase transitions on simple graphs, K-core percolation which study the emergence of K-core [112, 113] in the giant component (with $K \geq 2$) displays a discontinuous and hybrid phase transition at the critical threshold.

Recently, there is a surging interest in percolation defined on generalized network structures as simple pairwise networks are insufficient to capture many real-world phenomena. The classical percolation theory has been generalized thanks to the formulation of the interdependent percolation defined on multilayer networks [11, 108]. The interdependent percolation can display a discontinuous hybrid transition reflecting large avalanches and failure on multiplex networks. Moreover, it is known that the critical properties of interdependent percolation on multiplex networks are highly affected by the correlation of the generalized degree [49].

However, the critical properties of percolation transition on another type of generalized network structure, hypergraphs, have not yet been extensively explored. Recently, there are a few interesting results of core percolation on hypergraphs [23], yet the exploration of percolation on hypergraphs is still limited to simple hypergraphs in which all the hyperedges have the same cardinality [24].

In this chapter, we propose a multiplex hypergraph framework and in analogy to the generalized percolation processes defined on multiplex networks, we define higher-order percolation processes on the multiplex hypergraphs. Within the multiplex hypergraph framework, each layer captures the hyperedges with a given cardinality. By assigning

each node a generalized hyperdegree $\{k_i^{[m]}\}$ denoting the number of hyperedges with cardinality m that are associated with node i in layer m, we study the effect of correlation among generalized hyperdegrees. We reveal that the degree correlation can increase or decrease the critical threshold and we elucidate the mechanisms behind the effects. More importantly, we reveal how the multiplex nature of the multiplex hypergraph ensembles can be exploited to propose higher-order percolation problems which display rich interplays between higher-order topology and dynamics and a rich set of phenomena, including discontinuous hybrid transitions and multiple percolation transitions.

4.2 Models

4.2.1 Random hypergraph model

The random hypergraph is widely used in the literature. A random hypergraph $\mathcal{H} = (V, H)$ is formed by a set of nodes V with $N = |V|$ elements and a set of hyperedges of different cardinality $m \leq M$. The number of hyperedges incident to a node is called the hyperdegree of the node. Thus, if all the hyperedges have the cardinality $m = 2$, namely all edges describe pairwise interactions, the hypergraph will reduce to an ordinary network, and the hyperdegree will reduce to the degree. In a general random hypergraph composed of nodes and hyperedges with different cardinalities, the hyperdegree is obtained by counting the number of hyperedges incident to a node, despite their cardinalities.

The simplest model of hypergraph called here the *random hypergraph model* is a maximum entropy model with given hyperdegree distribution $P(k)$ and the cardinality distribution of hyperedges $\hat{P}(m)$. This maximum entropy ensemble of hypergraphs can be expressed as an ensemble of factor graphs. The factor graph is a bipartite network $G_B(\tilde{V}, \tilde{U}, \tilde{E})$ formed by a set of nodes $\tilde{V}$, a set of factor nodes $\tilde{U}$ and a set of pairwise links $\tilde{E}$ between nodes and factor nodes. Here we show how to map a hypergraph to a factor graph whose factor nodes connect to distinct sets of nodes. The set of nodes of a hypergraph V can be directly mapped to the set of nodes of the corresponding factor

graph; the hyperedges from H can be mapped to the factor nodes from $\tilde{U}$ and the interaction between a node and the hyperedges that it belongs to is expressed by the pairwise links between nodes and factor nodes. Note that though a hypergraph can always be mapped to a factor graph, the opposite is not always true, since it does not exclude a *priori* that two factor nodes connect the same set of nodes. Nevertheless, in the sparse network regime where structural cutoffs are present, the number of factor nodes that connect to the same set of nodes is negligible. Within this sparse limit, the hyperdegree distribution $P(k)$ and the cardinality distribution of hyperedges $\hat{P}(m)$ correspond to the degree distribution of nodes and factor nodes in the factor graph expression, respectively. In the uncorrelated hypergraph ensemble where the hyperdegree distribution $P(k)$ and cardinality distribution $\hat{P}(m)$ have structural cutoffs, the probability that a node i belongs to a hyperedge α (or equivalently, in the factor graph representation, a node i connects to a factor node α) is given by

$$\tilde{p}_{i\alpha} = \frac{k_i m_\alpha}{\langle k \rangle N} \tag{4.1}$$

where k_i and m_α indicate the hyperdegree of the node i and the cardinality of the hyperedge (or equivalently, the factor node) α respectively.

4.2.2 Random multiplex hypergraph model

The random hypergraph model introduced in the previous section is a maximum entropy model determined with hyperdegree distribution $P(k)$ and the hyperedge cardinality distribution $\hat{P}(m)$. This model reduces to the Poisson random network when the hyperedge cardinality distribution admits only links as hyperedges, *i.e.*, $\hat{P}(m) = \delta_{m,2}$. Therefore, this model neglects any heterogeneity between the nodes. In order to account for the heterogeneity we propose a hypergraph model called *multiplex hypergraph model* that accounts for this cardinality information. Specifically, we consider a maximum entropy hypergraph model determined by a generalized hyperdegree distribution $P(\mathbf{k}) \equiv P(k^{[2]}, k^{[3]}, \cdots, k^{[M]})$ and the hyperedge cardinality distribution $\hat{P}(m)$. The gen-

eralized hyperdegree of a node i, $\mathbf{k_i} \equiv (k_i^{[2]}, k_i^{[3]}, \cdots, k_i^{[M]})$ includes the information that the node belongs to $k_i^{[m]}$ hyperedges with cardinality m. This setting allows to control the number of hyperedges of a given cardinality incident to each node and it provides a more refined hypergraph model than the random hypergraph. As we will see, the model can be mapped to a multiplex network model, as its name indicates.

The random multiplex hypergraph $\mathcal{H} = (V, H)$ is formed by a set V of $N = |V|$ nodes and a set of hyperedges H with different cardinality $2 \leq m \leq M$. The structure of the hypergraph is fully characterized by a set of generalized adjacency tensor $A^{[m]}$ where $2 \leq m \leq M$. The tensor $A^{[m]}$ determines the hyperedges with cardinality m. Specifically, $A^{[m]}$ has the element $A^{[m]}_{i_1,i_2,\cdots,i_m} = 1$ if an hyperedge $\alpha = [i_1, i_2, \cdots, i_m] \in H$. Otherwise, $A^{[m]}_{i_1,i_2,\cdots,i_m} = 0$. Thus, $\mathbf{k_i} = (k_i^{[2]}, k_i^{[3]}, \cdots, k_i^{[m]}, \cdots, k_i^{[M]})$, the generalized hyperdegree of a node i is given by

$$k_i^{[m]} = \sum_{j_1,j_2,\cdots,j_{m-1}} A_{i,j_1,j_2,\cdots,j_{m-1}} \tag{4.2}$$

Now let us show that a random multiplex hypergraph can be mapped to a multiplex network where each layer of the multiplex network encodes the interactions of a given cardinality. Specifically, the layer m of a random multiplex hypergraph can be constructed starting from the well-established configuration model of pure $(m-1)$-simplicial complexes [164]. The random multiplex hypergraph can be generated by the following algorithm (see Figure 4.1).

(1) Consider a multiplex network with $M-1$ layers and hyperedges with cardinality m which $2 \leq m \leq M$ and N nodes corresponding to the N nodes of the hypergraph.

(2) A set of generalized hyperdegree $\{\mathbf{k_i}\}_{i=1,\cdots,N}$ is drawn from the generalized hyperdegree distribution $P(\mathbf{k})$. For layer m, first, we use the configuration model of simplicial complexes [164] with the generalized hyperdegree sequence $\{k^{[m]}\}_{i=1,2,\cdots,N} \equiv \{k_1^{[m]}, k_2^{[m]}, \cdots, k_N^{[m]}\}$ to generate a pure $(m-1)$-dimensional simplicial complex.

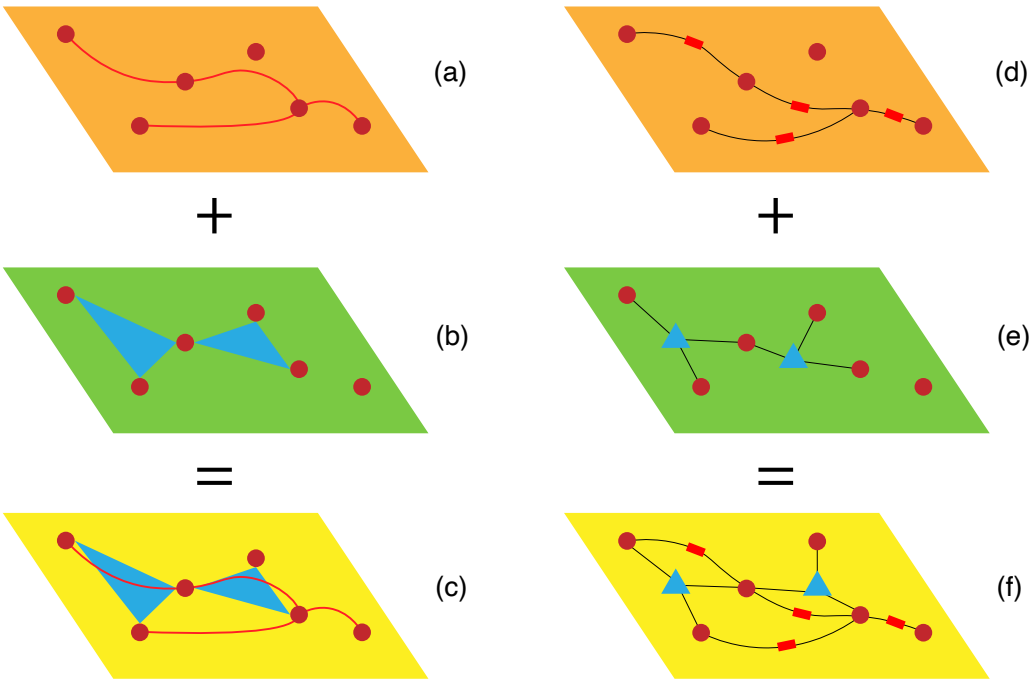

Figure 4.1: A schematic representation of the multiplex network construction of the hypergraph with given generalized hyperdegree sequences for hyperedges of cardinality $m_1 = 2$ (layer 1) and $m_2 = 3$ (layer 2). First, a configuration model is used to generate a simple network capturing the 2-body interactions of the hypergraph (panel a). Second, the configuration model of simplicial complexes [164] is used to generate a pure simplicial complex formed exclusively by triangles. Only the information about the 3-body interactions is retained (panel b). Finally, the information of the different layers is aggregated to generate the desired hypergraph including hyperedges of size $m = 2$ and $m = 3$ (panel c). This construction can be generalized to an arbitrary number of layers. The factor graph representation of the multiplex hypergraph is shown in panels (d), (e), and (f).

From this simplicial complex, we extract the hypergraph formed exclusively by the simplicial complex facets. This layer can be characterized by the aforementioned generalized adjacency tensor $A^{[m]}$ which encodes all the m-body interactions.

(3) The resulting multiplex hypergraph is obtained by aggregating all the layers, *i.e.*, including all the m-body interactions with $2 \leq m \leq M$. Note that this aggregated hypergraph, differently from the aggregated multiplex network with pairwise in-

teractions, retains its multilayer nature, as the hyperedges of different cardinality can be easily distinguished and the aggregated hypergraph can be precisely recovered to its multiplex representation, while this is not true for aggregated multiplex network with only pairwise interactions.

As we will show in the following sections, the random multiplex hypergraph provides a useful statistical mechanics tool to model unbiased random hypergraphs with hyperedge correlations. Moreover, the multiplex hypergraph model has a natural physical interpretation when hyperedges of different cardinality are associated with interactions of different natures and connotations. For instance, the multiplex hypergraph can be useful to model brain networks, to distinguish between brain regions connected by pairwise blood vessels [165] and higher-order functional interactions [42], or it can be useful to model real social networks where pairwise interactions (such as phone call interactions) and higher-order interactions (such as face-to-face interaction or online group interactions between more than two people) [160, 166] are present at the same time.

4.3 Percolation on random hypergraph model

Thanks to the mapping between a random hypergraph and the corresponding factor graph, the percolation theory on ordinary networks can be directly extended to factor graphs and subsequently to random hypergraphs. Since the factor graph considered here is in the sparse regime and hence locally tree-like, we can write self-consistent equations for $\hat{S}$ denoting the probability that starting from a node and following a link (in the factor graph representation) we reach a factor node (hyperedge) in the giant component, and S denoting the probability that starting from a factor node (hyperedge) and following a link we reach a node in the giant component. Assuming that nodes are initially retained with probability $p^{[N]}$ and hyperedges are retained with probability $p^{[H]}$ despite their

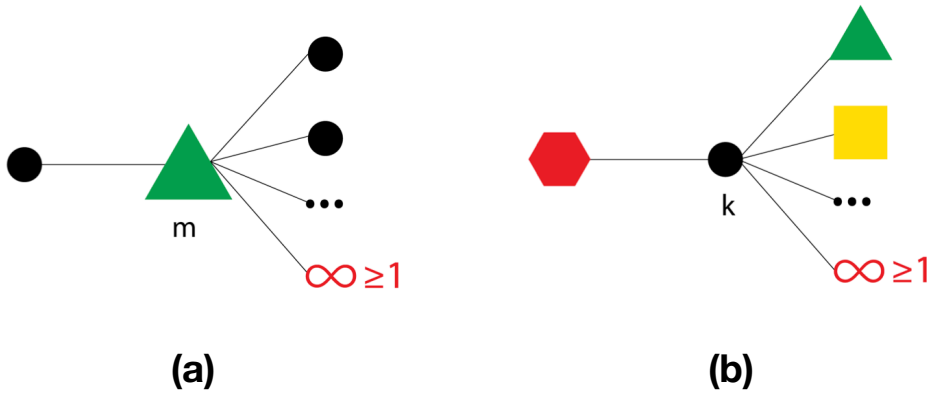

Figure 4.2: A schematic illustration of Eqs. 4.3 for $\hat{S}$ and S are shown in panels (a) and (b) respectively. Black circles represent nodes; triangles, squares, and hexagons represent factor nodes (hyperedges) with different cardinalities.

cardinality. The self-consistent equations of $\hat{S}$ and S read:

$$\begin{aligned} \hat{S} &= p^{[H]} \sum_m \frac{m}{\langle m \rangle} \hat{P}(m) \left[1 - (1-S)^{m-1} \right], \\ S &= p^{[N]} \sum_k \frac{k}{\langle k \rangle} P(k) \left[1 - \left(1 - \hat{S} \right)^{k-1} . \right] \end{aligned} \tag{4.3}$$

A diagrammatic representation of these two equations is shown in Figure 4.2. Following a link of a node in the factor graph representation, if we reach a factor node in the giant component (with probability $\hat{S}$), the factor node must connect to at least one node in the giant component and not initially be damaged. Similarly, following a link of a factor node, if we reach a node in the giant component, the node must connect to at least one hyperedge that is in the giant component. Note that in this model, when a node is damaged, the hyperedges that this node belongs to are not damaged. Instead, they act as active hyperedges with small cardinalities.

The percolation problem is fully characterized by the order parameters R and $\hat{R}$, indicating the probability of finding a node and a hyperedge in the giant component, respectively. In the case of the random hypergraph model, the order parameters R and

$\hat{R}$ can be expressed in terms of $\hat{S}$ and S:

$$\begin{aligned} R &= p^{[N]} \sum_k P(k) \left[1 - \left(1 - \hat{S} \right)^k \right], \\ \hat{R} &= p^{[H]} \sum_m \hat{P}(m) \left[1 - (1 - S)^m \right]. \end{aligned} \tag{4.4}$$

These self-consistent equations Eq. 4.4 and Eq. 4.3 are used in the percolation theory to investigate the critical properties, such as critical threshold p_c which reflects the robustness of a network. Particularly, by imposing $p^{[H]} = 1$ or $p^N = 1$, the percolation model above will reduce to node percolation or hyperedge percolation respectively. If the hypergraph exclusively contains hyperedges with cardinality $m = 2$, *i.e.*, $\hat{P}(m) = \delta_{m,2}$, the node (hyperedge) percolation on hypergraphs will reduce to node (link) percolation on networks.

The critical thresholds $p_c^{[H]}$ and $p_c^{[N]}$ that characterize the phase transition are obtained when the non-trivial solutions of Eq. 4.3 emerge. Since $S = \hat{S} = 0$ are always solutions of Eq. 4.3, the critical threshold is obtained when the trivial solutions lose stability. This happens when the largest eigenvalue Λ of the Jacobian matrix J of Eq. 4.3 is greater than 1. By imposing this condition at $S = \hat{S} = 0$, we find that $p_c^{[H]}$ and $p_c^{[N]}$ must satisfy

$$p_c^{[N]} p_c^{[H]} \frac{\langle k(k-1) \rangle}{\langle k \rangle} \frac{\langle m(m-1) \rangle}{\langle m \rangle} = 1. \tag{4.5}$$

Thus, the critical threshold p_c^H of hyperedge percolation (where $p^{[N]} = 1$) satisfies

$$p_c^{[H]} \frac{\langle k(k-1) \rangle}{\langle k \rangle} \frac{\langle m(m-1) \rangle}{\langle m \rangle} = 1. \tag{4.6}$$

and the critical threshold $p_c^{[N]}$ of node percolation where $p^{[H]}$ satisfies

$$p_c^{[N]} \frac{\langle k(k-1) \rangle}{\langle k \rangle} \frac{\langle m(m-1) \rangle}{\langle m \rangle} = 1. \tag{4.7}$$

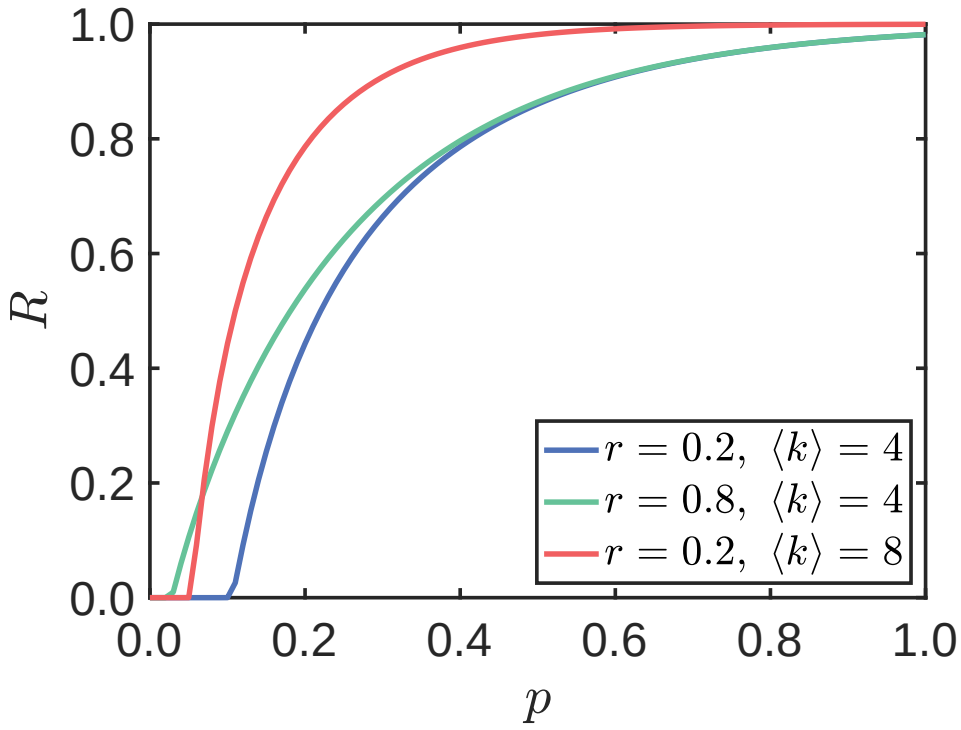

Figure 4.3: The fraction of nodes in the giant component R is shown versus $p^{[H]} = p$ for random hypergraphs. The hyperdegree distribution $P(k)$ is Poisson distribution and the distribution of cardinality of hyperedges $\hat{P}(m)$ is exponential distribution $\hat{P}(m) = r^{m-m_0}/(1-r)$ with minimum $m_0 = 3$.

In Figure 4.3 we show the result of hyperedge percolation ($p^{[N]} = 1$) on hypergraphs with Poisson hyperdegree distribution and exponential cardinality distribution. The order parameter R is displayed versus $p \equiv p^{[H]}$ with different average hyperdegree and cardinalities.

If the distribution $\hat{P}(m')$ reduces to $\delta_{m,m'}$, indicating that the hypergraph is formed exclusively by hyperedges with cardinality m, the critical thresholds $p_c^{[H]}$ and $p_c^{[N]}$ will satisfy

$$p_c^{[N]} p_c^{[H]} \frac{\langle k(k-1)\rangle}{\langle k\rangle}(m-1) = 1, \tag{4.8}$$

which has been reported in [24].

4.4 Percolation on multiplex hypergraph model

Similar to percolation defined on the random hypergraph model, here we study the percolation on the multiplex hypergraph model, *i.e.*, the nodes or hyperedges of a random multiplex hypergraph with generalized hyperdegree distribution $P(\mathbf{k})$ is initially retained with probability $p^{[N]}$ and $p^{[H]}$, respectively. The self-consistent equations that characterize the percolation process can be written in a similar fashion. Using the factor graph representation, we indicate with $\hat{S}_m$ the probability that following a link of a node in layer m we reach a m-factor node (m-hyperedge) that belongs to the giant component and S_m the probability that following a link of a m-factor node (m-hyperedge) in layer m we reach a node in the giant component. On a locally tree-like multiplex factor graph, the probabilities $\hat{S}_m$ and S_m satisfy the following self-consistent equations

$$\begin{aligned}
\hat{S}_m &= p^{[H]}\left[1-(1-S_m)^{m-1}\right], \\
S_m &= p^{[N]}\sum_{\mathbf{k}}\frac{k_m}{\langle k_m\rangle}P(\mathbf{k})\left[1-\prod_{m'}\left(1-\hat{S}_{m'}\right)^{k_{m'}-\delta_{m,m'}}\right].
\end{aligned} \tag{4.9}$$

The self-consistent equations can be interpreted diagrammatically as in Figure 4.4. Following a link of a node in layer m, if we reach a m-factor node in the giant component (with probability $\hat{S}_m$), the factor node must connect to at least one node in the giant component and not initially damaged. Similarly, following a link of a m-factor node in layer m, if we reach a node in the giant component, the node must connect to at least one hyperedge (despite its cardinality) that is in the giant component.

The order parameters for percolation on a random multiplex hypergraph, *i.e.*, the expected fraction of nodes R and the expected fraction of hyperedges $\hat{R}$ in the giant component, are given by:

$$\begin{aligned}
\hat{R} &= p^{[N]}\sum_{\mathbf{k}}P(\mathbf{k})\left[1-\prod_{m}\left(1-\hat{S}_{m}\right)^{k_m}\right], \\
R &= p^{[H]}\sum_{m}\hat{P}(m)\left[1-(1-S_m)^{m}\right].
\end{aligned} \tag{4.10}$$

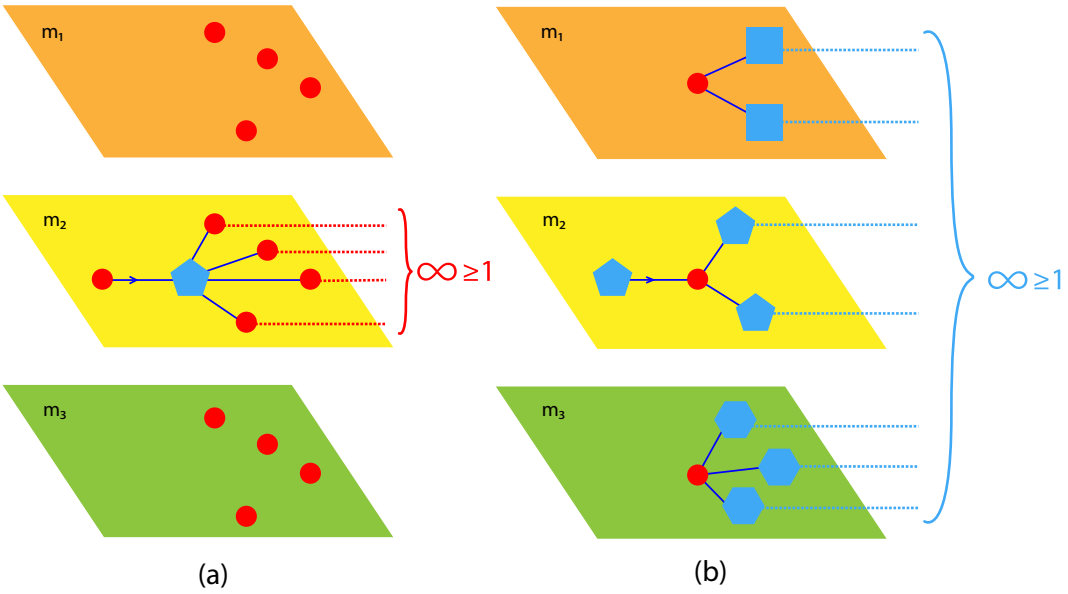

Figure 4.4: A schematic illustration of Eqs. 4.9 for $\hat{S}_m$ and S_m are shown in panels (a) and (b) respectively. Red circles represent nodes; squares, pentagons, and hexagons represent factor nodes (hyperedges) with different cardinalities.

Eq. 4.9 and Eq. 4.10 fully characterize the critical properties of the percolation process defined on the random multiplex hypergraph model. In particular, they can be used to investigate the effect of correlation between hyperedges in different layers on the robustness of the random multiplex hypergraph against random damage of nodes and hyperedges.

Using a similar approach to the random hypergraph model, we can write the Jobobian matrix of Eq. 4.9. Note that Eq. 4.9 is consisted of $2(M-1)$ equations (the equations of $\hat{S}_m$ and S_m with $2 \leq m \leq M$). We can merge the $2(M-1)$ equations to $(M-1)$ equations, by inserting the equation of S_m to the equation of $\hat{S}_m$. The Jacobian $\mathbf{G}$ of the modified equations with size $(M-1) \times (M-1)$ has entries:

$$G_{mn} = \begin{cases} p^{[H]}p^{[N]}(n-1)\langle k_n k_m \rangle / \langle k_m \rangle & \text{for} \quad m \neq n, \\ p^{[H]}p^{[N]}(m-1)\langle k_m(k_m-1) \rangle / \langle k_m \rangle & \text{for} \quad m = n. \end{cases} \tag{4.11}$$

Therefore, the critical threshold of node and hyperedge percolation $p_c^{[N]}$ and $p_c^{[H]}$ are obtained by imposing the largest eigenvalue Λ of $\mathbf{G}$ equals to 1.

In the following sections, we will study the percolation threshold in some important examples of random multiplex hypergraphs and we will characterize the role that correlations among hyperdegree of different layers plays on the robustness properties of random multiplex hypergraphs.

4.4.1 Case 1: Hypergraph with fixed cardinality of hyperedges

If the multiplex hypergraph is formed by one single layer that only includes hyperedges of cardinality m, we have

$$\hat{P}(m') = \delta_{m,m'}, \tag{4.12}$$

the Jacobian $\mathbf{G}$ reduces to a scalar given by

$$G \equiv G_{mm} = p^{[N]}p^{[H]}(m-1)\frac{\langle k_m(k_m-1\rangle}{\langle k_m\rangle}. \tag{4.13}$$

Thus by imposing $G = 1$, we recover the expression obtained in Eq. 4.8.

4.4.2 Case 2: Independent layers with Poisson generalized hyperdegree distribution

A more interesting case where we can appreciate the multiplex structure of the model is the one in which the hyperedge distribution of each layer of the random multiplex hypergraph is an independent Poisson distribution with layer-dependent average hyperdegree z_m. This case greatly simplifies the expression of the critical thresholds.

The generalized hyperdegree distribution with independent Poissonian layers is characterized by factorized form

$$P(\mathbf{k}) = \prod_m P_m(k_m) \tag{4.14}$$

where

$$P_m(k_m) = \frac{z_m^{k_m} \exp(-z_m)}{k_m!} \tag{4.15}$$

Using the well-known expressions of the moments of Poisson distribution and the independent condition, we have

$$\frac{\langle k_n k_m \rangle}{\langle k_n \rangle} = \frac{\langle k_m \rangle \langle k_n \rangle}{\langle k_n \rangle} = \langle k_m \rangle = z_m, \quad \frac{\langle k_m (k_m - 1) \rangle}{\langle k_m \rangle} = z_m. \tag{4.16}$$

Thus the Jacobian matrix $\mathbf{G}$ is simplified and has entries

$$G_{mn} = p_c^{[H]} p_c^{[N]} (m-1) z_m. \tag{4.17}$$

This expression indicates that the matrix $\mathbf{G}$ only depends on one index m, *i.e.*, $rank(G) = 1$. Thus, the only non-zero eigenvalue Λ equals the trace of the matrix:

$$\Lambda = Tr(G) = p_c^{[N]} p_c^{[H]} \sum_m (m-1) z_m. \tag{4.18}$$

By imposing $\Lambda = 1$, we find the critical threshold $p_c^{[N]}$ and $p_c^{[H]}$ satisfying

$$\frac{1}{p_c^{[N]} p_c^{[H]}} = \sum_m (m-1) z_m. \tag{4.19}$$

Notice that in Case 1 if we only consider a single layer of the multiplex hypergraph and the hyperdegree distribution $P_m(k_m)$ is a Poisson distribution with average hyperdegree z_m, Eq. 4.8 will further reduce to

$$p_c^{[H,m]} p_c^{[N,m]} = \frac{1}{z_m (m-1)} \tag{4.20}$$

Here we use $p_c^{[N,m]}$ and $p_c^{[H,m]}$ to denote the critical threshold of the node and hyperedge percolation that are defined on single-layer hypergraphs formed exclusively by m-hyperedges. Thus, comparing Eq. 4.20 and Eq. 4.19, we observe the relationship between

the critical threshold of the aggregated multiplex hypergraph and its component layers:

$$\frac{1}{p_c^{[N]}p_c^{[H]}} = \sum_m \frac{1}{p_c^{[H,m]}p_c^{[N,m]}} \tag{4.21}$$

This relationship implies that the product of the percolation threshold $p_c^{[H]}p_c^{[N]}$ for the multiplex hypergraph model is smaller than the corresponding product of percolation threshold $p_c^{[H,m]}p_c^{[N,m]}$ for each layer of the multiplex hypergraph, hence the multiplex hypergraph is more robust than each of its layers taken in isolation.

4.4.3 Case 3: Independent layers with power-law generalized hyperdegree distribution

In the case of independent layers with power-law hyperdegree distribution, the generalized hyperdegree distribution is given by

$$P(\mathbf{k}) = \prod_m P_m(k_m) \tag{4.22}$$

where

$$P_m(k_m) = c_m k_m^{-\gamma_m}, \tag{4.23}$$

with $\gamma_m > 2$ and c_m indicating the normalization constant. Note that the Jacobian $\mathbf{G}$ of the modified equations has elements

$$G_{mn} = \begin{cases} p^{[H]}p^{[N]}(n-1)\langle k_n k_m\rangle/\langle k_m\rangle & \text{for} \quad m \neq n, \\ p^{[H]}p^{[N]}(m-1)\langle k_m(k_m-1)\rangle/\langle k_m\rangle & \text{for} \quad m = n. \end{cases} \tag{4.24}$$

Since $\gamma_m > 2$, $\langle k_n\rangle$ is finite at the infinite network limit when $N \to \infty$, *i.e.*, all the layers are sparse. If one layer m is scale-free, *i.e.*, $\gamma_m \in (2, 3]$, $\langle k_m(k_m-1)\rangle/\langle k_m\rangle$ diverges as the second moment diverges. This implies the divergence of the trace of $\mathbf{G}$, as a consequence, the maximum eigenvalue diverges as well. Thus, as long as at least one

layer has a scale-free hyperdegree distribution,

$$p_c^{[N]} p_c^{[H]} \to 0 \tag{4.25}$$

in the infinite network limit $N \to \infty$. This result implies that for standard percolation on multiplex hypergraphs, having one scale-free layer can already significantly increase the robustness of the multiplex hypergraph.

4.5 Effects of hyperdegree correlation

In general, random multiplex hypergraphs have non-trivial correlations between the hyperdegree of the same nodes, *i.e.*, the hyperdegree distribution $P(\mathbf{k})$ does not always take the factorized form. Thus, in the general correlated cases

$$\langle k_n k_m \rangle \neq \langle k_n \rangle \langle k_m \rangle. \tag{4.26}$$

Let us define the correlation between the hyperdegrees of the same node connected to hyperedges of cardinality n and m respectively, *i.e.*,

$$C_{mn} = \langle k_n k_m \rangle - \langle k_n \rangle \langle k_m \rangle. \tag{4.27}$$

Here we consider a simple and exactly solvable 2-layer multiplex hypergraph, formed by hyperedges of cardinality m_1 and m_2. Without changing the structure of each layer, we are able to construct multiplex hypergraphs with different correlations by permuting the labels of nodes in one layer. In particular, we can permute the labels of replica nodes in such a way that the correlation between the generalized hyperdegree is maximized (either positively or negatively), namely the *Maximally Positive Correlated Multiplex Hypergraph (MPCMH)* and the *Maximally Negative Correlated Multiplex Hypergraph (MNCMH)*. This can be constructed via a similar way that constructs the maximally positive/negative correlated multiplex networks proposed in Ref. [14]. Therefore, in order to generate a *Maximally Positive Correlated Multiplex Hypergraph (MPCMH)*,

we can rank the hyperdegree of nodes in *both* layer in increasing order or decreasing order, then assign the same labels to nodes with the same rank in both layers. On the contrary, a *Maximally Negative Correlated Multiplex Hypergraph (MNCMH)* can be generated by first ranking hyperdegrees in one layer in increasing order and the other layer in decreasing order and assigning the same labels to nodes with the same rank in both layers. In order to compare the effects of hyperdegree correlation, we generate the *Uncorrelated Multiplex Hypergraph (UMH)* by randomly assigning labels to nodes in both layers as a null model. In order to assess the effects of correlation on critical thresholds, we investigate the dependency of the critical thresholds $p_c^{[H]}$ and $p_c^{[N]}$ on the correlation coefficient C_{mn} between two layers.

Consider a 2-layer multiplex hypergraph formed by hyperedges with cardinalities m_1 and m_2. The matrix $\mathbf{G}$ can be written explicitly as

$$G = p^{[H]}p^{[N]} \begin{pmatrix} \hat{m}_1\kappa_1 & \hat{m}_2\mathcal{K}_1 \\ \hat{m}_1\mathcal{K}_2 & \hat{m}_2\kappa_2 \end{pmatrix}, \tag{4.28}$$

where $\hat{m}_r \equiv m_r - 1$ for $r \in \{1, 2\}$ and we use κ_r and $\mathcal{K}_r$ to denote

$$\kappa_r \equiv \frac{\langle k_{m_r}(k_{m_r}-1)\rangle}{\langle k_{m_r}\rangle}, \quad \mathcal{K}_r \equiv \frac{\langle k_{m_1}k_{m_2}\rangle}{\langle k_{m_r}\rangle}, \quad r \in \{1, 2\}. \tag{4.29}$$

The critical thresholds are obtained by imposing the maximum eigenvalue of $\mathbf{G}$ equals to 1, which can be expressed explicitly in this duplex hypergraph as

$$p_c^{[N]}p_c^{[H]} = 2\left[\kappa_1\hat{m}_1 + \kappa_2\hat{m}_2 + \sqrt{\Delta}\right]^{-1} \tag{4.30}$$

where

$$\Delta = (\kappa_1\hat{m}_1 - \kappa_2\hat{m}_2)^2 + 4\mathcal{K}_1\mathcal{K}_2\hat{m}_1\hat{m}_2. \tag{4.31}$$

From Eq. 4.30 we observe that, for this specific percolation process, the hyperedge

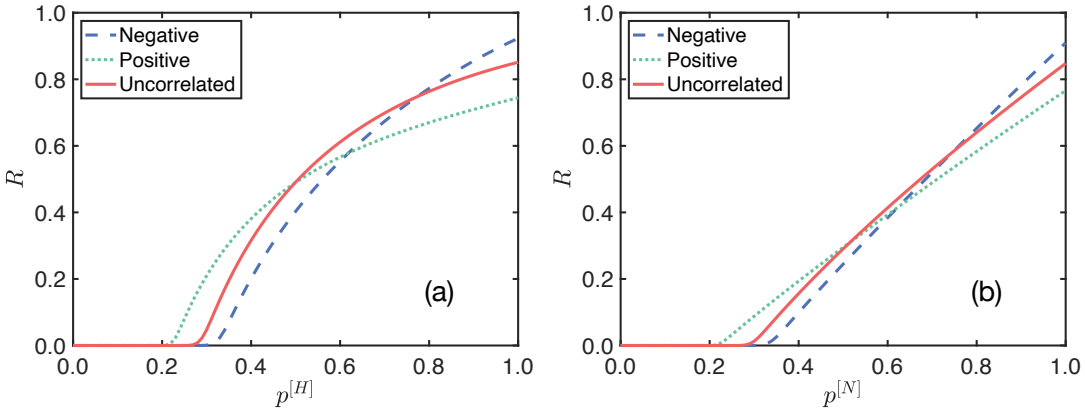

Figure 4.5: The fraction R of nodes in the giant component for *MPCMH* (Positive), for the *UMH* (Uncorrelated) and for *MNCMH* (Negative) is shown for hyperedge percolation (panel(a)) and for node percolation (panel (b)). The considered duplex hypergraph has $N = 10^4$ nodes and hyperedges of cardinality $m_1 = 2$ (layer 1) and $m_2 = 3$ (layer 2). The generalized hyperdegree distributions are Poisson distributions with $z_2 = 0.5$ (for layer 1), $z_3 = 1.5$ (for layer 2).

percolation (when $p^{[N]} = p_c^{[N]} = 1$) and node percolation (when $p^{[H]} = p_c^{[H]} = 1$) have the same critical threshold since $\mathcal{K}_1\mathcal{K}_2$ depends on the correlation coefficient in the following form:

$$\mathcal{K}_1\mathcal{K}_2 = \frac{(C_{m_1m_2} + \langle k_{m_1}\rangle\langle k_{m_2}\rangle)^2}{\langle k_{m_1}\rangle\langle k_{m_2}\rangle}. \tag{4.32}$$

Eq. 4.30 together with Eq. 4.31 and Eq. 4.32 indicates that positive correlations, which have a larger $\mathcal{K}_1\mathcal{K}_2$, increase the robustness of the multiplex hypergraph against random attack (a smaller critical threshold) and negative correlations decrease the robustness (a larger critical threshold). In Figure 4.5, we show the effects of degree correlation on both pure node percolation and hyperedge percolation. We observe that indeed *MPCMH* has a larger critical threshold compared with *MNCMH*, which agrees with the theoretical analysis above. Furthermore, we observe a worth-noting crossing of the curves of the fraction of nodes in the giant component R of *MPCMH* and *MNCMH*

versus the probability p of retaining a node ($p \equiv p^{[N]}$) or a hyperedge ($p \equiv p^{[H]}$). This indicates that different from the critical behavior, when the damage to the network is minor, *MNCMH* has greater stability compared with *MPCMH*.

This effect of degree correlation on the robustness of multiplex hypergraphs with the different entities of damage can be interpreted as follows. When the network is significantly damaged (p close to the critical threshold), the robustness of the multiplex hypergraph is determined by the high-degree nodes as they are less prone to be damaged in presence of positive correlations, leading to a smaller percolation threshold of *MPCMH*. On the contrary, when the damage to the network is minor, the robustness of the hypergraph is determined by the low-degree nodes. In particular, the role of low-degree nodes is more pronounced when in each layer there is a non-negligible number of isolated nodes. In presence of positive correlations, the number of nodes isolated in both layers or connected to a small number of hyperedges (regardless of their size) is larger. As a consequence, *MNCMH* have a larger fraction of nodes in the giant component than *MPCMH*. Indeed while in absence of isolated nodes, *i.e.*, there is only one connected component in the network, this effect remains but it is strongly suppressed.

4.6 Higher-order percolation on multiplex hypergraphs

The higher-order and multiplex nature of the random multiplex hypergraph allows for the investigation of various higher-order percolation problems. Higher-order percolation problems are characterized by collaborative phenomena, namely, the activation of one node (or hyperedge) requires the presence of multiple active neighbor hyperedges (or nodes). These higher-order percolation problems have highly non-trivial critical properties, as we will show in this section, including discontinuous hybrid phase transition, tricritical points, or even multiple phase transitions which have not been reported yet in this context.

In this section, we discuss four types of higher-order percolation, namely *Interdepen-*

dent Node percolation, *Interdependent Hyperedge percolation*, *Node K-core percolation*, *and Hyperedge K-core percolation*. Inspired by the parallelism between multiplex hypergraphs and multiplex networks, we can define the interlayer node dependency also on multiplex hypergraphs, *i.e.*, if a node is in the giant component (active), it must be in the giant component (active) in all layers. In particular, we will show that this higher-order percolation process displays a discontinuous hybrid phase transition at criticality. If partial dependence is considered, the transition will become continuous at the tricritical point.

Similarly, an interlayer dependency can be associated with hyperedges as well. Thus we can define *Interdependent Hyperedge percolation*, *i.e.*, a hyperedge is in the giant component (active), only when all the nodes that belong to this hyperedge are in the giant component (active). This highly non-trivial percolation problem displays a discontinuous hybrid transition at criticality if all the hyperedges are involving more than two nodes. In presence of hyperedges of cardinality two (links), the transition can become continuous at a tricritical point in some cases. More interestingly, with certain parameters, the percolation will display multiple transitions, characterized by more than one critical point, which has not been observed before in this context. Note that this interdependent hyperedge percolation is strongly related to the higher-order contagion model proposed and studied in Ref. [1, 3].

Another class of higher-order percolation problem we will discuss in this section is the higher-order K-core percolation inspired by K-core percolation on networks [112, 113]. In the case of *Node K-core percolation*, a node is in the giant component, if at least K hyperedges that include this node are in the giant component. Similarly, in the case of *Hyperedge K-core percolation*, a hyperedge is in the giant component if at least K nodes that belong to it are in the giant component. In either one of these last two models, the transition is discontinuous as long as $K > 2$ and the distributions $P(k)$ and $\hat{P}(m)$ have finite second moments. These different higher-order percolation processes are summarized in Figure 4.6.

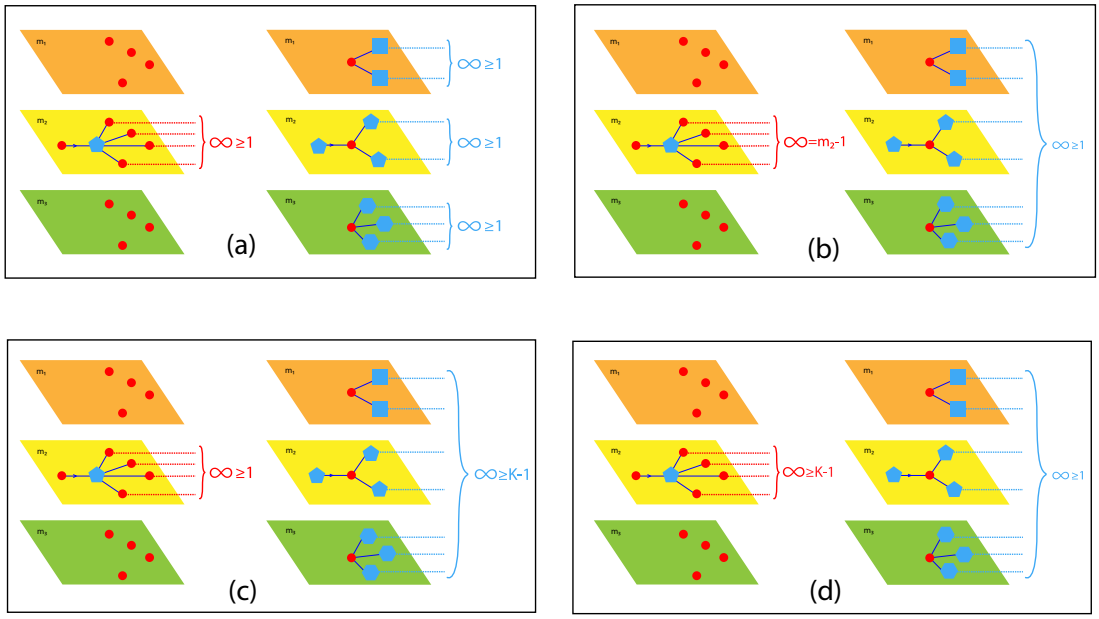

Figure 4.6: Schematic representation of the equations for $\hat{S}_m$ and for S_m determining higher-order percolation models defined on multiplex hypergraphs. Panel (a) represents node interdependent percolation. Panel (b) represents hyperedge interdependent percolation. Panel (c) represent Node K-core percolation. Panel (d) represent hyperedge K-core percolation.

4.6.1 Interdependent node percolation

4.6.1.1 General framework

The interdependent node percolation on multiplex hypergraphs formulated here is an analogy with interdependent node percolation on multiplex networks. In a multiplex hypergraph, a node is in the giant component if each of its replica nodes belongs to at least one hyperedge that is in the giant component. The rationale behind this definition is that in real networks, hyperedges with different cardinalities can encode interactions of different natures. For instance, in a duplex hypergraph that represents a brain network, the giant component of interdependent node percolation (active component) is formed by brain regions (nodes) connected by both blood vessels (pairwise interactions) and functional interactions (higher-order interactions). Similarly, in social networks, we can consider agents (nodes) connected in both mobile phone connection networks (pairwise

interactions) and face-to-face or online group networks (higher-order interactions). The order parameters of the interdependent node percolation on multiplex hypergraphs can be obtained in the following way. Let us define the probability $\hat{S}_m$ that starting from a node we reach a m-factor node (hyperedge with cardinality m) that is active and the probability S_m that starting from a m-factor node (hyperedge with cardinality m) we reach a node that is active. $\hat{S}_m$ and S_m follow the relationship

$$\hat{S}_m = p^{[H]}\left[1-(1-S_m)^{m-1}\right] \tag{4.33}$$

$$S_m = p^{[N]}\sum_{\mathbf{k}}\frac{k_m}{\langle k_m\rangle}P(\mathbf{k})\prod_{m'}\left[1-\left(1-\hat{S}_{m'}\right)^{k'_m-\delta_{m,m'}}\right]. \tag{4.34}$$

Subsequently, the order parameters R denoting the probability of a node belonging to the giant component and $\hat{R}$ denoting the probability of a hyperedge belonging to the giant component follow the relationship

$$R = p^{[N]}\sum_{\mathbf{k}}P(\mathbf{k})\prod_{m}\left[1-\left(1-\hat{S}_m\right)^{k_m}\right] \tag{4.35}$$

$$\hat{R} = p^{[H]}\left[1-\sum_{m}\hat{P}(m)(1-S_m)^m\right] \tag{4.36}$$

4.6.1.2 Independent layers

In order to reveal the mechanism behind the discontinuous phase transition, we consider a simpler model, in which the hyperdegrees of a node are independent. This indicates that the generalized hyperdegree distribution $P(\mathbf{k})$ factorizes according to $P(\mathbf{k})=\prod_m P_m(k_m)$, Eq. 4.34 and Eq. 4.35 reduce to

$$S_m = p^{[N]}\left(1-G_{1,m}(1-\hat{S}_m)\right)\prod_{m'\neq m}\left(1-G_{0,m'}(1-\hat{S}_{m'})\right) \tag{4.37}$$

$$R = p^{[N]}\prod_{m'}\left(1-G_{0,m'}(1-\hat{S}_{m'})\right) \tag{4.38}$$

where $G_{0,m}(x)$ and $G_{1,m}(x)$ denote the generating function

$$
\begin{aligned}
G_{0,m}(x) &= \sum_{k_m} P_m(k_m) x^{k_m} \\
G_{1,m}(x) &= \sum_{k_m} \frac{k_m}{\langle k_m \rangle} P_m(k_m) x^{k_m - 1}
\end{aligned}
\tag{4.39}
$$

By choosing then hyperdegree distribution $P_m(k_m)$ in each layer to be Poisson distribution with expectation z_m, the generating functions reduce to

$$
G_{0,m}(x) = G_{1,m}(x) = 1 - \exp\left(-z_m(1-x)\right) \tag{4.40}
$$

Thus, according to Eq. 4.37 and Eq. 4.38, $S_m \equiv S = R$ for all m. Inserting Eq. 4.33 into Eq. 4.38, we obtain that the order parameter $R = S$ obeys a single equation

$$
h(S) \equiv S - p^{[N]} \prod_m \left[1 - \exp\left(-p^{[H]} z_m S^{m-1}\right)\right] = 0. \tag{4.41}
$$

For multiplex hypergraphs with more than one layer, the node interdependent percolation displays a discontinuous hybrid phase transition it can be obtained by imposing (see Figure 4.7)

$$
h(S_c) = h'(S_c) = 0. \tag{4.42}
$$

4.6.1.3 Effects of the generalized hyperdegree correlation

The generalized hyperdegree correlation has a significant effect on the higher-order node interdependent percolation transition of multiplex hypergraphs as well. This phenomenon is the higher-order version of the corresponding phenomenon known to occur on pairwise multiplex networks [14, 49]. Here we again consider the duplex hypergraph with tunable correlations of the generalized hyperdegrees that we use in Sec. 4.5. We

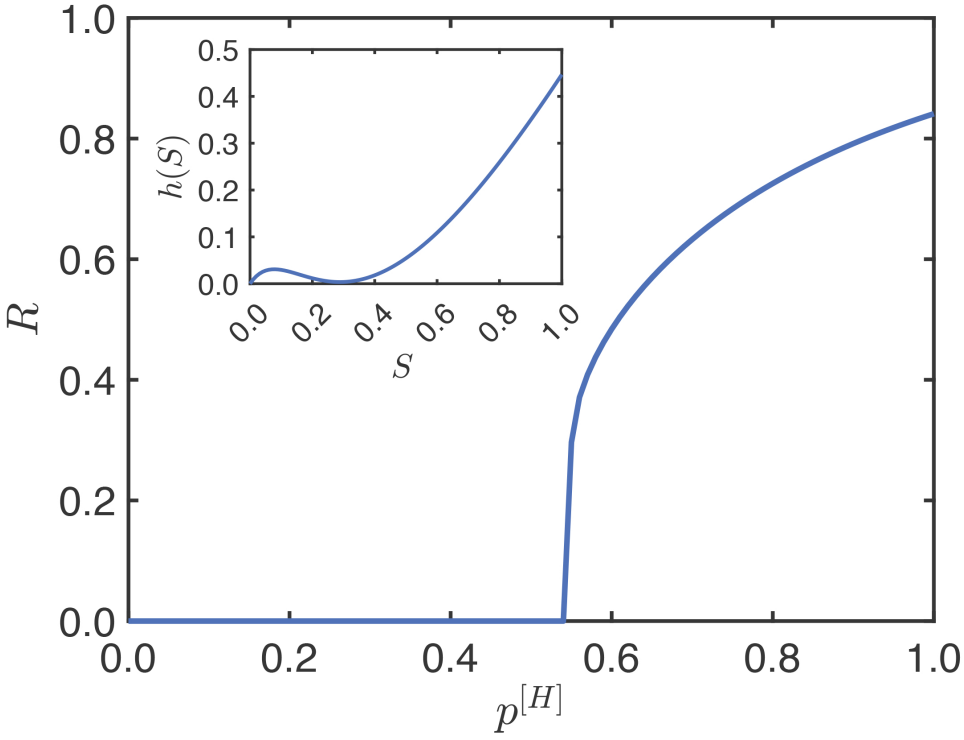

Figure 4.7: The fraction R of active nodes in interdependent node percolation is shown versus $p^{[H]}$ for a duplex multiplex hypergraph with $p^{[N]} = 1$. The layers of the duplex networks are formed by hyperedges of cardinality $m_1 = 3$ (layer 1), and $m_2 = 4$ (layer 2). Both layers have Poisson generalized degree distribution with $z_3 = z_4 = 2.5$. The inset displays the function $h(R)$ defined in Eq. 4.41 calculated at the critical point, *i.e.*, for $p^{[H]} = p_c^{[H]}$.

observe that *MPCMH* are always more robust than *MNCMH* for every entity of the damage, *i.e.*, positive correlations between generalized hyperdegrees of different layers always increase the robustness of the multiplex hypergraph (see Figure 4.8), which is different from our observations for standard percolation on multiplex hypergraphs discussed in Sec. 4.5. This difference has a simple interpretation. The maximum positive correlation will minimize the number of isolated nodes (thus inactive) in at least one layer while the maximum negative correlation will maximize this quantity. In the node-interdependent percolation problem, an isolated (inactive) node in one layer will deactivate its replica node in another layer, while this is not the case for standard percolation on multiplex hypergraphs. This explains the difference between Figure 4.8 and Figure 4.5: for node

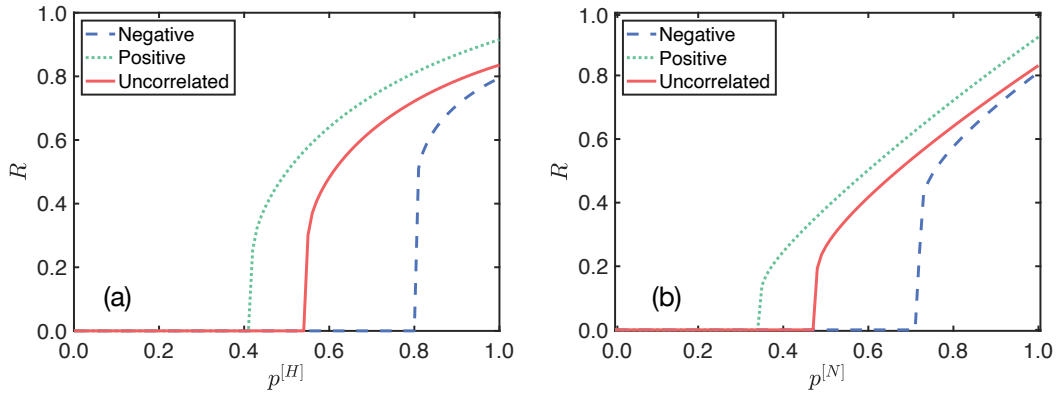

Figure 4.8: The fraction of active nodes R for interdependent node percolation is plotted versus $p^{[H]}$ when $p^{[N]} = 1$ (panel a) and versus $p^{[N]}$ when $p^{[H]} = 1$ (panel b) for a *MPCMH* (Positive) a *MNCMH* (Negative) and for a *UMH* (Uncorrelated). The layers of the duplex hypergraph are formed by hyperedges of cardinality $m_1 = 3$ (layer 1), $m_2 = 4$ (layer 2), with Poisson layers of average generalized degree $z_3 = 2.5$, $z_4 = 2.5$.

interdependent percolation, the order parameter R for percolation on *MPCMH* is always larger than percolation on *MNCMH*, while we observe a crossing of the two curves in standard percolation.

4.6.1.4 Partial interdependence

Partial interdependence has been introduced and investigated in detail for pairwise multiplex networks [11, 12, 49, 122]. On pairwise multiplex networks, when partial interdependence is considered, it is possible to observe a change of critical behavior at the so-called tricritical point. By decreasing the strength of partial interdependence, the discontinuous transition could shift to a continuous transition at the tricritical point. Here we extend this notion to multiplex hypergraphs to highlight the similarities and differences between the two models. To be more precise, by partial interdependence, we mean that the interdependence is not always present between replica nodes, but only with a probability r. Therefore, for $r = 1$ we recover node interdependent percolation discussed above, which displays a discontinuous hybrid transition, while for $r = 0$, the replica nodes in two layers are independent and we recover the standard percolation dis-

cussed in Sec. 4.4 which displays a continuous transition. Let us restrict our discussion to the simple case of independent generalized hyperdegrees where the joint hyperdegree distribution $P(\mathbf{k})$ takes the factorized form according to $P(\mathbf{k}) = \prod_m P_m(k_m)$. In this case, the equations for $\hat{S}_m$ and $\hat{R}$ remain unchanged (Eq. 4.33 and Eq. 4.36) while the equations for S_m and R (Eq. 4.34 and Eq. 4.35) become

$$S_m = p^{[N]} \left(1 - G_{1,m}(1 - \hat{S}_m)\right) \prod_{m' \neq m} \left(1 - rG_{0,m'}(1 - \hat{S}_{m'})\right) \tag{4.43}$$

$$R = p^{[N]} \left(1 - G_{0,m}(1 - \hat{S}_m)\right) \prod_{m' \neq m} \left(1 - rG_{0,m'}(1 - \hat{S}_{m'})\right) \tag{4.44}$$

Interestingly, due to the higher-order nature of the multiplex hypergraph model, these equations cannot be reduced to a single equation even in the simple case of layers with Poissonian generalized hyperdegree distribution. Nevertheless, the phase diagram of the model can be investigated numerically. The phase diagram is characterized by a tricritical point separating a regime of continuous transition ($r < r_T$) and a regime of discontinuous hybrid transition ($r > r_T$). If we consider either node percolation ($p^{[H]=1}$, $p^{[N]} \equiv p$) or hyperedge percolation ($p^{[N]=1}$, $p^{[H]} \equiv p$), the tricritical point (r_T, p_T) can be found numerically by solving the self-consistent equations Eq. 4.33 and Eq. 4.43 together with $\Lambda = 1$, where Λ is the largest eigenvalue of the Jacobian matrix of the equations determining $\hat{S}_m$ and S_m (see Figure 4.9).

4.6.2 Interdependent hyperedge percolation

4.6.2.1 General framework

The higher-order interdependency can be defined not only on nodes but also on hyperedges. In the interdependent hyperedge percolation, a hyperedge is active only if all its nodes are active as well, and a node is active if at least one of the hyperedges it belongs to is active. The model considered here is complementary of the node interdependent percolation, as in node interdependent percolation, a node is active if all of its replica nodes are active, *i.e.*, all of its replica nodes belong to at least one active hyperedge. The

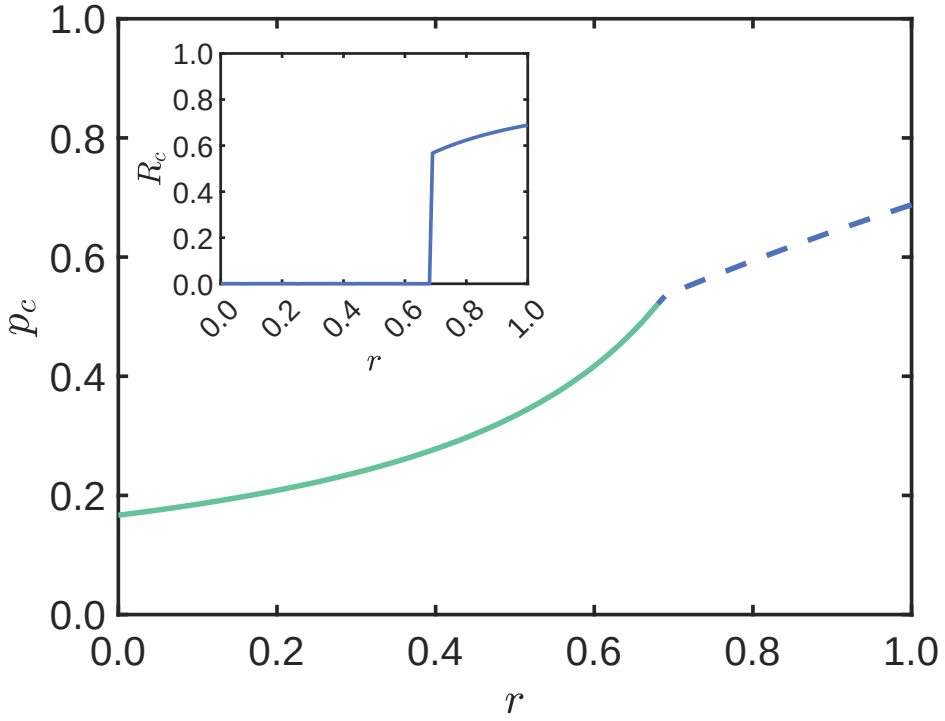

Figure 4.9: The percolation threshold $p_c = p_c^{[H]}$ of a duplex multiplex hypergraph is plotted versus r for the interdependent node percolation process with partial interdependence. The solid line corresponds to the line of the continuous critical point, the dashed line corresponds to the line of discontinuous, hybrid transitions. The tricritical point separating the two lines is obtained for $r = r_T = 0.68\ldots$. The inset displays the value $R = R_c$ of the fraction of active nodes at the critical point as a function of r showing that $R_c > 0$ for $r > r_T$ indicating that the transition is discontinuous. The layers of the duplex hypergraph are formed by hyperedges of cardinality $m_1 = 3$ (layer 1), $m_2 = 4$ (layer 2), with Poisson layers of average generalized degree $z_3 = 2$, $z_4 = 2$. Here $p^{[N]}$ is set equal to one.

interdependent hyperedge percolation model can be closely related to the higher-order social contagion model proposed in [3] and investigated on random hypergraph in [1], since in the higher-order contagion model, a node is infected if it belongs to at least one $m-$hyperedge which contains $m-1$ infected nodes. Nevertheless, there are two major differences between the higher-order contagion model and interdependent hyperedge percolation: The first difference is that higher-order contagion models are usually studied under the Susceptible-Infected-Susceptible (SIS) setting while the percolation model is

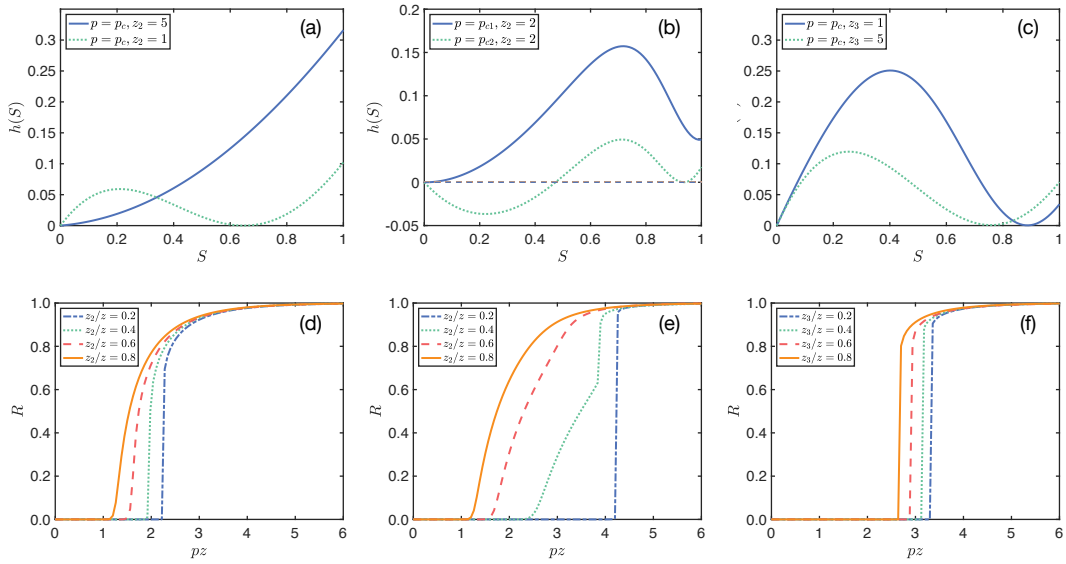

Figure 4.10: The critical behavior of the interdependent hyperedge percolation process on a duplex hypergraph is investigated by plotting the function $h(S)$ defined in Eq. 4.41 versus S (panels (a) and (c)) and by displaying the fraction of active nodes R for different values of $p = p^{[H]}$ (panels (d) and (f)). The duplex hypergraphs have layers with hyperedge cardinalities $m_1 = 2$, $m_2 = 3$ (panel (a) and (d)), $m_1 = 2$, $m_2 = 10$ (panel (b) and (e)), and $m_1 = 3$, $m_2 = 5$ (panel (c) and (f)). Each layer is characterized by Poisson hyperdegree distributions with average degree z_{m_1} (layer 1) and z_{m_2} (layer 2) with $z_{m_1} + z_{m_2} = z = 6$. In panel (d) we observe continuous transitions and discontinuous transitions occurring for different values of z_2. In panel (e) we observe that the model can display, for the same value of z_3, two critical points p_{c1} and p_{c2} corresponding to a continuous and discontinuous transition occurring at a non-zero value of the order parameter. In panel (f) we show that all the transitions are discontinuous.

known to map to the SIR model. This difference impedes a precise mapping between the percolation model and SIS-type dynamic, however, it will not be critical here since we are mainly concerned about the nature of the phase transition rather than the actual dynamic processes, and the SIR model and SIS model display very similar critical behaviors. More importantly, the second difference is that in the higher-order contagion model, bistable regimes can be observed, *i.e.*, the contagion spreads either until it becomes pandemic, or the epidemic dies out, depending on the initial conditions. While in

interdependent hyperedge percolation, such bistability does not exist, as in percolation problems, we always take the largest solutions of the order parameters R and $\hat{R}$ from the self-consistent equations, even if there are multiple non-trivial solutions.

In the interdependent hyperedge percolation model, the probability $\hat{S}_m$ that starting from a random structural node we reach an active m-factor node (in the factor graph representation), and the probability S_m that starting from a m-factor node, we reach an active structural node satisfy

$$\hat{S}_m = p^{[H]} S_m^{m-1} \tag{4.45}$$

$$S_m = p^{[N]} \sum_{\mathbf{k}} \frac{k_m}{\langle k_m \rangle} P(\mathbf{k}) \left[1 - \prod_{m'} (1 - \hat{S}_{m'})^{k_{m'} - \delta_{m,m'}} \right]. \tag{4.46}$$

The order parameter $\hat{R}$ and R indicating the fraction of nodes and hyperedges in the giant component respectively are given by

$$\hat{R} = p^{[H]} \sum_{m} \hat{P}(m) S_m^m \tag{4.47}$$

$$R = p^{[N]} \sum_{\mathbf{k}} \frac{k_m}{\langle k_m \rangle} P(\mathbf{k}) \left[1 - \prod_{m'} (1 - \hat{S}_{m'})^{k_{m'}} \right]. \tag{4.48}$$

Here we note that in the simplest case, the multiplex hypergraph is formed by a single layer containing hyperedges with cardinality $m = 2$, the equations will reduce to link percolation on simple networks. Nevertheless, as long as the hypergraph contains some hyperedges with cardinality $m > 2$, the equations of interdependent hyperedge percolation are different from the simple link percolation.

In the following sections, we will characterize the phase transition of interdependent hyperedge percolation and investigate the effect of the generalized hyperdegree correlation.

4.6.2.2 Interdependent layers

In order to study the critical properties of the interdependent hyperedge percolation transition, let us consider the simple case of interdependent layers. In this case, Eqs. 4.45, 4.46, 4.47, 4.48 will reduce to

$$\begin{aligned}
\hat{S}_m &= p^{[H]} S_m^{m-1}, \\
S_m &= P^{[N]} \left[1 - G_{1,m}\left(1 - \hat{S}_m\right) \prod_{m' \neq m} G_{0,m'}\left(1 - \hat{S}'_m\right) \right], \\
R &= p^{[N]} \left[1 - \prod_m G_{0,m}\left(1 - p^{[H]} S_m^{m-1}\right) \right], \\
\hat{R} &= p^{[H]} \sum_m \hat{P}(m) S_m^m.
\end{aligned} \tag{4.49}$$

The generating functions $G_{0,m}(x)$ and $G_{1,m}(x)$ are defined in Eq. 4.39. By choosing the generalized degree distributions as Poisson distribution defined in Eq.4.15, we observe that $S_m = R = S$ for any m with S satisfying

$$S = p^{[N]} \left[1 - \exp\left(-p^{[H]} \sum_m z_m S^{m-1} \right) \right]. \tag{4.50}$$

In the simplified case of 2-layer multiplex hypergraph with cardinality m_1, m_2 and corresponding average generalized degree z_{m_1} and z_{m_2}, S satisfies

$$S = p^{[N]} \left\{ 1 - \exp\left[-p^{[H]} \left(z_{m_1} S^{m_1 - 1} + z_{m_2} S^{m_2} \right) \right], \right\} \tag{4.51}$$

or equivalently we write the equation above as

$$h(S) = S - p^{[N]} \left\{ 1 - \exp\left[-p^{[H]} \left(z_{m_1} S^{m_1 - 1} + z_{m_2} S^{m_2} \right) \right] \right\} = 0. \tag{4.52}$$

Let us fix the expected number of hyperedges incident to a node despite their cardinality by imposing

$$z_{m_1} + z_{m_2} = z \tag{4.53}$$

and we will characterize the interdependent hyperedge percolation transition as a function of z_{m_1}. As a specific example, let us set $m_1 = 2$ and $m_2 = 3$. In one extreme case that $z_2 = z$ and $z_3 = 0$, the multiplex hypergraph reduces to a single network with only pairwise connections. Thus the transition will reduce to standard link percolation whose critical point is characterized by the following condition:

$$h(0) = h'(0) = 0. \tag{4.54}$$

In the other extreme case where $z_3 = z$ and $z_2 = 0$, the multiplex hypergraph reduces to a single hypergraph that includes only 3-hyperedges. In this case, the transition is discontinuous and is obtained at a non-zero value $S = S_c$ which is characterized by

$$h(S_c) = h'(S_c) = 0. \tag{4.55}$$

By increasing z_2 from 0 to z, the percolation transition shifts from the region of continuous phase transition to the region of discontinuous phase transition. These two regions are separated by a tricritical point observed at $z_2 = z_T$ that satisties

$$h(0) = h'(0) = h''(0) = 0. \tag{4.56}$$

For hyperedge interdependent percolation with $p^{[N]} = 1$, we obtain the tricritical point at

$$z_T = \frac{2}{3}z, \quad p_T^{[H]} = \frac{3}{2z}. \tag{4.57}$$

For hyperedge interdependent percolation with $p^{[H]} = 1$, on the other hand, the tricritical point is found at

$$z_T = \sqrt{1+2z} - 1, \quad p_T^{[N]} = \frac{\sqrt{1+2z}+1}{2z}. \tag{4.58}$$

Interestingly, if we still limit our discussion to 2-layer duplex hypergraphs and as we change the value of m_1 and m_2, different scenarios of phase transitions emerge. For $m_1 > 2$ and $m_2 > 2$, the transition is always discontinuous. However, as we show in Figure 4.10(b), when $m_1 = 2$ and $m_2 > 3$, the percolation transition can display not just one but also two percolation transitions. The first transition describes the emergence of the giant component which is continuous, while the second discontinuous transition indicates an abrupt jump of the order parameter R from a non-zero value to a higher non-zero value. To the best of our knowledge, this phenomenon has not been reported before, not even for the higher-order contagion model studied in Refs. [1, 3]. These multiple transitions can have an interesting interpretation as a sudden activation of hyperedges of larger cardinality.

4.6.2.3 Effect of the generalized hyperdegree correlation

The general equations characterizing the hyperedge interdependent percolation can be also used to study the effects of correlation between the generalized hyperdegrees of the replica nodes. In this case, we observe (see Figure 4.11) that *MPCMH* displays a critical threshold smaller than *MNCMH* which indicates that *MPCMH* is more robust. For small entities of the damage, on the other hand, *MPCMH* has a smaller giant component than *MNCMH*. This observation is expected as it has the same explanation of the corresponding phenomenon observed and discussed in Sec. 4.5 for the case of standard percolation on multiplex hypergraphs (see Figure 4.5).

4.6.3 Node K-core percolation

In this section, we discuss the node higher-order K-core percolation on multiplex hypergraphs, as a generalization of both K-core percolation [112, 113] on simple networks and aforementioned node interdependent percolation on multiplex hypergraphs. In standard K-core percolation on simple networks, a node is active if it has at least K active neighbors, while in node K-core percolation defined on multiplex hypergraphs, a node is active if it belongs to at least K hyperedges regardless of their cardinalities. In this

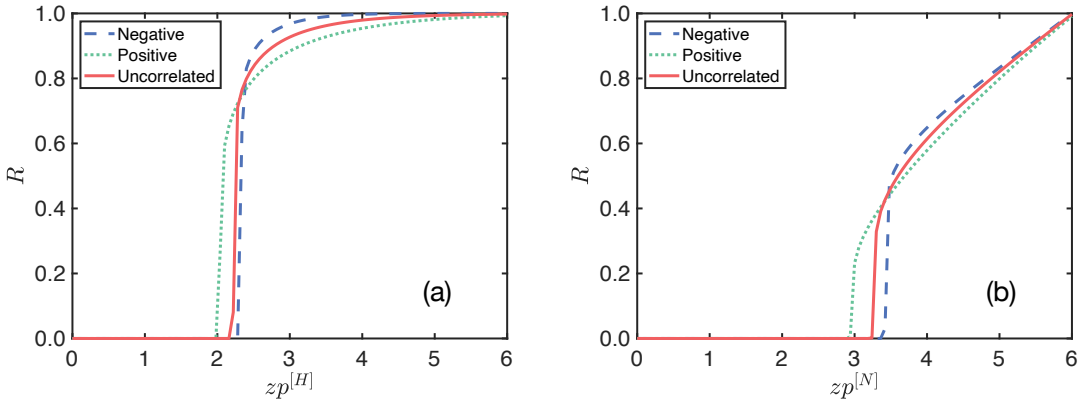

Figure 4.11: The fraction of active nodes R in the interdependent hyperedge percolation is plotted versus $p^{[H]}$ when $p^{[N]} = 1$ (panel a) and versus $p^{[N]}$ when $p^{[H]} = 1$(panel b) for a *MPCMH* (Positive) a *MNCMH* (Negative) and for a *UMH* (Uncorrelated). The layers of the duplex hypergraph are formed by hyperedges of cardinality $m_1 = 2$ (layer 1), $m_2 = 3$ (layer 2), with Poisson layers of average generalized degree $z_2 = 4.8$, $z_3 = 1.2$ and $z = z_2 + z_3 = 6$.

case, the percolation equations read:

$$\begin{aligned} \hat{S}_m &= p^{[H]} \left[1 - (1 - S_m)^{m-1}\right], \\ S_m &= p^{[N]} {\sum_{\mathbf{k}}}' \frac{k_m}{\langle k_m \rangle} P(\mathbf{k}) \left[1 - \sum_{q=0}^{K-2} B_q(\mathbf{k})\right] \end{aligned} \tag{4.59}$$

where ${\sum_{\mathbf{k}}}'$ indicates the sum over $\mathbf{k}$ such that

$$\sum_m k_m \geq K. \tag{4.60}$$

Here $B_q(\mathbf{k})$ is given by

$$B_q(\mathbf{k}) = {\sum_{\{q'_m\}}}'' \prod_{m'} \left[\binom{k'_m - \delta_{m,m'}}{q_{m'}} \hat{S}_{m'}^{q_{m'}} \left(1 - \hat{S}_{m'}\right)^{k'_m - \delta_{m,m'} - q_{m'}} \right], \tag{4.61}$$

where $\sum''_{\{q'_m\}}$ indicates the sum $\{q'_m\}$ such that

$$\sum_m^{'} q'_m = q. \tag{4.62}$$

The order parameters R and $\hat{R}$, denoting the fraction of nodes and hyperedges in the giant component respectively, are given by

$$\begin{aligned} \hat{R} &= p^{[H]} \left[1 - \sum_m \hat{P}(m) \left(1 - S_m\right)^m \right], \\ R &= p^{[N]} \left[1 - \sum_{\mathbf{k}}^{'} P(\mathbf{k}) \sum_{q=0}^{K-1} D_q \right] \end{aligned} \tag{4.63}$$

where D_q is given by

$$D_q = \sum_{\{q_{m'}\}}^{''} \prod_{m'} \left[\begin{pmatrix} k'_m \\ q_{m'} \end{pmatrix} \hat{S}_{m'}^{q_{m'}} \left(1 - \hat{S}_{m'}\right)^{k'_m - q_{m'}} \right]. \tag{4.64}$$

The node K-core percolation on multiplex hypergraphs will reduce to standard K-core percolation if the multiplex hypergraph is formed by a single-layer hypergraph containing exclusively hyperedges with cardinality m_2 (simple network). For K-core percolation on pairwise networks [112, 113], it is known that the phase transition becomes discontinuous and hybrid as long as $K > 2$. Here for node K-core percolation on multiplex hypergraphs, we observe similar phenomena provided that the hyperdegree distribution has a finite second moment (see Figure 4.12).

4.6.4 Hyperedge K-core percolation

Similar to the node K-core percolation, we can define the K-core percolation on hyperedges. In this case, a hyperedge is active only if at least K nodes belonging to it are also active. In other words, it describes the physical scenario in which a node is active only if a critical number of nodes belonging to the same hyperedge is active, thus it can describe

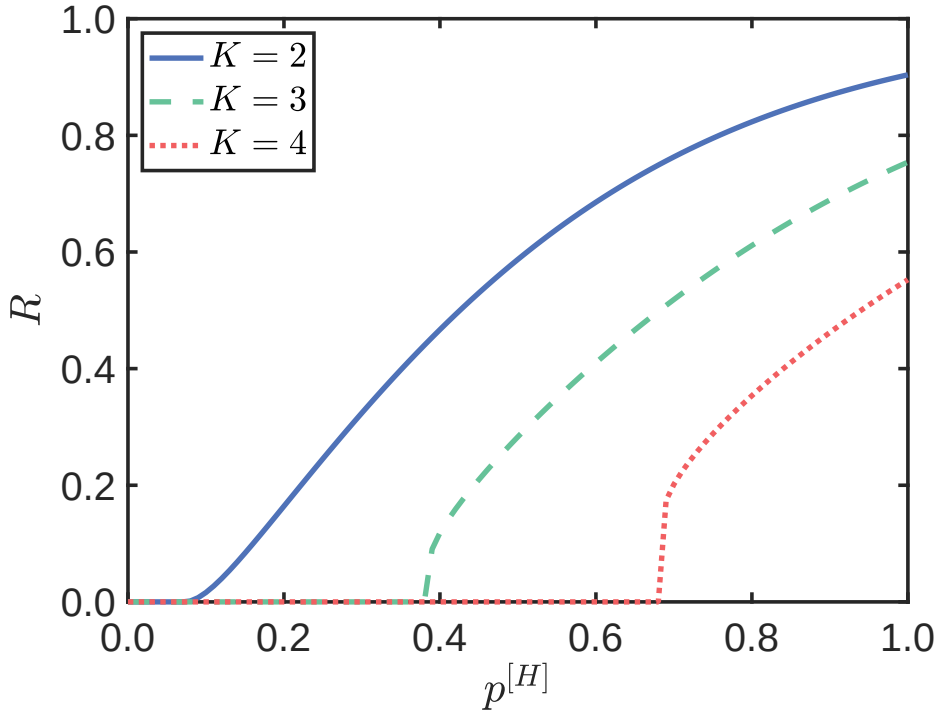

Figure 4.12: The fraction R of active nodes for the node K-core percolation on duplex hypergraphs with independent Poisson layers is shown versus the probability of retaining a hyperedge $p^{[H]} = p$. The duplex hypergraph includes $N = 10^4$ nodes and has layers formed by hyperedges of cardinality $m_1 = 4$ and $m_2 = 5$ with independent Poisson generalized hyperdegree distributions with average $z_4 = z_5 = 2$. Here $p^{[N]}$ is fixed to the constant value $p^{[N]} = 1$. The node K-core percolation is discontinuous for $K > 2$.

another variation of contagion models or threshold models [167, 168]. The probability $\hat{S}_m$ that starting from a node we reach a m-hyperedge that is active and the probability S_m that starting from a m-hyperedge we reach a node that is active are given by

$$\begin{aligned} \hat{S}_m &= \begin{cases} p^{[H]}\left[1 - \sum_{q=0}^{K-2} \hat{B}_q(m)\right] & \text{for} \quad m \geqslant K \\ 0 & \text{for} \quad m < K \end{cases}, \\ S_m &= p^{[N]}\left[1 - \sum_{\mathbf{k}} \frac{k_m}{\langle k_m \rangle} P(\mathbf{k}) \prod_{m'} \left(1 - \hat{S}_{m'}\right)^{k_{m'} - \delta_{m,m'}}\right], \end{aligned} \tag{4.65}$$

where $B_q(m)$ can be expressed as

$$\hat{B}_q(m) = \begin{pmatrix} m-1 \\ q \end{pmatrix} (S_m)^q \, (1 - S_m)^{m-1-q} \, . \tag{4.66}$$

Similarly, the order parameters R and $\hat{R}$ denoting the fraction of node and hyperedge that are in the giant component as

$$\begin{aligned} \hat{R} &= p^{[H]} \sum_{m \geqslant K} \hat{P}(m) \left[1 - \sum_{q=0}^{K-1} \begin{pmatrix} m-1 \\ q \end{pmatrix} S_m^q \, (1 - S_m)^{m-q} \right] \\ R &= p^{[N]} \left[1 - \sum_{\mathbf{k}} P(\mathbf{k}) \prod_{m'} \left(1 - \hat{S}_{m'} \right)^{k_{m'}} \right] . \end{aligned} \tag{4.67}$$

For hyperedge K-core percolation, we observe that the percolation transition is discontinuous and hybrid as long as $K > 2$ provided that the distribution of hyperedge cardinality $\hat{P}(m)$ has a finite second moment, which is consistent with the K-core percolation on pairwise networks [112, 113]. (see Figure 4.13)

4.7 Conclusion

In this chapter, we propose a random multiplex hypergraph model on which we investigate standard and higher-order percolation processes. Random multiplex networks are a natural generalization of random hypergraphs as the hyperedges of different cardinality are associated with different layers of the multiplex. This comprehensive framework allows for exploring the rich interplay between the topology of the hypergraphs and properties of standard and higher-order percolation defined on these topological structures. Moreover, thanks to the multilayer structure, we can explore the effects of interlayer correlation on the critical properties of standard and higher-order percolation. In particular, we show that for standard percolation processes, close to the percolation transition, positive correlations increase the robustness of the hypergraph while when the damage is minor, negative correlations can enhance the network robustness. On the other hand,

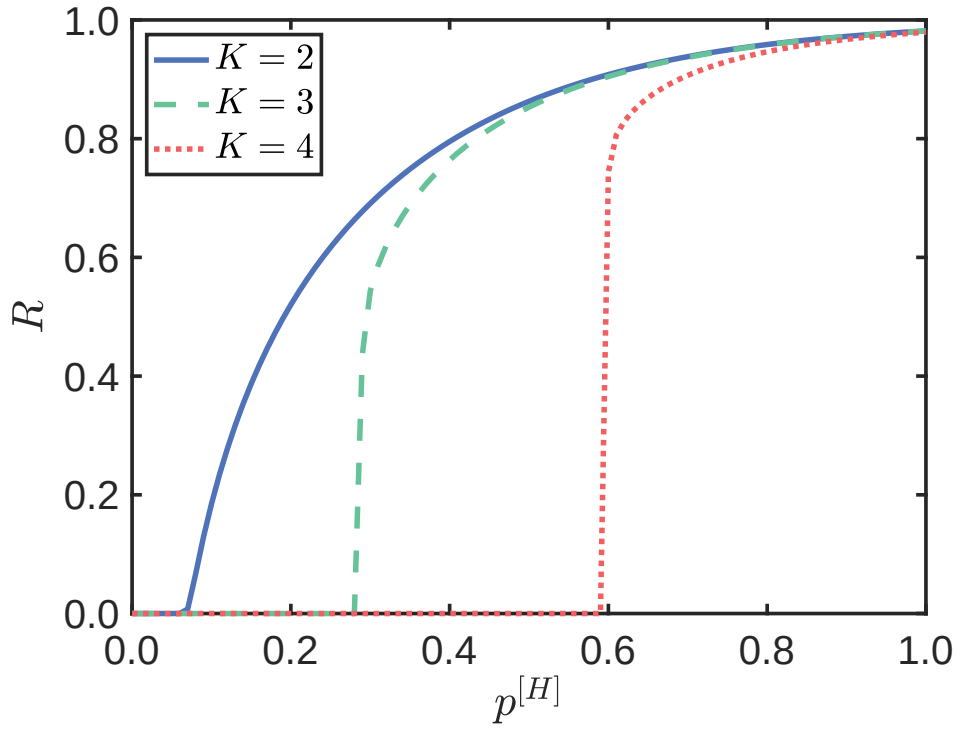

Figure 4.13: The fraction R of active nodes for the hyperedge K-core percolation on duplex hypergraphs with independent Poisson layers is shown versus the probability of retaining a hyperedge $p^{[H]} = p$. The duplex hypergraph includes $N = 10^4$ nodes and has layers formed by hyperedges of cardinality $m_1 = 4$ and $m_2 = 5$ with independent Poisson generalized hyperdegree distributions with average $z_4 = z_5 = 2$. Here $p^{[N]}$ is fixed to the constant value $p^{[N]} = 1$. The transition is discontinuous for $K > 2$.

for node interdependent percolation, positive correlations always increase the robustness of the hypergraph despite the level of damage to the hypergraph. Moreover, we have formulated two higher-order percolation models that generalize the contagion model on hypergraphs and interdependent percolation on multiplex networks (node interdependent percolation, hyperedge interdependent percolation) and two higher-order percolation models that generalize the K-core percolation on networks. These models display a rich phenomenology including discontinuous hybrid transition, tricritical points, and multiple phase transitions.

In this chapter, we have provided a comprehensive view of the possible higher-order

percolation processes on random multiplex hypergraphs, nevertheless, the processes investigated in this chapter do not exhaustively cover all relevant percolation processes that *can be* defined on these structures. We hope that this work can generate further interest in the interplay between the topological structure of higher-order networks and the dynamical processes defined on them. The critical properties of percolation processes defined on multiplex hypergraphs can provide new insights for the study of other dynamical processes such as epidemic spreading and social contagion.

Chapter 5

Higher-order network model of epidemic spreading

Mathematical models of epidemics have played a significant role in pandemic control and public health efforts. However, most of these models fail to capture the complexity of real-world scenarios due to two defects. Firstly, they neglect the higher-order structure of infections, which is a characteristic feature of transmission through environments such as workplaces, restaurants, and households. Secondly, they assume a linear relationship between exposure to infected contacts and the risk of infection. In this chapter, we propose a higher-order epidemic spreading model that overcomes the defects above, and considers the heterogeneity of environment and individual participation in these environments. We show that the heterogeneous exposure to the infected contacts and the concept of minimal infective dose induces a universal nonlinear relationship between the exposure and infection risk. With nonlinear infection kernels, the epidemic spreading processes display discontinuous transitions, super-exponential spread, and hysteresis. The results presented in this chapter are published in [78].

5.1 Introduction

Epidemic spreading models are playing an increasingly important role in modern society [169]. Numerous theoretical models have been proposed to characterize the mechanism of the spreading dynamic from various perspectives [170]. However, large-scale forecasting comparisons show that statistical models often outperform mechanistic models that make assumptions about the dynamic [171]. This suggests that there are potential defects in the assumptions used by these mechanistic models.

In this chapter, we examine the two commonly used assumptions in the models: The random mixing assumption and the linearity between infection risk and exposures to infected individuals. While it is mathematically convenient to assume random mixing in models of infectious diseases, this approach treats all contacts between susceptible and infectious individuals as effectively equivalent. There are various models that lift this assumption by introducing heterogeneity among individuals. For instance, in Ref. [172, 173], individuals are distinguished by features such as their intrinsic susceptibility or reaction to the infections, or in Ref. [8, 174], the underlying contact networks including the heterogeneity are specified. However, almost all disease models rely on the assumption of linearity. Doubling the number of contacts between susceptible and infectious individuals doubles the risk of infection for the susceptible individuals. There are few works in mathematical biology that consider the non-linear infection rates [175, 176] but rarely used in practice. In other fields such as sociology, complex contagions that introduce the non-linear relationship between infection rate and sources of infection allow the model to consider mechanisms such as social reinforcement, *i.e.*, multiple exposures can have more impact than the mere sum of unique exposures.

In addition, the linearity assumption implies that all increments in total exposure to infectious individuals are equivalent, which contradicts evidence from immunology. The concept of minimal infective dose indicates that not all exposures are equal and a minimal dose is required for an infection to occur. More precisely, the ID_{50} value is a measure of the dose needed to cause an infection in 50% of individuals. This concept is

needed since our immune system is usually able to handle microscopic challenges posed by pathogens. While an infective dose of tuberculosis might only require between 1 and 5 bacteria [177], some enterics might require up to 10^9 pathogenic particles [178], and others like common respiratory infections still require further study [179]. There are indeed multiple different physical mechanisms behind immune evasion, for example, some airborne viruses need to find their receptors on lung epithelial cells, while some bacteria might instead require interaction with the immune system [180]. These mechanisms are reviewed in Refs. [180–184] , and all of them combine to determine the ID_{50} of specific pathogens. Likewise, the decay or clearing rates of pathogens in non-infectious courses can also vary a lot, potentially requiring days for bacteria to hours for airborne viral infections. For example, mathematical models for the pathogenesis of SARS-CoV-2 or influenza A use decay rates of the order of 7-18 hours but empirical estimates vary wildly (see Refs. [185] and [186]).

In order to study the effect of simultaneously relaxing these two assumptions, we consider a social structure where individuals attend a certain number of environments such as workplaces, gyms, or supermarkets. This division of contact structure in environments is motivated by the known role of superspreading events, which are for example critical to the spreading of COVID-19 [187–194]. While variations at the individual level are often used to explain superspreading [195], we focus here on the variability of environments and of temporal patterns [51, 160, 196–200] at *group* level, which undoubtedly affects epidemics [189], especially when a certain exposure within a certain time window is needed to confidently spark an infection. Interestingly, available case data highlight how there is no expected size or duration for such events. Transmission is highly context-dependent on the settings (for instance, ventilation) and activity (for instance, singing and shouting) such that the resulting superspreading events are heterogeneous in size, duration and attack rate, as shown in Figure 5.1(a). Higher-order contact structures and heterogeneous temporal patterns are therefore key ingredients for more realistic models of spreading dynamics.

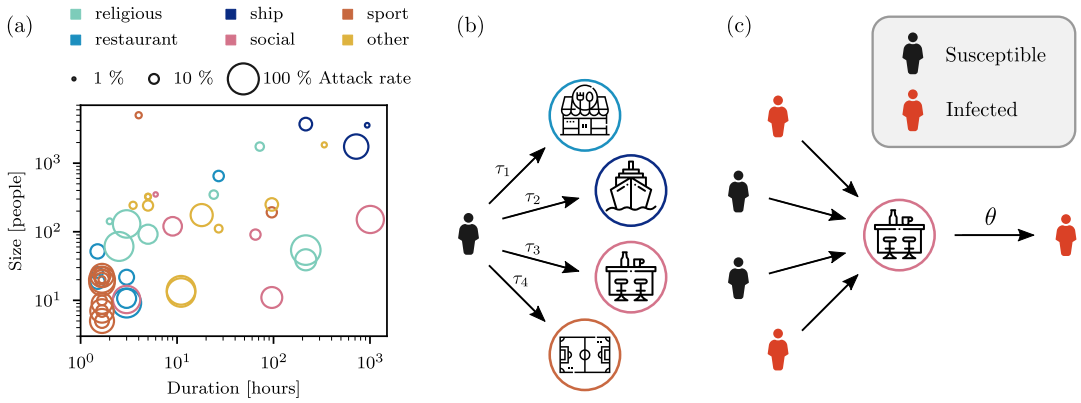

Figure 5.1: Modeling contagions and superspreading events through higher-order networks. (a) Scatter plot of superspreading events of COVID-19 where the number of people involved (size), the duration of the event, and the resulting proportion of infected individuals (attack rate) are all available (extracted from Refs. [201, 202]. (b)-(c) Framework for contagions on hypergraphs [203], where the size m of the hyperedges (environment), the hyperdegree k of the nodes (individuals), and the participation time to the environment τ are all heterogeneous, distributed according to $\hat{P}(m)$, $\tilde{P}(k)$, and $P(\tau)$ respectively. For the sake of simplicity, we assume the same distribution $P(\tau)$ for all environments. (b) At each time step t, an individual participates for a time τ (drawn independently) to each environment. (c) An individual gets infected with probability $\theta_m(\rho)$ in the environment at time step t, which depends on the size m and the fraction infected ρ.

Mathematically, the structure of higher-order contact is encoded in a hypergraph [75, 204, 205]. Environments are described by hyperedges and we denote the cardinality of a hyperedge m, indicating that the hyperedge contains m individuals. The hyperdegree of a node is denoted as k, representing the node incident to k hyperedges. Here we consider all hyperedges of the same cardinality m to be equivalent. To model the heterogeneous temporal patterns, we consider a discrete-time process, where at each time step $t = 1, 2, \cdots$, we draw for each individual a *participation time* $\tau \in [1, \tau_{\max}]$ for each environment to which they are connected (see Figure 5.1(b)). The time steps correspond to fixed temporal windows of size $\tau_{\max}$, during which susceptible individuals can get infected through their participation in environments.

We first study the impact of the spatiotemporal co-location patterns on the *infection*

kernel $\theta_m(\rho)$, *i.e.*, the probability of getting infected in an environment of size m when a fraction ρ of the other participants are infected (see Figure 5.1(b)). We then analyze the properties of the resulting contagion process.

5.2 Universal infection kernel from heterogeneous exposure

Let us consider a susceptible individual participating in an environment of size m for a duration $\tau \in [0, \tau_{\max}]$, where a fraction ρ of the other participants are infected. During this exposure period, the susceptible individual might receive an infective dose from other infected individuals and here we assume the infective dose received takes the value $\kappa \in [0, \infty]$ distributed according to $\pi(\kappa; \lambda)$ where $\lambda \equiv \langle \kappa \rangle$ representing the average of the dose distribution. A reasonable assumption is that the mean dose received is proportional to the time spent in the environment and to the proportion of infectious people, *i.e.*,

$$\lambda = \beta f(m) \tau \rho, \tag{5.1}$$

where β is a rate of dose accumulation and $f(m)$, unitless, modulates the typical number of contacts in environments frequented by m individuals. We further assume that the random variable for the dose can be written as $\kappa = \lambda u$, where u is a random variable that is independent of λ. In this case, u can be regarded as an intrinsic property of the contagion process– determined by rates of viral shedding, diffusion in the environment, variability of human interactions, *etc*, while λ acts as a scale parameter, *i.e.*,

$$\pi(\kappa; \lambda) = \pi(k/\lambda; 1) \equiv \pi(k/\lambda)\lambda. \tag{5.2}$$

To incorporate the concept of minimal infective dose, we assume that an individual is infected if the dose received $\kappa > K$, a perspective analogous to standard threshold models [206–208] and related to the assumption that successful host invasion necessitates

multiple attempts by the pathogen [209]. The probability of getting infected in the environment is therefore

$$\bar{\Pi}(K/\lambda) = \int_{K/\lambda}^{\infty} \pi(\kappa) \mathrm{d}\kappa. \tag{5.3}$$

Thus the infection kernel $\theta_m(\rho)$ is calculated as the average of $\pi(\kappa;\lambda)$ over the distribution of participation duration $P(\tau)$. Note that here for our dose mechanism to be well defined, we can only average over participation times $\tau \in [1, \mathcal{T}]$ where $\mathcal{T} \leq \tau_{\max}$ is the *clearing window*, *i.e.*, the characteristic time for the immune system to remove any dose $\kappa < K$. Due to the threshold K, the characteristic time τ_c of getting infected in the environment is obtained when

$$K = \langle \kappa \rangle = \beta f(m) \rho \tau_c, \quad i.e., \quad \tau_c = \frac{K}{\beta f(m) \rho}. \tag{5.4}$$

If we assume that the clearing window is sufficiently large compared to the characteristic time τ_c, the events where $\tau \geq \mathcal{T}$ can be neglected as they do not contribute significantly to the infection kernel.

Here we focus on the case of heterogeneous exposure, where the distribution of participation time $P(\tau)$ is described by a power-law distribution

$$P(\tau) = C_\alpha \tau^{-\alpha-1} \tag{5.5}$$

where C_α is the normalization constant, $\alpha > 0$ and $\tau \in [1, \tau_{\max}]$. Therefore the infection kernel $\theta_m(\rho)$ reads

$$\begin{aligned} \theta_m(\rho) &= \int_1^{\mathcal{T}} \bar{\Pi}(\tau_c/\tau) P(\tau) \mathrm{d}\tau \\ &= \frac{C_\alpha}{\alpha} \left[\bar{\Pi}(\tau_c) - \bar{\Pi}(\tau_c/\mathcal{T}) \mathcal{T}^{-\alpha} + \tau_c^{-\alpha} \int_{\tau_c/\mathcal{T}}^{\tau_c} \pi(y) y^\alpha \mathrm{d}y \right]. \end{aligned} \tag{5.6}$$

When $1 \ll \tau_c \ll \mathcal{T}$ and $\pi(y)$ decreases faster than $y^{-\alpha-1}$, then the integral on the right

converges to a constant, the term in $\mathcal{T}^{-\alpha}$ can be neglected, and $\bar{\Pi}(\tau_c) \ll \tau_c^{-\alpha}$, which implies

$$\theta_m(\rho) \sim D_\alpha \tau_c^{-\alpha} \propto \rho^\alpha, \tag{5.7}$$

where D_α is a constant. The form of infection kernel is universal and driven by temporal patterns, and it does not depend on the value of K (given $K > 0$) or on the particular form of π. We illustrate it in Figure 5.2(a) using an exponential for the dose distribution $\pi(k; \lambda)$.

In fact, as long as $P(\tau)$ is asymptotically power-law for large τ, we can still obtain a universal infection kernel $\theta_m(\rho) \propto \rho^\nu$ in most cases but ν is not always directly equal to α. In the following discussion, we limit our discussion to the power-law distributed participation time $P(\tau)$.

5.3 Epidemic spreading with nonlinear infection kernel

Now we consider the dynamic of epidemic spreading on hypergraphs with nonlinear infection kernel. To simplify the mathematical analysis, we consider a discrete Susceptible-Infective-Susceptible (SIS) model. At each time step, infected individuals recover with probability μ while susceptible nodes are infected with probability $\theta_m(\rho)$ via hyperedges with cardinality m. Here we assume the probability of infection through each hyperedge that a node belongs to is independent. This assumption indicates that the infective dose cannot accumulate across multiple environments. For instance, if $\mathcal{T}$ is of the magnitude of a few hours, and an individual participates in an environment once a day, the night allows the immune system to clear any dose $\kappa < K$ accumulated the day before.

In order to obtain analytical results, we consider an *annealed* infinite random hypergraph [76] of hyperdegree distribution $\tilde{P}(k)$ and cardinality distribution $\hat{P}(m)$. By annealed we mean that at each time step, the connections between nodes and hyperedges are reshuffled. With the mean-field approximation, the probability of a node being

infected at time t only depends on its hyperdegree k, which is denoted as $\rho_k(t)$. The global prevalence is hence expressed as

$$I(t) = \sum_k \rho_k(t)\tilde{P}(k) \tag{5.8}$$

and the SIS-dynamic reads

$$\rho_k(t+1) = (1-\mu)\rho_k(t) + [1-\rho_k(t)]\,\Theta_k(\bar{\rho}). \tag{5.9}$$

where

$$\Theta_k(\bar{\rho}) = 1 - \left[1-\bar{\theta}(\bar{\rho})\right]^k \tag{5.10}$$

denoting the probability for a susceptible node of hyperdegree k to be infected. $\bar{\rho}(t)$ is the probability that a node belonging to any hyperedge is infected and $\bar{\theta}(\bar{\rho})$ indicates the probability for a susceptible node to get infected in any hyperedge, *i.e.*,

$$\bar{\rho}(t) = \sum_k \frac{k\tilde{P}(k)}{\langle k\rangle}\rho_k(t) \quad \text{and} \quad \bar{\theta}(\bar{\rho}) = \sum_m \frac{m\hat{P}(m)}{\langle m\rangle}\bar{\theta}_m(\bar{\rho}) \tag{5.11}$$

where $\bar{\theta}_m(\bar{\rho})$ is the probability for a node being infected in a hyperedge of cardinality m. Due to the annealed structure, all the hyperedges with the same cardinality are equivalent, thus $\bar{\theta}_m(\bar{\rho})$ is simply the average of $\theta_m(\rho)$ defined in Eq. 5.6 with $\rho = i/(m-1)$ over a binomial distribution:

$$\bar{\theta}_m(\bar{\rho}) = \sum_{i=1}^{m-1} \begin{pmatrix} m-1 \\ i \end{pmatrix} \bar{\rho}^i (1-\bar{\rho})^{m-1-i} \theta_m\left(\frac{i}{m-1}\right). \tag{5.12}$$

The SIS dynamic reaches a steady state when

$$\rho_k^* = (1-\mu)\rho_k^* + [1-\rho_k^*]\,\Theta_k(\bar{\rho}^*). \tag{5.13}$$

thus

$$\rho_k^* = \frac{\Theta_k(\bar{\rho}^*)}{\Theta_k(\bar{\rho}^*) + \mu}. \tag{5.14}$$

$\bar{\rho}^*$ is associated with ${\rho_k}^*$ via Eq. 5.11:

$$\bar{\rho}^* = \sum_k \frac{k\tilde{P}(k)}{\langle k \rangle} \rho_k^* = \sum_k \frac{k\tilde{P}(k)}{\langle k \rangle} \frac{\Theta_k(\bar{\rho}^*)}{\Theta_k(\bar{\rho}^*) + \mu} \equiv G(\bar{\rho}^*) \tag{5.15}$$

5.4 Results

For contagions with a nonlinear infection kernel, the phase transition associated with the order parameter, *i.e.*, the global prevalence I^* can be either continuous or discontinuous with a bistable regime. Here, let us define the *invasion threshold* β_c such that for all $\beta > \beta_c$, the absorbing state $I^* = 0$ is unstable. Let us also define the *persistence threshold* β_p such that for all $\beta < \beta_p$, the absorbing state $I^* = 0$ is globally attractive. For continuous phase transition, $\beta_c = \beta_p$, and is called the *epidemic threshold*; while for a discontinuous phase transition, $\beta_p < \beta_c$, and for all $\beta \in (\beta_p, \beta_c)$, there exists typically three solutions, *i.e.*, $I_1^* = 0$ and $I_2^*,\ I_3^* > 0$, with I_1^* and I_3^* locally stable.

The invasion threshold β_c can be found by imposing $G'(0) = 1$, while the persistence threshold β_p is obtained by imposing

$$\bar{\rho}^* = G(\bar{\rho}^*) \quad \text{and} \quad G'(\bar{\rho}^*) = 1. \tag{5.16}$$

Finally, any tricritical point can be found by imposing

$$G'(0) = 1 \quad \text{and} \quad G''(0) = 0. \tag{5.17}$$

Let us derive the exact expression for the invasion threshold β_c. The derivative of $G(\bar{\rho}^*)$

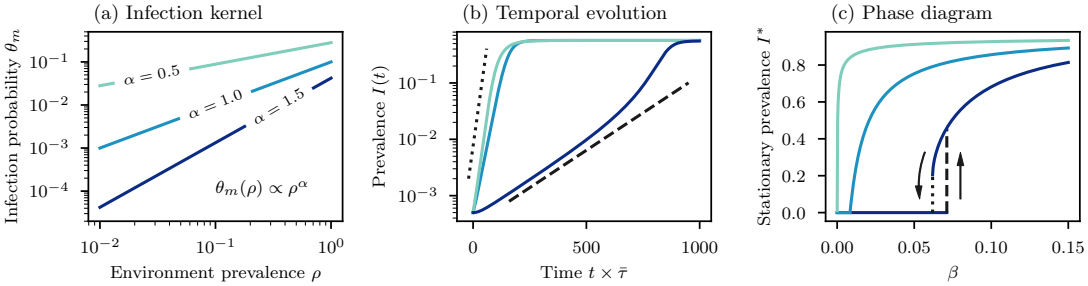

Figure 5.2: Properties of contagions with nonlinear infection kernels induced by heterogenous exposure. We use an exponential dose distribution $\pi(\kappa;\lambda) \propto e^{-\kappa/\lambda}$ with a power-law distribution of participation time $P(\tau) \propto \tau^{-\alpha-1}$, a clearing window $\mathcal{T} \to \infty$, and $f(m) = 1$. (a) Effective infection kernel using $\beta = 0.1$. The infection probability has a power law scaling $\theta_m(\rho) \propto \rho^\alpha$. (b)-(c) We use Poisson distributions for both $\tilde{P}(k)$ and $\hat{P}(m)$, with $\langle k \rangle = 5$ and $\langle m \rangle = 10$, and set $\mu = 0.05$. We use Eqs. (5.9-5.11) to evolve the system. (b) Supra-linear kernels $\alpha > 1$ lead to a super-exponential growth for the global prevalence $I(t)$. We use $\beta = 5 \times 10^{-4}$, $\beta = 0.025$ and $\beta = 0.077$ for $\alpha = 0.5$, $\alpha = 1$ and $\alpha = 1.5$ respectively. $\bar{\tau}$ is the median exposure period. (c) The phase diagram for stable solutions in the stationary state ($t \to \infty$) can be continuous or discontinuous with a bistable regime. Sub-linear and linear kernels $\alpha \leq 1$ lead to a continuous phase transition, and the invasion threshold β_c vanishes for $\alpha \to 0$. Supra-linear kernels $\alpha > 1$ can lead to a discontinuous phase transition with a bistable regime.

defined in Eq. 5.3 reads

$$G'(\bar{\rho}^*) = \sum_k \frac{k\tilde{P}(k)}{\langle k \rangle} \left[\frac{\Theta'_k(\bar{\rho}^*)}{\mu + \Theta_k(\bar{\rho}^*)} - \frac{\Theta_k(\bar{\rho}^*)\Theta'_k(\bar{\rho}^*)}{(\Theta_k(\bar{\rho}^*) + \mu)^2} \right]. \tag{5.18}$$

where

$$\Theta'_k(\bar{\rho}^*) = \frac{\partial}{\partial \bar{\rho}^*} \left\{ 1 - \left[1 - \bar{\theta}(\bar{\rho}^*) \right]^k \right\} = k \left[1 - \bar{\theta}(\bar{\rho}^*)^{k-1} \right] \sum_m \frac{m\hat{P}(m)}{\langle m \rangle} \bar{\theta}'_m(\bar{\rho}^*) \tag{5.19}$$

and

$$\bar{\theta}'_m(\bar{\rho}^*) = \sum_{i=1}^{m-1} \binom{m-1}{i} \theta_m\left(\frac{i}{m-1}\right) \left[i\bar{\rho}^{*i-1}(1-\bar{\rho}^*)^{m-1-i} - (m-1-i)\bar{\rho}^{*m-2-i}\bar{\rho}^{*i} \right] \tag{5.20}$$

When $\bar{\rho}^* = 0$, we have $\theta(\bar{\rho})^* = 0$ and $\Theta_k(\bar{\rho}^*) = 0$, thus

$$\begin{aligned}
\Theta_k'(0) &= k\bar{\theta}'(0), \\
\bar{\theta}'(0) &= \frac{1}{\langle m \rangle}\langle m\theta_m'(0)\rangle, \\
\bar{\theta}_m'(0) &= (m-1)\theta_m\left(\frac{1}{m-1}\right)
\end{aligned} \tag{5.21}$$

At invasion threshold β_c

$$G'(0) = \frac{\langle k^2\rangle\bar{\theta}'(0)}{\mu\langle k\rangle} = \frac{\langle k^2\rangle\langle m(m-1)\theta_m(\frac{1}{m-1})\rangle}{\mu\langle k\rangle\langle m\rangle} = 1. \tag{5.22}$$

Recall Eq. 5.7 and the characteristic time of getting infected in the environment $\tau_c \equiv K/\beta f(m)\rho$, hence the infection kernel reads

$$\theta_m(\rho) \sim D_\alpha\left(\frac{K}{\beta f(m)\rho}\right)^{-\alpha}. \tag{5.23}$$

Thus, the invasion threshold β_c reads

$$\beta_c \propto \left(\frac{\mu\langle m\rangle\langle k\rangle}{\langle m(m-1)^{1-\alpha}[f(m)]^\alpha\rangle}\langle k^2\rangle\right)^{1/\alpha}. \tag{5.24}$$

In analogy to the calculation above, the tricritical point (α_t, β_t) and persistence threshold β_p can be obtained numerically. However, we can get some insights for minimal kernel exponent α_t leading to a discontinuous phase transition from an asymptotic expansion.

At tricritical point (α_t, β_t),

$$G'(0) = 1 \quad \text{and} \quad G''(0) = 0 \tag{5.25}$$

where $G'(0)$ is given by Eq. 5.22 and $G''(0)$ reads

$$\begin{aligned} G''(0) &= \frac{1}{\langle k \rangle} \left\langle \frac{k\Theta_k''(0)}{\mu} - \frac{2k\left[\Theta_k'(0)\right]^2}{\mu^2} \right\rangle \\ &= \frac{1}{\mu\langle k \rangle} \left\{ \left\langle k^2 \right\rangle \bar{\theta}''(0) - \left(\left\langle k^2(k-1) \right\rangle + \frac{2\left\langle k^3 \right\rangle}{\mu} \right) \left[\bar{\theta}'(0)\right]^2 \right\} . \end{aligned} \tag{5.26}$$

and

$$\begin{aligned} \bar{\theta}''(0) &= \frac{1}{\langle m \rangle} \langle m\theta_m''(0) \rangle, \\ \bar{\theta}_m''(0) &= (m-1)(m-2)\left[\theta_m\left(\frac{2}{m-1}\right) - 2\theta_m\left(\frac{1}{m-1}\right) \right] \end{aligned} \tag{5.27}$$

From Eq. 5.22 we know that at tricritical point (α_t, β_t)

$$\bar{\theta}'(0) = \frac{\mu\langle k \rangle}{\langle k^2 \rangle}, \tag{5.28}$$

Thus Eq. 5.26 reduces to

$$G''(0) = \frac{1}{\mu\langle k \rangle} \left\{ \left\langle k^2 \right\rangle \bar{\theta}''(0) - \left(\left\langle k^2(k-1) \right\rangle + \frac{2\left\langle k^3 \right\rangle}{\mu} \right) \frac{\mu^2 \langle k \rangle^2}{\langle k^2 \rangle^2} \right\} . \tag{5.29}$$

Meanwhile, inserting the asymptotic approximation Eq. 5.23 into Eq. 5.27 we obtain

$$\bar{\theta}''(0) \propto \frac{\beta^\alpha}{\langle m \rangle} \left\langle m(m-1)^{1-\alpha}(m-2)[f(m)]^\alpha \left(2^\alpha - 2\right) \right\rangle . \tag{5.30}$$

Note that at the tricritical point, $\beta = \beta_c$, which is given by Eq. 5.24, hence Eq. 5.30 further reduces to

$$\bar{\theta}''(0) \propto \mu \frac{\langle k \rangle}{\langle k^2 \rangle} \frac{\left\langle m(m-1)^{1-\alpha}(m-2)[f(m)]^\alpha \left(2^\alpha - 2\right) \right\rangle}{\left\langle m(m-1)^{1-\alpha}\left[f(m)\right]^\alpha \right\rangle} . \tag{5.31}$$

We get three insights from Eqs. 5.26 and 5.31.

1. The condition $\alpha > 1$ is necessary to have a tricritical point, but not sufficient: it depends on the first three moments of $\tilde{P}(k)$, and in a more complicated manner

on the distribution $\hat{P}(m)$.

2. It is necessary to have $\hat{P}(m) > 0$ for at least one value $m > 2$, i.e., environments of size $m = 2$ cannot lead to a discontinuous phase transition.

3. A more heterogeneous $\tilde{P}(k)$ will typically require a larger α to reach a tricritical point. Indeed, if we keep $\langle k \rangle$ fixed, but increase the value for the second and third moments (using a broader distribution for instance), the negative term on the right in Eq. 5.26 increases, while the positive term is invariant.

5.5 Conclusion

Our framework captures many properties that are usually overlooked for the sake of simplicity in epidemic models: the higher-order structure of contacts, the temporal heterogeneity of human activity, and threshold effects over the exposure due to the host immune system. In particular, we recover a universal nonlinear infection kernel that provides a connection between complex contagions based on nonlinear infection kernels [210] and threshold models [206–208].

Our results challenge a key assumption of most epidemic models: Why assume a linear relationship between the number of infectious contacts and the risk of infection? This question is critical since three of the basic insights gathered from epidemic models break down under nonlinear infection kernels: they can lead to a discontinuous relationship between disease transmissibility and epidemic size, to a bistable regime where macroscopic outbreak and disease-free state co-exist, and to a super-exponential growth. In fact, the super-exponential spread has been observed for influenza-like illness [211].

The phenomenology being drastically different from standard epidemiological models induces the following question: Why do linear models work? Even for a nonlinear kernel $\theta_m(\rho)$, the probability of infection $\bar{\theta}_m(\bar{\rho})$ (given by Eq. 5.12) is linear in $\bar{\rho}$ if $\bar{\rho} \ll 1$. Therefore, linear models are a good approximation when the prevalence is sufficiently low, but it breaks down at higher prevalence, for instance, as illustrated in Figure 5.2(b)

when $\alpha = 1.5$.

The mathematical framework we use to solve the SIS model depends on a mean-field approximation, as in other studies [1, 3, 6, 212], thereby suppressing dynamic correlations within hyperedges. Future works could investigate more thoroughly the interplay between dynamical correlations, nonlinear kernels, and spatiotemporal heterogeneity. Moreover, although we considered the SIS model to simplify the analysis, the universal infection kernel $\theta_m(\rho) \propto \rho^\alpha$ could be directly integrated into other models such as SEIR or SIRS models.

Altogether, our conclusions stress the need to embrace heterogeneity in disease modeling; in the infection dynamics itself, in patterns of temporal activity, and in the higher-order structure of contact networks. Epidemics should be seen as the result of a collective process, where higher-order structure and temporal patterns can drive complex dynamics.

Chapter 6

Mitigation of epidemic spreading with mobile apps

In this chapter, we consider a stylised SIR-like model for the epidemic spreading under interventions, namely automated contact-and-tracing with mobile apps and isolation, which has been widely used during the COVID-19 pandemic. With the help of percolation theory and the powerful message-passing approach, we are able to analyze how this containment measure can affect the epidemic-spreading process and the critical threshold of a massive outbreak. Moreover, we propose optimal strategies for distributing the contact-and-tracing app under limited resources available. Despite various empirical studies of the contact tracing app [213–215] have been published recently, the present model is one of the first theoretical studies on the subject. In this chapter, we do not intend to apply this framework to real-world problems, however, this work might be insightful to study the role of contact-and-tracing in real pandemics. The results presented in this chapter are published in [138].

6.1 Introduction

With the hit of new pandemic threats, scientific frameworks are needed to understand the unfolding of epidemic spreading. The recent outbreak of the COVID-19 pandemic has displayed some new features and requires new tools to control the spread. Due to the asymptomatic transmission, only isolating infected individuals with symptoms is insufficient to mitigate the pandemic. Thus, digital contact-and-tracing with mobile apps has been extensively used in some countries to control new infections and contain further propagation, as the traditional manual contact tracing is infeasible due to the fast transmission. The basic mechanism behind contact-and-tracing with mobile apps is as follows. Within a population that has adopted the tracing app, infected individuals can upload their infectious status on the app when they are diagnosed. The app will send this message to individuals who have adopted the app and have been in close contact with this infected individual. These people will isolate themselves immediately to prevent the further propagation due to the asymptomatic infection.

In order to obtain some theoretical insights about the above-mentioned process, the traditional SIR model is insufficient, and a new theoretical framework for understanding the epidemic processes in presence of contact tracing is therefore needed. In the past years, a large variety of epidemiological models have been proposed, with different flavors of complexity, while arguably the most popular one would be the SIR model, which allows to find analytical expressions for the epidemic threshold in several scenarios. Although these results might be only an approximation of observed features in real epidemics, they still constitute a fundamental theoretical cornerstone in the field of epidemic processes. Meanwhile, the SIR model can be mapped to a link percolation problem [7, 8] and the percolation theory provides a simple mathematical framework that naturally applies to critical diffusion (such as epidemic spreading in heterogeneous structures). Therefore, a percolation theory based framework seems to be a natural option to understand the epidemic spreading process with digital contact and tracing.

Recently, there have been several studies [213–215] investigating the effectiveness of

contact-and-tracing policies as a measure to contain epidemic spreading from different perspectives. In Ref. [214], Ferretti *et al.* propose a mathematical model to estimate the basic reproductive number using real epidemic data and explore the feasibility of controlling the epidemic with a digital contact tracing approach. They reveal that the use of a contact-tracing app with immediate notification to contacts of positive cases would be sufficient to stop the epidemic if used by enough people. In Ref. [213], the authors discuss the effectiveness of the contact tracing approach under the different ratios of asymptomatic transmissions and find that contact tracing is effective only for intermediate level of asymptomatic infection and the impact of contact tracing depends on the efficacy of reporting and isolation of the symptomatic cases.

There are several mathematical arguments proposed in the literature to justify the above-mentioned effect. For instance, in [215] a simple generating function argument is proposed in order to compute the probability that contact tracing stops the epidemic propagation, however, a solid percolation approach that is able to capture analytically the impact of a tracing app on the non-linear aspect of epidemic spreading has not been proposed so far. In [138], we take a step forward in filling this gap by proposing a stylized model for epidemic spreading with contact-and-tracing and testing policies based on link percolation.

Here we propose a modified version of the Message-passing (MP) equation to capture the dynamic of the epidemic-spreading process with contact-and-tracing and isolation. We derive different MP equations that are able to predict the epidemic spreading depending on the level of information available about the structure of the network and the user adoption of the app [49]. The theoretical predictions are validated by comparing them with extensive Monte Carlo simulations. Our results show that in general the more the app is adopted by the population, the higher the value of the critical threshold p_c. Furthermore, we study different allocation strategies to mitigate the epidemic spreading given a fixed app coverage on a random network ensemble. We find that the optimal strategy which maximizes p_c is the hub-targeting strategy. By applying the message-

passing algorithm to real networks we also show that this strategy gives excellent results compared with other state-of-the-art ranking algorithms for the centrality of nodes in epidemic spreading.

6.2 Model description

Consider a contact network $G(V, E)$ formed by $|V| = N$ individuals $i = 1, 2, 3, \cdots, N$ and the set of edges E among them. Each individual i is assigned a binary variable T_i, indicating if the individual has the mobile app for contact-and-tracing ($T_i = 1$) or not ($T_i = 0$). We formulate the spreading process based on the following rationale. Infected individuals transmit the virus to a susceptible neighbor with probability p, called *transmissibility*. Under an ideal assumption (with might be far from reality, but helps simplify the analysis), an individual who has the app, will know almost instantaneously if he/she has been contacted by an infected individual who also has the app, and he/she will self-isolate immediately to prevent the further propagation of the virus. However, if the infection comes from someone who does not have the app, he/she will only know until the symptom shows, thus he/she can still spread the virus during the asymptomatic period. In other words, individuals with the app ($T_i = 1$) can infect only if previously infected by individuals without the app ($T_i = 0$), while individuals without the app can infect regardless of the T_i value of the individual that has infected them (see Figure 6.1). Now, we propose a stochastic infection model as follows: for every link (i, j) we draw a random variable $x_{ij} \in \{0, 1\}$ indicating whether the eventual contact between one infected and one susceptible node, found at the two ends of the link, leads to the infection. We parametrize this dynamic by taking $\langle x_{ij} \rangle = p$, where p indicates the transmissibility of the epidemic. The stationary state of this spreading process on any network topology can be simulated with the following Monte Carlo algorithm, thanks to the mapping between the spreading process and percolation theory. We will show in the following, how to implement the Monte Carlo algorithm to simulate the phase diagram and the critical threshold, and more importantly, we will show the message-passing approach to

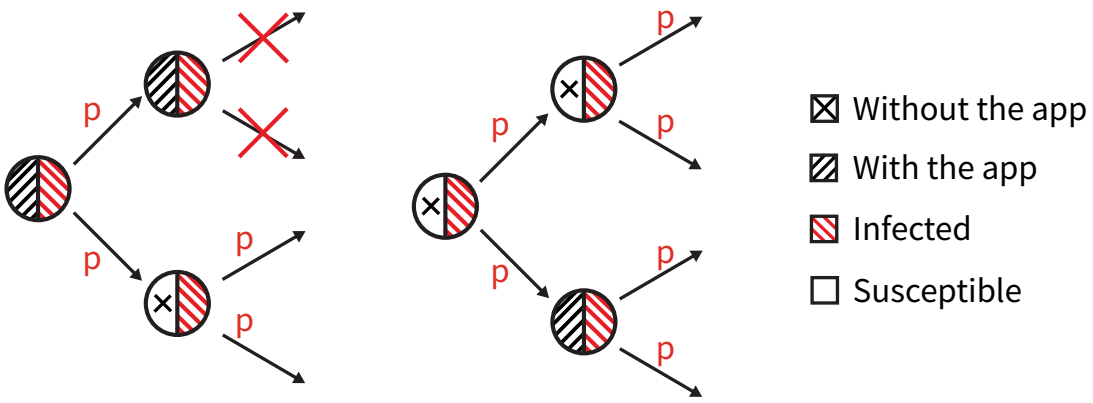

Figure 6.1: Sketch of the infection pathways that leads to the epidemic spreading in a population in which there are individuals that have adopted the app and individual that have not adopted the app.

the model proposed above.

6.3 Monte Carlo simulation

In order to find which are the nodes infected in the epidemic outbreak, we adopt the following algorithm that takes advantage of the mapping of the stationary state of the epidemic to percolation. Firstly, we notice that the virus cannot propagate via a T-T link. By T-T link we refer to the links connecting two individuals that both have adopted the app. Therefore initially we remove all T-T links from the network. In practice, we associate to each link (i, j) a variable $y_{ij} \in \{0, 1\}$ defined as

$$y_{ij} = x_{ij}(1 - T_i T_j), \tag{6.1}$$

indicating whether the link contributes or not to the spread of the disease in the network. Note that although the virus cannot be transmitted via a T-T link, both nodes at the end of a T-T link still can be infected by other neighbors.

Secondly, using the mapping between epidemic spreading and link percolation, we find the nodes in the giant component of the resulting percolation problem. In practice, we assign to each node an indicator variable $m_i \in \{0, 1\}$ indicating if node i belongs or

not to the giant component of the network with links according to the indicator function y_{ij}. The nodes in the giant component are those who are infected by a chain of contacts, in which we can never find two consecutive infected nodes with the app (as all the T-T links have been removed).

Finally, we calculate the fraction of infected individuals. We need to sum not only all the nodes in the giant component which is indicated by $m_i = 1$, but also the nodes with the app infected by nodes with the app. Here we define the indicator σ_i which indicates if a node i is infected ($\sigma_i = 1$) or not ($\sigma_i = 0$). The value of σ_i is calculated by

$$\sigma_i = m_i + (1 - m_i) \left(1 - \prod_{i \in N(i)} (1 - m_j T_j T_i x_{ij}) \right). \tag{6.2}$$

The second term of Eq. 6.2 means that a node i which is not in the giant component can also be infected if, for at least one of its neighbor j, (1) node j is in the giant component; (2) both node i and j have adopted the app; (3) an infection has taken place between i and j.

6.4 Message passing approach

To analytically predict the propagation of the epidemic on a network, we use the powerful MP approach [49, 140]. This approach is well-known to be very robust in the case of real-world networks with loops [142], as long as the underlying MP converges, while the approach is proven to give exact results only on locally tree-like networks. In this work, we adopt the MP approach and we use it to predict the phase diagram of the spreading process on network ensembles as a function of the level of adoption of the app in the population.

6.4.1 MP algorithm when the microscope structure of the infection is known

The considered spreading model is stochastic and has different sources of randomness that can be taken into account by different MP algorithms in which we average different levels of information [49]. The simplest case of MP algorithm is the original stochastic infection model proposed in Sec. 2.3. In this case, we know everything about the spreading dynamics. This would entail first knowing the contact network, secondly knowing which individuals have the app, *i.e.*, the configuration $\{T_i\}_{i\in V}$, and finally knowing which links have led to an actual infection, *i.e.*, $\{x_{ij}\}_{(i,j)\in E}$. In this case, we can derive the message-passing equation based on the following rationale. We denote $\tilde{\sigma}_{i\to j}=1$ if the node i spreads the virus to node j and $\tilde{\sigma}_{i\to j}=0$ otherwise. If node i has the app, *i.e.*, $T_i=1$, the node i can spread the virus to node j only in the case when (1) node i has been infected by at least one neighbor node without the app and (2) the link between node i and j that lead to the actual infection exists, *i.e.*, $x_{ij}=1$. If the node i does not have the app ($T_i=0$), on the other hand, the infection from node i to j will happen if node i (1) is infected by at least one neighbor node (despite if the nodes have the app or not) and (2) $x_{ij}=1$. Now the message-passing algorithm reads

$$\tilde{\sigma}_{i\to j}=x_{ij}T_i\left[1-\prod_{\ell\in N(i)\setminus j}(1-(1-T_\ell)\tilde{\sigma}_{\ell\to i})\right]+x_{ij}(1-T_i)\left[1-\prod_{\ell\in N(i)\setminus j}(1-\tilde{\sigma}_{\ell\to i})\right], \tag{6.3}$$

where $N(i)$ denotes the set of neighbors of node i. Moreover, the quantity $\tilde{\sigma}_i$ which indicates if the node i is infected ($\tilde{\sigma}_i=1$) or not ($\tilde{\sigma}_i=0$) is given by

$$\tilde{\sigma}_i=\left[1-\prod_{\ell\in N(i)}(1-\tilde{\sigma}_{\ell\to i})\right]. \tag{6.4}$$

and the fraction of nodes infected, *i.e.*, the size of the outbreak is given by

$$S=\frac{1}{N}\sum_{i=1}^{N}\tilde{\sigma}_i. \tag{6.5}$$

The epidemic threshold is determined by

$$\Lambda(\mathcal{B}) = 1 \tag{6.6}$$

where $\Lambda(\mathcal{B})$ is the leading eigenvalue of the modified non-backtracking matrix $\mathcal{B}$ of elements

$$\mathcal{B}_{\ell i \to ij} = x_{ij}(1 - T_i T_\ell)\mathcal{A}_{\ell i \to ij} \tag{6.7}$$

with $\mathcal{A}$ defined in terms of the adjacency matrix of network a as

$$\mathcal{A}_{\ell i \to ij} = a_{\ell i} a_{ij}(1 - \delta_{\ell j}) \tag{6.8}$$

where $\delta_{\ell j}$ is the Kronecker delta.

6.4.2 MP algorithm when only the transmissibility of the disease is known

In the case in which we only know the transmissibility of the disease $p = \langle x_{ij} \rangle$, the algorithm above should be modified. In this case, the messages have real values $\sigma_{i \to j} \in [0, 1]$, which indicate the probability that node i infects node j. The modified messages can be obtained by averaging over all the configurations of $\{x_{ij}\}_{(i,j)\in E}$ [49]. The probability of having a given configuration of $\{x_{ij}\}_{(i,j)\in E}$ is given by

$$P(\{x_{ij}\}) = \prod_{(i,j)\in E} p^{x_{ij}}(1-p)^{1-x_{ij}} \tag{6.9}$$

and the average messages read:

$$\sigma_{i \to j} = \sum_{\{x_{ij}\}} P(\{x_{ij}\})\tilde{\sigma}_{i \to j} \tag{6.10}$$

Using the definitions above, one can write the averaged message-passing equation as

$$\sigma_{i\to j} = pT_i \left[1 - \prod_{\ell\in N(i)\setminus j} (1-(1-T_\ell)\sigma_{\ell\to i})\right] + p(1-T_i)\left[1 - \prod_{\ell\in N(i)\setminus j}(1-\sigma_{\ell\to i})\right], \quad (6.11)$$

and the averaged marginal probabilities σ_i read

$$\sigma_i = \left[1 - \prod_{\ell\in N(i)}(1-\sigma_{\ell\to i})\right]. \quad (6.12)$$

The non-backtracking matrix reads

$$\mathcal{B}_{\ell i\to ij} = p(1-T_iT_\ell)\mathcal{A}_{\ell i\to ij} \quad (6.13)$$

and the epidemic threshold $p = p_c$ is determined by Eq. 6.6. Here we note that Eq. 6.13 (as well as Eq. 6.7) clearly indicates that the epidemic threshold is dictated by the non-backtracking matrix of the network where all the T-T links have been removed, which is consistent with the above-mentioned Monte Carlo algorithm.

6.4.3 MP algorithm when only the adoption probability of the app is known

In order to model different scenarios corresponding to different adoption patterns of the mobile app, we might also assume that the configuration $\{T_i\}_{i\in V}$ is not known exactly. A simple assumption can be that we will have access to the probability that a node adopt the app, and the probability is a function of the degree of the nodes, *i.e.*, $\langle T_i\rangle = T(k_i)$ with $T(k)$ describing the probability that a node of degree k adopts the app. Although in reality, the willingness to adopt the tracing app might be affected by many factors, for instance, an additional social contagion process [216], here we use the minimum assumption, without assuming any other information about the network, but using only the intrinsic topological property of the network. Meanwhile, this minimum assumption allows for deriving analytical calculations. For formulating the message passing algorithm

in this case, we consider for every ordered pair of linked nodes (i, j) two messages

$$\hat{\sigma}^T_{i\to j} = \langle T_i \sigma_{i\to j}\rangle, \quad \hat{\sigma}^N_{i\to j} = \langle (1-T_i)\sigma_{i\to j}\rangle, \tag{6.14}$$

indicating the probability that node i infects node j given that node i has adopted the app ($\hat{\sigma}^T_{i\to j}$) or not ($\hat{\sigma}^N_{i\to j}$). Then the message passing equation averaged over all configurations $\{T_i\}_{i\in V}$ and $\{x_{ij}\}_{(i,j)\in E}$ reads

$$\begin{aligned}
\hat{\sigma}^T_{i\to j} &= pT(k_i)\left[1 - \prod_{\ell\in N(i)\setminus j}(1-\hat{\sigma}^N_{\ell\to i})\right] \\
\hat{\sigma}^N_{i\to j} &= p(1-T(k_i))\left[1 - \prod_{\ell\in N(i)\setminus j}(1-\hat{\sigma}^N_{\ell\to i} - \hat{\sigma}^T_{\ell\to i})\right],
\end{aligned} \tag{6.15}$$

and the marginal probability that node i is infected $\hat{\sigma}_i$ is given by

$$\hat{\sigma}_i = \left[1 - \prod_{\ell\in N(i)}\left(1-\hat{\sigma}^N_{\ell\to i} - \hat{\sigma}^T_{\ell\to i}\right)\right]. \tag{6.16}$$

Now we use the method introduced in Sec. 2.3 to derive the critical threshold. By linearizing the message passing equation Eq. 6.15 we obtain

$$\begin{aligned}
\hat{\sigma}^T_{i\to j} &= pT(k_i)\sum_{\ell\in N(i)\setminus j}\hat{\sigma}^N_{\ell\to i} = pT(k_i)\sum_{\ell\in N(i)}\mathcal{A}_{\ell i\to ij}\hat{\sigma}^N_{\ell\to i}, \\
\hat{\sigma}^N_{i\to j} &= p\left(1-T(k_i)\right)\sum_{\ell\in N(i)\setminus j}\left(\hat{\sigma}^N_{\ell\to i} + \hat{\sigma}^T_{\ell\to i}\right) \\
&= p(1-T(k_i))\sum_{\ell\in N(i)}\mathcal{A}_{\ell i\to ij}(\hat{\sigma}^N_{\ell\to i} + \hat{\sigma}^T_{\ell\to i}).
\end{aligned} \tag{6.17}$$

Combining the two equations above, we have

$$\begin{aligned}\hat{\sigma}^N_{i\to j} &= p(1-T(k_i))\sum_{\ell\in N(i)}\mathcal{A}_{\ell i\to ij} \\ &\times \left[\hat{\sigma}^N_{\ell\to i}+pT(k_\ell)\sum_{\ell'\in N(\ell)}\mathcal{A}_{\ell'\ell\to\ell i}p(1-T(k_i))\sum_{\ell\in N(i)}\mathcal{A}_{\ell i\to ij}\hat{\sigma}^N_{\ell'\to\ell}\right].\end{aligned} \tag{6.18}$$

Therefore the modified non-backtracking matrix reads

$$\mathcal{B}_{\ell'\ell\to ij}=p\delta_{\ell,i}\mathcal{A}_{\ell' i\to ij}(1-T_{k_i})+p^2\mathcal{A}_{\ell'\ell\to\ell i}T_{k_\ell}\mathcal{A}_{\ell i\to ij}(1-T_{k_i}), \tag{6.19}$$

and the epidemic threshold $p=p_c$ is determined by Eq. 6.6. We check the validity of the message-passing approach (Eq. 6.15 and Eq. 6.16) by comparing directly to the Monte Carlo algorithm proposed in Sec. 6.3 (see Figure 6.2). The comparison is conducted on both synthetic random networks and real networks and we find an excellent agreement between the two approaches.

6.5 Ensemble method

In the case with the least information, we do not know the exact topology of the contact network, *i.e.*, we only know that the network is a random uncorrelated network with a given degree distribution $P(k)$, as well as the statistical properties of the configurations $\{T_i\}_{i\in V}$ and $\{x_{ij}\}_{(i,j)\in E}$ which illustrated in the sections above. Here we use the ensemble approach, as introduced in Sec. 2.2.1, to derive the self-consistent equations, which is the message-passing equation averaged over the uncorrelated network ensemble. We consider the variables S'_T and S'_N indicating the probability that by randomly following a link, we reach an infected individual with the app or without the app, respectively.

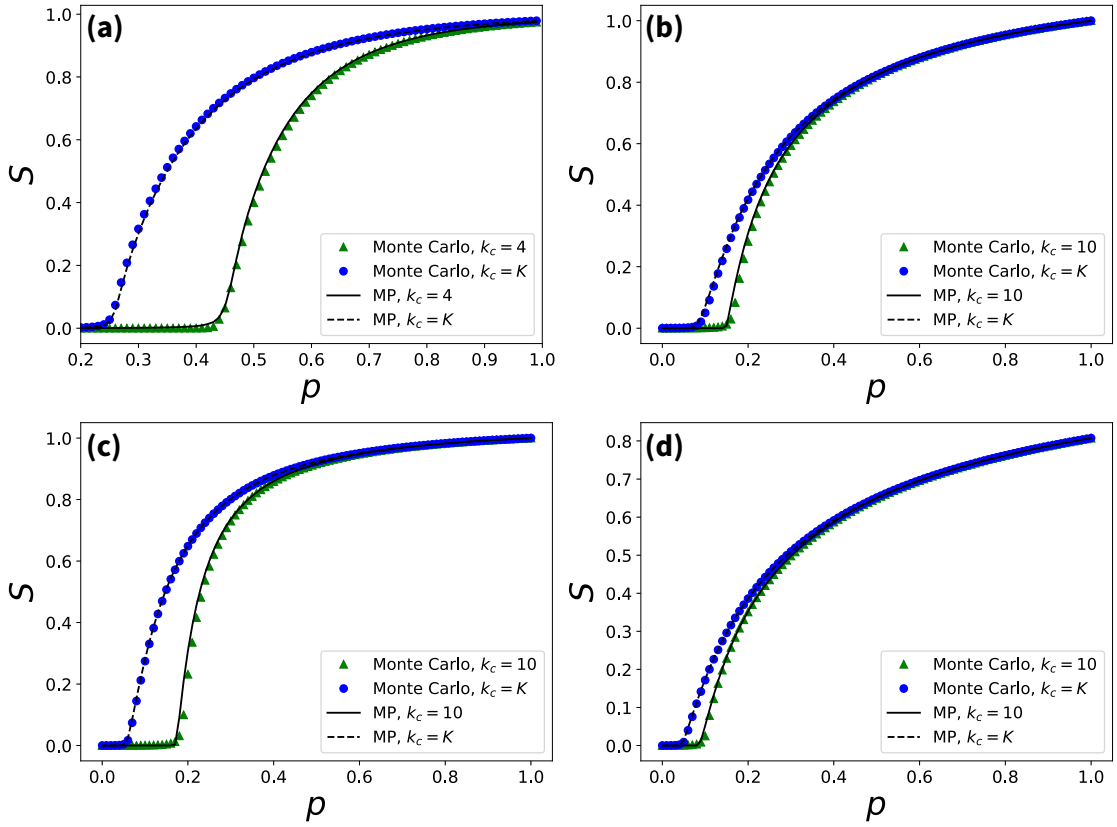

Figure 6.2: The fraction of infected nodes S is plotted versus p for several networks. The results obtained by averaging the Monte Carlo simulations of the configurations $\{T_i\}_{i\in V}$ and $\{x_{ij}\}_{(i,j)\in E}$ are compared with the results of the MP algorithm defined by Eq. 6.15 and Eq.6.16, where $T(k)$ is given by Eq. 6.29 with $\alpha = 0$ and k_c as indicated in the legend of each panel. The value K in all panels corresponds to the largest degree of the network and therefore corresponds to the case of no app coverage. **(a)** Poisson network with $N = 5 \times 10^4$ nodes and average degree $\lambda = 4$. **(b),(c),(d)** Friendship networks from the music streaming site Deezer in the countries of Romania ($N = 41773$), Hungary ($N = 47538$) and Croatia ($N = 54573$) respectively [217].

The self-consistent equations of S'_T and S'_N read:

$$\begin{aligned} S'_T &= p\sum_k \frac{kP(k)}{\langle k\rangle}(T(k))\left[1-(1-S'_N)^{k-1}\right] \\ S'_N &= p\sum_k \frac{kP(k)}{\langle k\rangle}(1-T(k))\left[1-(1-S'_N-S'_T)^{k-1}\right], \end{aligned} \tag{6.20}$$

where $T(k)$ indicates the probability that a node of degree k adopts the app. The probability that a random node gets infected is given by

$$S = \sum_k P(k) \left[1 - \left(1 - S'_T - S'_N\right)^k\right]. \tag{6.21}$$

In order to calculate the critical threshold, we re-write Eq. 6.20 as

$$\begin{aligned} S'_T &= p \sum_k \frac{kP(k)}{\langle k \rangle} (T(k)) \left[1 - (1 - S'_N)^{k-1}\right] = 0 \\ S'_N &= p \sum_k \frac{kP(k)}{\langle k \rangle} (1 - T(k)) \left[1 - (1 - S'_N - S'_T)^{k-1}\right] = 0, \end{aligned} \tag{6.22}$$

Using the same approach demonstrated in Sec. 2.2.1, the Jacobian of the equations is given by

$$\mathbf{J} = \begin{pmatrix} 1 & -p\kappa_T \\ -p\kappa_N & 1 - p\kappa_N \end{pmatrix}, \tag{6.23}$$

where

$$\begin{aligned} \kappa_N &= \frac{\langle k(k-1)(1 - T(k)) \rangle}{\langle k \rangle}, \\ \kappa_T &= \frac{\langle k(k-1)T(k) \rangle}{\langle k \rangle}. \end{aligned} \tag{6.24}$$

Imposing that the determinant of the Jacobian is zero we obtain that the transition is achieved for

$$p_c = \min\left(1, \frac{1}{2\kappa_T}\left[-1 + \sqrt{1 + 4\frac{\kappa_T}{\kappa_N}}\right]\right). \tag{6.25}$$

6.6 Optimization

In the previous section, we have obtained the analytical expression of critical threshold p_c on the uncorrelated network ensemble. Here we study the optimization of the critical

threshold, *i.e.*, how to maximize p_c to delay the massive outbreak, with limited resources. A simple and reasonable assumption is that the expected number of people who has the app is restricted, due to some factors, for instance, the accessibility of the contact-and-tracing app, personal concerns related to the privacy risk of the tracing app, *etc.* The constraint reads

$$\sum_k P(k)T(k) = \mathcal{T}. \tag{6.26}$$

From Eq. 6.25 we notice that p_c is an increasing function of κ_T, hence we simply need to maximize κ_T under the constraint given by Eq. 6.26.

Thus, the optimization problem reads

$$\max_{T(k)} \mathcal{O} = \sum_k k(k-1)P(k)T(k) \quad \text{subject to} \quad \begin{cases} \sum_k P(k)T(k) = \mathcal{T}, \\ 0 \leq T(k) \leq 1. \end{cases} \tag{6.27}$$

gives the discrete Heaviside step function (see details in Appendix C.)

$$\tilde{T}(k) = \theta(k - k_c, \alpha) \tag{6.28}$$

taking the value $0 \leq \alpha = \mathcal{T} - \sum_{k>k_c} P(k) < 1$ at $k = k_c$. Therefore the optimal solution is to have all nodes of degree $k > k_c$ with 100% app adoption and the node with exactly $k = k_c$ with the maximal adoption allowed by the constraint in Eq. 6.26.

6.7 Improvement on p_c

From Eq. 6.25, we have learned that on an uncorrelated random network, given a fixed app coverage $\mathcal{T}$, the optimal strategy of app allocation in order to maximize the critical threshold p_c, *i.e.*, maximally delay the outbreak of the pandemic, is targeting the hub nodes. In order to verify the optimality of Eq. 6.25 compared to other strategies, we

consider a more general form of $T(k)$ given by:

$$T(k) = \rho + (1 - \rho)\theta(k - k_c, \alpha), \tag{6.29}$$

where $\theta(k-k_c, \alpha)$ is the aforementioned discrete Heaviside step function taking the value α at $k = k_c$, and $\rho \in [0, 1]$ indicates a uniform fraction of indivuduals adopting the app. Using Eq. 6.29 we can interpolate between a purely random strategy (when $k_c \to \infty$) and the optimal strategy (when $\rho \to 0$).

Thanks to the analytical expression of p_c given by Eq. 6.25, we are able to investigate the phase diagram characterized by the epidemic threshold p_c of a Poisson random network as a function of ρ and k_c (see Figure 6.3). We observe that the adoption of the contact tracing app can significantly increase p_c, reflected in the phase diagram when increasing ρ or decreasing k_c.

To show the effect of increasing p_c due to the adoption of the app, we consider an epidemic spreading process on a real network, Livemocha social-network [218] (see Figure 6.4). We observe the random adoption strategy indicated by $k_c \to \infty$ yields a very small increase in the value of p_c, compared to the optimal distribution indicated by $\rho \to 0$. Hence, in a scenario of limited resources, represented by the constraint defined in Eq. 6.26, the optimal strategy corresponds to distributing the app from higher-degree nodes to lower-degree ones until the resources are exhausted. The resulting increase in p_c computed according to Eq. 6.25 is dramatic and non-linear. For instance from Figure 6.4, if the app is optimally distributed among $\sim 40\%$ of the population, the increase of p_c is $\sim$ 17-fold, while if the same percentage is covered randomly, the increase is$\sim$ 1.2-fold.

In order to check how the obtained optimal strategy compares with other possible mechanisms driving the adoption of the app, we compare the hub-targeting strategy with other strategies, for instance targeting nodes with high eigenvector centrality [219], or the high non-backtracking centrality [220] in a number of real datasets (see Figure 6.5). In the investigated datasets, targeting nodes with high eigenvector centrality is not as

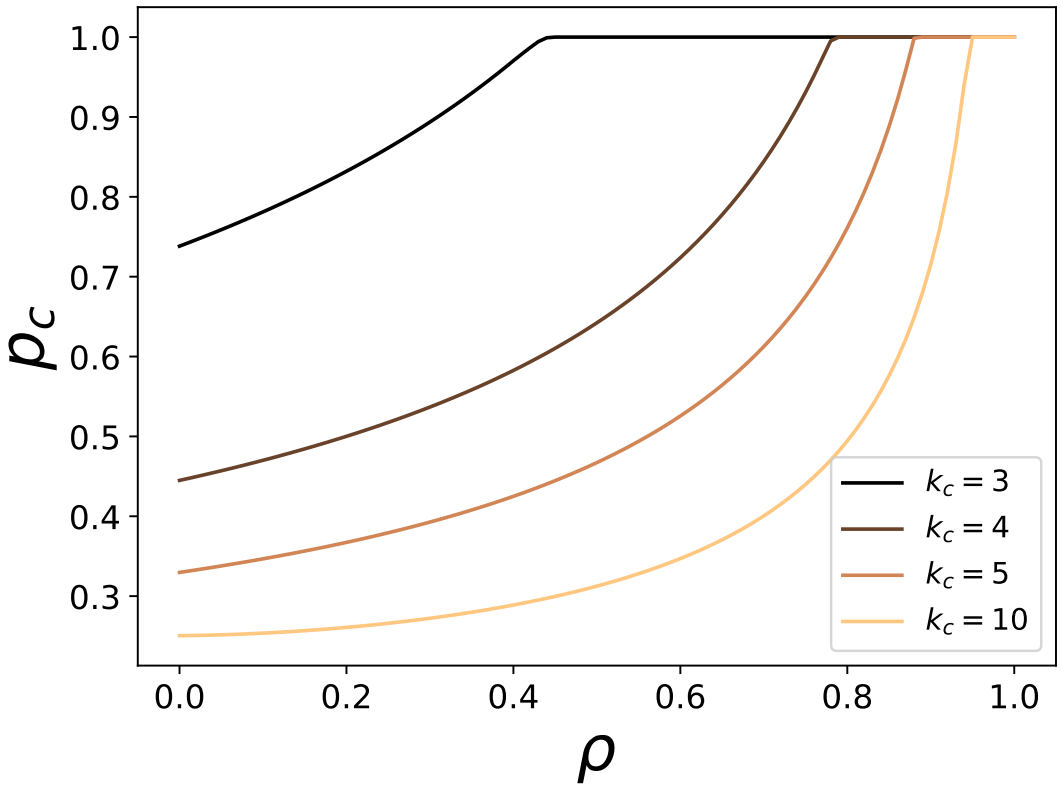

Figure 6.3: The phase diagram of the epidemic model mitigated by the adoption of the app is shown for a Poisson network of $N = 10^4$ nodes with average degree $\lambda = 4$. Here $T(k)$ is given by Eq. 6.29 with $\alpha = 0$. The epidemic threshold p_c is plotted as a function of ρ for different values of the cutoff k_c.

efficient as targeting high-degree nodes, while targeting nodes with high non-backtracking centrality performs much better, nevertheless, it does not change significantly the results obtained by targeting high-degree nodes. These numerical results suggest that in a wide range of real scenarios, targeting high-degree nodes can still be a very efficient algorithm for mitigating an epidemic outbreak.

6.8 Conclusion

In this chapter, we have discussed a message-passing approach proposed in [138] that predicts the epidemic threshold of a disease spreading among a population using a contact-tracing app. The simplicity of this model allows for deriving a simple analytical estima-

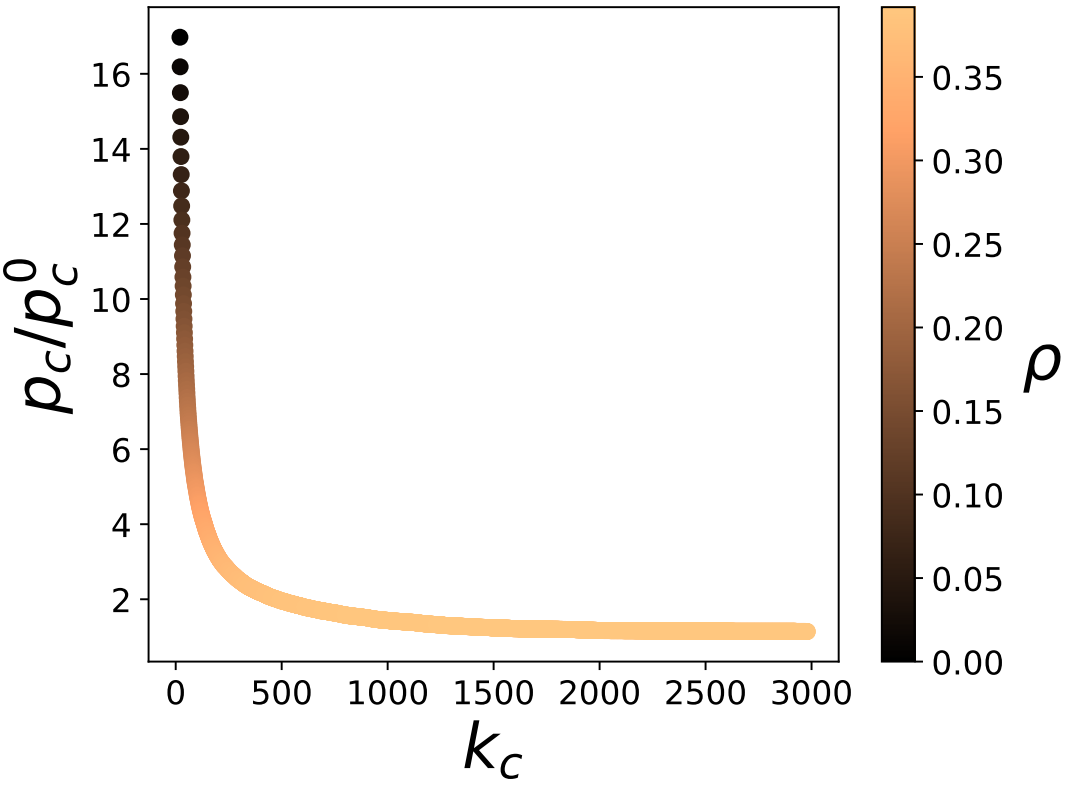

Figure 6.4: (Color online) Relative increase of p_c computed from Eq. 6.25 on the Livemocha social network ($N \sim 104 \times 10^3$ nodes, $E \sim 2 \times 10^6$ edges) [218], where $T(k)$ is given by Eq. 6.29 under the constraint 6.26, and $p_c^0 = \langle k \rangle / \langle k(k-1) \rangle$ represents the value of the percolation threshold in the absence of app coverage (which can be obtained from Eq. 6.25 in the limit $\kappa_T \to 0$). Here $p_c^0 = 0.00306$, while the app coverage is fixed at $\mathcal{T} = 0.39175$, corresponding to an optimal $\tilde{T}(k)$ with $k_c = 20$ and $\alpha = 1$. The plot shows that for this particular value of $\mathcal{T}$, corresponding to ∼40% of the nodes having the app, the optimal distribution is reached at $\rho = 0$ and corresponds to a ∼17-fold increase of p_c, whereas in the case of a purely random strategy, obtained at $\rho = \mathcal{T}$, the increase of p_c is ∼1.2-fold.

tion for the epidemic threshold on uncorrelated random networks and leaves plenty of room for taking into account more complex and realistic factors. The proposed mathematical framework can be used to assess the expected impact of digital contact tracing in the course of an epidemic. Our results show both numerically and theoretically that the adoption of the app by a large fraction of the population increases the value of the

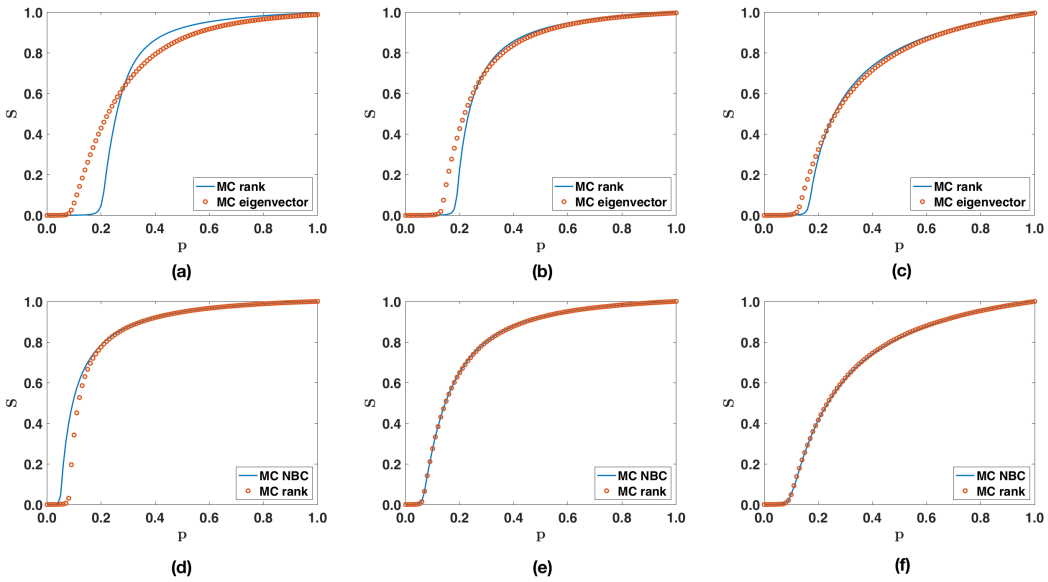

Figure 6.5: We compare the efficiency of different strategies for targeting the adoption of the app including targeting the nodes of high degrees, the nodes of high eigenvector centrality and the nodes of high non-backtracking centrality (NBC) on three different real social network datasets. Specifically, we compare the fraction of infected individuals S as a function of the transmissibility p obtained with the Monte Carlo simulations when the same fraction f of nodes of high centrality adopts the app but the centrality measures can change. In panels (a), (b) and (c) we report results obtained on the real datasets by comparing the strategy in which nodes of high eigenvector centrality are targeted with the strategy in which the same fraction of high-degree nodes are targeted. In panels (d) (e) and (f) a similar comparison is made between the strategy targeting nodes with high non-backtracking centrality and the strategy in which nodes of high degree are targeted. Panels (a)&(d), (b)&(e) and (c)&(f) show the results obtained on the friendship networks from the music streaming site *Deezer* in the countries of Croatia ($N = 54573$), Hungary ($N = 47538$) and Romania ($N = 41773$) respectively [217].

epidemic threshold. In the scenario of uncorrelated random networks, we are able to derive a closed analytical expression for p_c which turns out to depend on both the degree distribution $P(k)$ of the network and the average app distribution $T(k)$. Taking advantage of this closed-form expression, we prove in the scenario of limited resources that the critical threshold p_c is maximized when high-degree nodes are targeted. Our results

show that optimal targeting gives rise to a dramatic increase in the value of p_c when compared to a strategy in which the same amount of resources is uniformly distributed, and an increase of the randomness in app allocation will contribute to the decrease of the effectiveness of the tracing app. In summary, our results show that even if the adoption of a tracing app has the effect of preventing an epidemic wave, the app can still be optimally distributed, by taking into account the heterogeneity of the contact network among the population, in order to obtain a significantly better mitigation effect.

Although this framework is not proposed to precisely fit the current pandemic of COVID-19 (for the sake of analytical results, in the simple model many realistic factors which will also affect the epidemic spreading process have been excluded and some assumptions used may not be precise in the real-world scenarios), the physical intuition we grasp from the presented analysis may prove fundamental to prescribe the best strategy for app adoption, as well as it captures the highly non-linear effect on the reduction of the incidence provided by a certain fraction of app adoption, which may provide some insights to the control of the current pandemic.

Chapter 7

Conclusions

In this thesis, new insights into the relationship between network structure and their dynamic properties are provided. The main contributions of this thesis are two-fold. From the perspective of percolation, percolation theories on higher-order network models are developed, with two main contributions on *Networks with Triadic Interactions* and *Random Multiplex Hypergraphs*. These novel percolation models deepen our understanding of critical behaviors on higher-order networks. From the perspective of epidemic spreading, two novel epidemic models, *i.e.*, epidemic spreading on hypergraphs and epidemic spreading with contact-and-tracing are presented. These models enrich our understanding of the non-linear dynamic of epidemics on networks and provide new insights into real pandemics.

In Chapter 3 and 4, we show how percolation is affected by higher-order network topology on two examples, *i.e.*, networks with triadic interactions and multiplex random hypergraph model. The percolation on networks with triadic interactions provides a framework for modeling systems with time-dependent functioning connectivity such as brain networks and climate networks. By introducing signed triadic interactions that regulate the connectivity of structural links, we define triadic percolation. Triadic percolation behaves very differently from ordinary percolation in the sense that the order

parameter of triadic percolation is a time-dependent variable when both positive and negative regulations are present. The order parameter of triadic percolation can display period doubling and a route to chaos as we change the control parameter, while for ordinary percolation, the order parameter is always a fixed value. The results of triadic percolation radically change our understanding of percolation on networks. It provides new insights that can shed light on the study of brain networks and climate networks. On the other hand, the simple and higher-order percolation processes defined on the random multiplex hypergraph model [76] display very rich phenomenology including the discontinuous phase transition, the tricritical point, and multiple phase transitions which are reported for the first time in this context. Comparing simple and higher-order percolation, we reveal that the collaboration effect, *i.e.*, the requirement of multiple activations leads to discontinuous transition. Indeed, this requirement can be found in many critical phenomena that display discontinuous transitions, such as K-core percolation [112], complex contagion [221], also in empirical studies [222]. Moreover, the multilayer structure allows for defining hyperdegree correlations and investigating the effect on critical behaviors. We show that hyperdegree correlations strongly affect the percolation threshold and have different effects on simple percolation and higher-order percolation. The multiplex hypergraph can be a suitable candidate for modeling brain networks where interactions of different natures (for instance pairwise blood vessels between neurons and higher-order functioning brain interactions) coexist. These percolation models might be used to understand the mechanism of brain functioning.

There are several theoretical generalizations of these models that can be explored in the future. In Chapter 3, we explore the networks with triadic interactions formed by random structural networks and random regulatory networks. This simplified consideration allows us to derive analytical results. In real systems such as brain networks, climate networks, and biochemical reaction networks, the nodes interact in more complicated ways. For instance, in brain networks that are formed by neuron-neuron structural connectivity and glia-neuron regulatory connectivity is *spatial* due to the physical con-

straints. Moreover, since neurons and glia are different types of cells, they can be modeled by a multilayer network. Another example is the biochemical reaction network where enzymes can regulate biochemical reactions that involved multiple reactants. All these examples motivate generalizations of networks with triadic interactions, *i.e.*, spatial networks, multilayer networks and hypergraphs with triadic interactions. Moreover, in [87] we investigate the fraction of active nodes in the network, while there might be other quantities of interest, for example, spatial features of active nodes which might provide more insights into the modeling of brain networks.

In Chapter 5 and Chapter 6, we show how higher-order interactions and containment measures affect the epidemic spreading process in a highly non-trivial way. The epidemic model with digital contact-and-tracing [138] provides theoretical insights into the long-lasting discussion on the effectiveness of this novel way to tackle the COVID-19 pandemic: automated contact-tracing can effectively increase the epidemic threshold hence mitigate a pandemic, and does not require 100% of the population adopting the contact-and-tracing app. The theory further reveals analytically the non-linear relationship between the increment in the level of app adoption and the epidemic threshold. The epidemic model on hypergraphs [78], on the other hand, challenges a commonly used assumption in most epidemic models which is the linear relationship between the number of contact with infected individuals and the risk of infection. We find that higher-order interactions among individuals together with heterogeneous temporal human activity and the threshold effects over the exposure induce a nonlinear infection kernel, which could lead to a discontinuous relationship between disease transmission and epidemic size, to a bistable regime where macroscopic outbreak and disease-free state coexist, and to a super-exponential growth.

The theoretical results obtained in Chapter 5 and Chapter 6 provide rich insights into real pandemics. Many directions can be further explored from the perspective of applications. In the epidemic model with digital contact and tracing, some assumptions used might be relaxed in real scenarios. For instance, in reality, tracing and isolation

might be imperfect, and the probability that an individual adopting a tracing app might not simply depend solely on the degree but on some external information or external dynamic processes. There is some very recent literature examining the effectiveness of the digital contact-and-tracing approach from various perspectives. Ref. [223] designs a controlled experiment in a population to examine the effectiveness while Ref. [224] checks high-resolution empirical data of contact. The results of both studies show evidence of the usefulness of the digital contact-and-tracing approach. There are also a few new theoretical models that consider other realistic factors. Ref. [225] proposes a SIR-like model where awareness of prevention is controlled by the global and local prevalence of the pandemic. Ref. [226] extends the model we propose in [138] by considering a homophilic adoption of contact tracing apps in a population. These theoretical models also suggest novel strategies to improve the mitigation of epidemic waves.

Altogether, we show in this thesis the rich interplay between network structures and their dynamic properties from both perspectives of percolation and epidemic spreading. Novel models proposed in this thesis have deepened our understanding of critical phenomena on networks and their generalizations and we have answered some open questions in this research area. We hope this thesis can generate further interest in the interplay between the topological structure of networks and the dynamical processes defined on them.

Appendix A

Universality class of the route to chaos of triadic percolation

In the main texts of Chapter 3, we have studied triadic percolation in different settings and we have shown that the process can undergo a period-doubling transition. Here we demonstrate that triadic percolation undergoes a route to chaos in the universality class of the logistic map as long as the structural and regulatory degrees are uncorrelated and the distributions $P(\hat{\kappa}^{\pm})$ are Poisson.

Triadic percolation can be captured at the mean-field level by a map

$$R^{(t)} = h(R^{(t-1)}) \tag{A.1}$$

determining the relative size $R^{(t)}$ of the giant component at time t, given the relative size $R^{(t-1)}$ of the giant component at time $t-1$. Examples of these maps obtained from uncorrelated structural Poisson networks are shown in Figure C.1.

Here we show that this map is in the universality class of the logistic map. In order to show that, according to Feigenbaum classic result [147], it is enough to demonstrate that the function $h(R)$ is unimodal, *i.e.*, has a single maximum at $R = R^{\star}$, and that close to

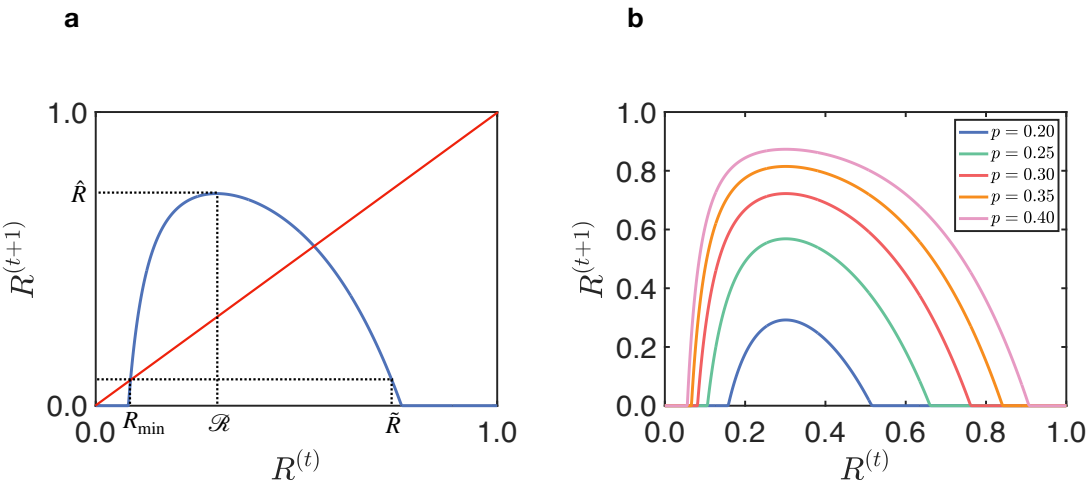

Figure C.1: Example of the maps capturing triadic percolation. Panel (a) shows the map $R^{(t)} = h(R^{(t-1)})$ (in blue) obtained for $p = 0.3$ in the case of a Poisson structural network and uncorrelated regulatory network with Poisson distributions $P(\hat{\kappa}^{\pm})$. The intersections between the red line $R^{(t)} = R^{(t-1)}$ and the map (indicated in blue) determine the fixed points. Here $\underline{R}$ denotes the minimum non-trivial fixed point of the map. The map reaches its maximum $\hat{R}$ for $R = R^{\star}$. We denote with $\bar{R} > \underline{R}$ the point where $h(\bar{R}) = \underline{R}$. Panel (b) displays the map $R^{(t)} = h(R^{t-1})$ for different parameter p. In both panels the structural network is a Poisson network with average degree $c = 30$ and the distributions $\hat{P}_{\pm}(\hat{\kappa}_{\pm})$ are Poisson with average degrees $\langle \hat{\kappa}^{+} \rangle = c^{+} = 1.8$, $\langle \hat{\kappa}^{-} \rangle = c^{-} = 2.5$.

its maximum, *i.e.*, for $|R - R^{\star}| \ll 1$, the function $h(R)$ has a quadratic approximation, with

$$h(R) \simeq h(R^{\star}) + \frac{1}{2} h''(R^{\star})(R - R^{\star})^2. \tag{A.2}$$

To demonstrate this scaling of the function $h(R)$ close to its maximum we provide here the explicit expression of the derivative $dR^{(t)}/dR^{(t-1)}$ in terms of $R^{(t-1)}$ and $R^{(t)} = h(R^{(t-1)})$.

Our starting point will be the formulation of triadic percolation for uncorrelated structural and regulatory degrees of the nodes dictated by the Eqs. 3.7, 3.8 and 3.9,

which we rewrite here for completeness,

$$S^{(t)} = 1 - G_1\left(1 - p_L^{(t-1)} S^{(t)}\right) = F_1\left(p_L^{(t-1)}, S^{(t)}\right), \tag{A.3}$$

$$R^{(t)} = 1 - G_0\left(1 - p_L^{(t-1)} S^{(t)}\right) = F_2\left(p_L^{(t-1)}, S^{(t)}\right), \tag{A.4}$$

$$p_L^{(t)} = pG_0^-\left(1 - R^{(t)}\right)\left[1 - G_0^+\left(1 - R^{(t)}\right)\right] = F_3\left(R^{(t)}\right), \tag{A.5}$$

where $G_1(x)$, $G_0(x)$ and $G_0^{\pm}(x)$ are defined in Eq. (3.10). Starting from Eq. (A.3) and using the chain rule we get

$$\frac{dS^{(t)}}{dR^{(t-1)}} = \frac{\partial F_1}{\partial p_L^{(t-1)}} \frac{dp_L^{(t-1)}}{dR^{(t-1)}} + \frac{\partial F_1}{\partial S^{(t)}} \frac{dS^{(t)}}{dR^{(t-1)}}. \tag{A.6}$$

Thus,

$$\frac{dS^{(t)}}{dR^{(t-1)}} = \frac{\partial F_1}{\partial p_L^{(t-1)}} \frac{dp_L^{(t-1)}}{dR^{(t-1)}} \left(1 - \frac{\partial F_1}{\partial S^{(t)}}\right)^{-1}. \tag{A.7}$$

Similarly, we can use the chain rule starting from Eq. (A.4) to express the derivative $dR^{(t)}/dR^{(t-1)}$, *i.e.*,

$$\frac{dR^{(t)}}{dR^{(t-1)}} = \frac{\partial F_2}{\partial p_L^{(t-1)}} \frac{dp_L^{(t-1)}}{dR^{(t-1)}} + \frac{\partial F_2}{\partial S^{(t)}} \frac{dS^{(t)}}{dR^{(t-1)}}. \tag{A.8}$$

Using Eq.(A.7) and the relation

$$\frac{\partial F_2}{\partial p_L^{(t-1)}} \frac{\partial F_1}{\partial S^{(t)}} = \frac{\partial F_1}{\partial p_L^{(t-1)}} \frac{\partial F_2}{\partial S^{(t)}}, \tag{A.9}$$

we obtain

$$\frac{dR^{(t)}}{dR^{(t-1)}} = \frac{\partial F_2}{\partial p_L^{(t-1)}} \frac{dp_L^{(t-1)}}{dR^{(t-1)}} \left(1 - \frac{\partial F_1}{\partial S^{(t)}}\right)^{-1}, \tag{A.10}$$

where

$$\frac{\partial F_1}{\partial p_L^{(t-1)}} = S^{(t)}\langle k\rangle G_1\left(1-p_L^{(t-1)}S^{(t)}\right), \quad \frac{\partial F_1}{\partial S^{(t)}} = p_L^{(t)}\langle k\rangle G_1\left(1-p_L^{(t-1)}S^{(t)}\right),$$
$$\frac{\partial F_2}{\partial p_L^{(t-1)}} = S^{(t)}G_1'\left(1-p_L^{(t-1)}S^{(t)}\right), \quad \frac{\partial F_2}{\partial S^{(t)}} = p_L^{(t)}G_1'\left(1-p_L^{(t-1)}S^{(t)}\right), \quad \text{(A.11)}$$

and

$$\frac{dp_L^{(t-1)}}{dR^{(t-1)}} = p\left[G_0^-(1-R^{(t-1)})\left\langle\hat{\kappa}^+\right\rangle G_1^+(1-R^{(t-1)}) - \langle\hat{\kappa}^-\rangle G_1^-(1-R^{(t-1)})\left(1-G_0^+(1-R^{(t-1)}\right)\right].$$

Note that here $G_1'(x) = \sum_k k(k-1)x^{k-2}/\langle k\rangle$. From Eq.(A.10) and Eqs.(A.11) it follows that the derivative $dR^{(t)}/dR^{(t-1)}$ vanishes if and only if either $S^{(t)} = 0$ or $dp_L^{(t-1)}/dR^{(t-1)} = 0$. Consequently, the maximum of the map is determined by the condition $dp_L^{(t-1)}/dR^{(t-1)} = 0$. Let us now consider the case in which the distributions $P(\hat{\kappa}^{\pm})$ are Poisson with average degree $c^{\pm}$. In this case $G_0^+(1-R^{(t-1)}) = G_1^+(1-R^{(t-1)}) = \exp(-c^+R^{(t-1)})$ and $G_0^-(1-R^{(t-1)}) = G_1^-(1-R^{(t-1)}) = \exp(-c^-R^{(t-1)})$ and hence

$$\frac{\partial p_L^{(t-1)}}{\partial R^{(t-1)}} = pe^{-c^-R^{(t-1)}}\left[-c^- + (c^+ + c^-)e^{-c^+R^{(t-1)}}\right]. \quad \text{(A.12)}$$

In this case there is only one singular value $R^{(t-1)} = R^\star$ at which $dp_L^{(t-1)}/dR^{(t-1)} = 0$ given by

$$R^\star = \frac{1}{c^+}\ln\left(\frac{c^+ + c^-}{c^-}\right). \quad \text{(A.13)}$$

It is straightforward to show that

$$\left.\frac{d^2p_L^{(t-1)}}{d(R^{(t-1)})^2}\right|_{R^{(t-1)}=R^\star} = -pe^{-(c^-+c^+)R^\star}(c^+ + c^-)c^+, \quad \text{(A.14)}$$

and, as long as $\hat{R} = h(R^\star) > 0$, it follows immediately that

$$\left.\frac{d^2R^{(t)}}{d(R^{(t-1)})^2}\right|_{R^{(t-1)}=R^\star} = \frac{\partial F_2}{\partial p_L^{(t-1)}}\frac{\partial^2 p_L^{(t-1)}}{\partial (R^{(t-1)})^2}\left(1-\frac{\partial F_1}{\partial S^{(t)}}\right)^{-1}\Bigg|_{R^{(t-1)}=R^\star} < 0. \quad \text{(A.15)}$$

Hence the scaling of the map close to the maximum is quadratic proving that the universality class of triadic percolation is the one of the logistic map as long as the structural and the regulatory degrees are uncorrelated and $P(\hat{\kappa}^{\pm})$ are Poisson distributions.

Appendix B

Further information about the real datasets

We provide further information about the two datasets studied in Figure 3.7 of the main text. In Table D.1 we provide the major structural properties of the networks and in Figure D.1 we report their degree distribution.

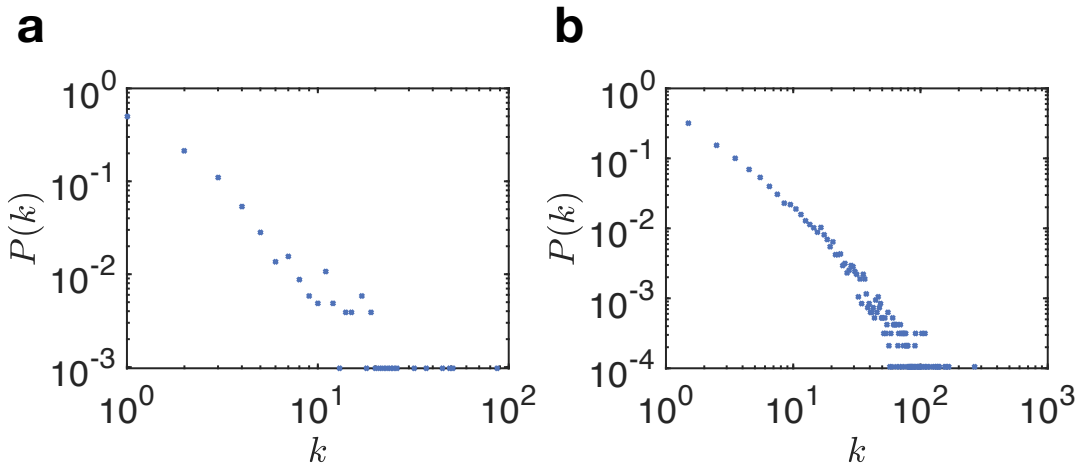

Figure D.1: Degree distribution $P(k)$ of structural mouse brain network (a) and structural Human bio grid network (b) from [154].

Network	C	k_{min}	k_{max}	N	L	R
Mouse Brain [154]	0	1	123	1029	1559	0.9592
Human bio grid [154]	0.1612	1	308	9436	31182	0.9642

Table D.1: Structural properties of the real-world networks: the averaged clustering coefficient C, minimum degree k_{min}, maximum degree k_{max}, number of nodes N, number of links L and the fraction of node in the giant component R. Both networks are treated as undirected networks.

Appendix C

Optimization

In Chapter 6 we study the optimization problem that reads

$$\max_{T(k)} \mathcal{O} = \sum_k k(k-1)P(k)T(k) \;\text{ subject to }\; \begin{cases} \sum_k P(k)T(k) = \mathcal{T}, \\ 0 \leq T(k) \leq 1. \end{cases} \tag{C.1}$$

where k denotes the degree of a node, $P(k)$ denotes a given degree distribution and $T(k)$ denotes the probability for a node with degree k to adopt the contact-and-tracing app. The objective function indicates that when using the same amount of budget $P(k)T(k)$ from the constraint $\sum_k P(k)T(k) = \mathcal{T}$, the terms with larger k in the summation have more significant contributions to the objective. Thus, the maximum of the objective is obtained by maximizing $k(k-1)P(k)T(k)$ from larger k. Each term $k(k-1)P(k)T(k)$ reaches its maximum when $T(k) = 1$ hence we impose $T(k) = 1$ for all $k > k_c$ where k_c is a threshold that due to the constraint $T(k) = 1$ cannot be achieved at $k = k_c$. Instead $T(k) = \alpha$ where

$$0 \leq \alpha = \mathcal{T} - \sum_{k>k_c} P(k) < 1. \tag{C.2}$$

In other words, at $k = k_c$, all the remaining budget $\alpha = \mathcal{T} - \sum_{k>k_c} P(k)$ is allocated. Hence the optimal $\tilde{T}(k)$ is in the form of a discrete Heaviside step function that reads

$$\tilde{T}(k) = \theta(k - k_c, \alpha) \tag{C.3}$$

taking the value $0 \leq \alpha = \mathcal{T} - \sum_{k>k_c} P(k) < 1$ at $k = k_c$.

References

[1] N. W. Landry and J. G. Restrepo, "The effect of heterogeneity on hypergraph contagion models," *Chaos*, vol. 30, no. 10, p. 103117, 2020.

[2] A. P. Millán, J. J. Torres, and G. Bianconi, "Explosive higher-order kuramoto dynamics on simplicial complexes," *Physical Review Letters*, vol. 124, no. 21, p. 218301, 2020.

[3] I. Iacopini, G. Petri, A. Barrat, and V. Latora, "Simplicial models of social contagion," *Nature communications*, vol. 10, no. 1, pp. 1–9, 2019.

[4] J. T. Matamalas, S. Gómez, and A. Arenas, "Abrupt phase transition of epidemic spreading in simplicial complexes," *Physical Review Research*, vol. 2, no. 1, p. 012049, 2020.

[5] G. F. de Arruda, G. Petri, and Y. Moreno, "Social contagion models on hypergraphs," *Physical Review Research*, vol. 2, no. 2, p. 023032, 2020.

[6] B. Jhun, M. Jo, and B. Kahng, "Simplicial SIS model in scale-free uniform hypergraph," *J. Stat. Mech.*, vol. 2019, p. 123207, 2019.

[7] M. E. Newman, "Spread of epidemic disease on networks," *Physical review E*, vol. 66, no. 1, p. 016128, 2002.

[8] R. Pastor-Satorras, C. Castellano, P. Van Mieghem, and A. Vespignani, "Epidemic processes in complex networks," *Reviews of modern physics*, vol. 87, no. 3, p. 925, 2015.

[9] M. E. Newman, S. H. Strogatz, and D. J. Watts, "Random graphs with arbitrary degree distributions and their applications," *Physical review E*, vol. 64, no. 2, p. 026118, 2001.

[10] R. Cohen, K. Erez, D. Ben-Avraham, and S. Havlin, "Resilience of the internet to random breakdowns," *Physical review letters*, vol. 85, no. 21, p. 4626, 2000.

[11] S. V. Buldyrev, R. Parshani, G. Paul, H. E. Stanley, and S. Havlin, "Catastrophic cascade of failures in interdependent networks," *Nature*, vol. 464, no. 7291, pp. 1025–1028, 2010.

[12] R. Parshani, S. V. Buldyrev, and S. Havlin, "Interdependent networks: Reducing

the coupling strength leads to a change from a first to second order percolation transition," *Physical review letters*, vol. 105, no. 4, p. 048701, 2010.

[13] F. Radicchi and G. Bianconi, "Redundant interdependencies boost the robustness of multiplex networks," *Physical Review X*, vol. 7, no. 1, p. 011013, 2017.

[14] B. Min, S. Do Yi, K.-M. Lee, and K.-I. Goh, "Network robustness of multiplex networks with interlayer degree correlations," *Physical Review E*, vol. 89, no. 4, p. 042811, 2014.

[15] V. Nicosia and V. Latora, "Measuring and modeling correlations in multiplex networks," *Physical Review E*, vol. 92, no. 3, p. 032805, 2015.

[16] D. Cellai, S. N. Dorogovtsev, and G. Bianconi, "Message passing theory for percolation models on multiplex networks with link overlap," *Physical Review E*, vol. 94, no. 3, p. 032301, 2016.

[17] B. Min, S. Lee, K.-M. Lee, and K.-I. Goh, "Link overlap, viability, and mutual percolation in multiplex networks," *Chaos, Solitons & Fractals*, vol. 72, pp. 49–58, 2015.

[18] S. Boettcher, V. Singh, and R. M. Ziff, "Ordinary percolation with discontinuous transitions," *Nature communications*, vol. 3, no. 1, p. 787, 2012.

[19] G. Bianconi and R. M. Ziff, "Topological percolation on hyperbolic simplicial complexes," *Physical Review E*, vol. 98, no. 5, p. 052308, 2018.

[20] I. Kryven and G. Bianconi, "Enhancing the robustness of a multiplex network leads to multiple discontinuous percolation transitions," *Physical Review E*, vol. 100, no. 2, p. 020301, 2019.

[21] G. Bianconi, I. Kryven, and R. M. Ziff, "Percolation on branching simplicial and cell complexes and its relation to interdependent percolation," *Physical Review E*, vol. 100, no. 6, p. 062311, 2019.

[22] H. Sun, R. M. Ziff, and G. Bianconi, "Renormalization group theory of percolation on pseudofractal simplicial and cell complexes," *Physical Review E*, vol. 102, no. 1, p. 012308, 2020.

[23] B. C. Coutinho, A.-K. Wu, H.-J. Zhou, and Y.-Y. Liu, "Covering problems and core percolations on hypergraphs," *Physical Review Letters*, vol. 124, no. 24, p.

248301, 2020.

[24] G. Ghoshal, V. Zlatić, G. Caldarelli, and M. E. Newman, "Random hypergraphs and their applications," *Physical Review E*, vol. 79, no. 6, p. 066118, 2009.

[25] S. Gomez, A. Diaz-Guilera, J. Gomez-Gardenes, C. J. Perez-Vicente, Y. Moreno, and A. Arenas, "Diffusion dynamics on multiplex networks," *Physical review letters*, vol. 110, no. 2, p. 028701, 2013.

[26] A. Sole-Ribalta, M. De Domenico, N. E. Kouvaris, A. Diaz-Guilera, S. Gomez, and A. Arenas, "Spectral properties of the laplacian of multiplex networks," *Physical Review E*, vol. 88, no. 3, p. 032807, 2013.

[27] J. J. Torres and G. Bianconi, "Simplicial complexes: higher-order spectral dimension and dynamics," *Journal of Physics: Complexity*, vol. 1, no. 1, p. 015002, 2020.

[28] M. T. Schaub, A. R. Benson, P. Horn, G. Lippner, and A. Jadbabaie, "Random walks on simplicial complexes and the normalized hodge 1-laplacian," *SIAM Review*, vol. 62, no. 2, pp. 353–391, 2020.

[29] S. Majhi, M. Perc, and D. Ghosh, "Dynamics on higher-order networks: A review," *Journal of the Royal Society Interface*, vol. 19, no. 188, p. 20220043, 2022.

[30] L. Böttcher and M. A. Porter, "Complex networks with complex weights," *arXiv preprint arXiv:2212.06257*, 2022.

[31] T. Mendes-Santos, M. Schmitt, A. Angelone, A. Rodriguez, P. Scholl, H. Williams, D. Barredo, T. Lahaye, A. Browaeys, M. Heyl *et al.*, "Wave function network description and kolmogorov complexity of quantum many-body systems," *arXiv preprint arXiv:2301.13216*, 2023.

[32] E. Bairey, E. D. Kelsic, and R. Kishony, "High-order species interactions shape ecosystem diversity," *Nature communications*, vol. 7, no. 1, p. 12285, 2016.

[33] J. Grilli, G. Barabás, M. J. Michalska-Smith, and S. Allesina, "Higher-order interactions stabilize dynamics in competitive network models," *Nature*, vol. 548, no. 7666, p. 210, 2017.

[34] A. D. Letten and D. B. Stouffer, "The mechanistic basis for higher-order interactions and non-additivity in competitive communities," *Ecology letters*, vol. 22,

no. 3, pp. 423–436, 2019.

[35] J. M. Levine, J. Bascompte, P. B. Adler, and S. Allesina, "Beyond pairwise mechanisms of species coexistence in complex communities," *Nature*, vol. 546, no. 7656, pp. 56–64, 2017.

[36] J. Jost and R. Mulas, "Hypergraph laplace operators for chemical reaction networks," *Advances in mathematics*, vol. 351, pp. 870–896, 2019.

[37] A. E. Sizemore, C. Giusti, A. Kahn, J. M. Vettel, R. F. Betzel, and D. S. Bassett, "Cliques and cavities in the human connectome," *Journal of computational neuroscience*, vol. 44, pp. 115–145, 2018.

[38] C. Giusti, E. Pastalkova, C. Curto, and V. Itskov, "Clique topology reveals intrinsic geometric structure in neural correlations," *Proceedings of the National Academy of Sciences*, vol. 112, no. 44, pp. 13 455–13 460, 2015.

[39] E. Kuzmin, B. VanderSluis, W. Wang, G. Tan, R. Deshpande, Y. Chen, M. Usaj, A. Balint, M. Mattiazzi Usaj, J. Van Leeuwen *et al.*, "Systematic analysis of complex genetic interactions," *Science*, vol. 360, no. 6386, p. eaao1729, 2018.

[40] N. Boers, B. Goswami, A. Rheinwalt, B. Bookhagen, B. Hoskins, and J. Kurths, "Complex networks reveal global pattern of extreme-rainfall teleconnections," *Nature*, vol. 566, no. 7744, pp. 373–377, 2019.

[41] Z. Su, H. Meyerhenke, and J. Kurths, "The climatic interdependence of extreme-rainfall events around the globe," *Chaos: An Interdisciplinary Journal of Nonlinear Science*, vol. 32, no. 4, p. 043126, 2022.

[42] C. Giusti, R. Ghrist, and D. S. Bassett, "Two's company, three (or more) is a simplex," *Journal of computational neuroscience*, vol. 41, no. 1, pp. 1–14, 2016.

[43] J. Faskowitz, R. F. Betzel, and O. Sporns, "Edges in brain networks: Contributions to models of structure and function," *Network Neuroscience*, vol. 6, no. 1, pp. 1–28, 2022.

[44] E. Schneidman, M. J. Berry, R. Segev, and W. Bialek, "Weak pairwise correlations imply strongly correlated network states in a neural population," *Nature*, vol. 440, no. 7087, pp. 1007–1012, 2006.

[45] C. Castellano, S. Fortunato, and V. Loreto, "Statistical physics of social dynamics,"

Reviews of modern physics, vol. 81, no. 2, p. 591, 2009.

[46] A. Barrat, M. Barthelemy, and A. Vespignani, *Dynamical processes on complex networks*. Cambridge university press, 2008.

[47] A. Arenas, A. Díaz-Guilera, J. Kurths, Y. Moreno, and C. Zhou, "Synchronization in complex networks," *Physics reports*, vol. 469, no. 3, pp. 93–153, 2008.

[48] N. Masuda, M. A. Porter, and R. Lambiotte, "Random walks and diffusion on networks," *Physics reports*, vol. 716, pp. 1–58, 2017.

[49] G. Bianconi, *Multilayer networks: structure and function*. Oxford university press, 2018.

[50] S. Wasserman and K. Faust, "Social network analysis: Methods and applications," 1994.

[51] P. Holme and J. Saramäki, "Temporal networks," *Physics reports*, vol. 519, no. 3, pp. 97–125, 2012.

[52] ——, *Temporal network theory*. Springer, 2019, vol. 2.

[53] J. Gao, S. V. Buldyrev, S. Havlin, and H. E. Stanley, "Robustness of a network of networks," *Physical review letters*, vol. 107, no. 19, p. 195701, 2011.

[54] G. Bianconi and S. N. Dorogovtsev, "Multiple percolation transitions in a configuration model of a network of networks," *Physical Review E*, vol. 89, no. 6, p. 062814, 2014.

[55] G. Bianconi, S. N. Dorogovtsev, and J. F. Mendes, "Mutually connected component of networks of networks with replica nodes," *Physical Review E*, vol. 91, no. 1, p. 012804, 2015.

[56] K. Lewis, J. Kaufman, M. Gonzalez, A. Wimmer, and N. Christakis, "Tastes, ties, and time: A new social network dataset using facebook. com," *Social networks*, vol. 30, no. 4, pp. 330–342, 2008.

[57] E. Omodei, M. De Domenico, and A. Arenas, "Characterizing interactions in online social networks during exceptional events," *Frontiers in Physics*, vol. 3, p. 59, 2015.

[58] H. Abdi and L. J. Williams, "Principal component analysis," *Wiley interdisciplinary reviews: computational statistics*, vol. 2, no. 4, pp. 433–459, 2010.

[59] J. Bennett, S. Lanning *et al.*, "The netflix prize," in *Proceedings of KDD cup and*

workshop, vol. 2007. New York, 2007, p. 35.

[60] P. Kazienko, K. Musial, and T. Kajdanowicz, "Multidimensional social network in the social recommender system," *IEEE Transactions on Systems, Man, and Cybernetics-Part A: Systems and Humans*, vol. 41, no. 4, pp. 746–759, 2011.

[61] A. Cardillo, J. Gómez-Gardenes, M. Zanin, M. Romance, D. Papo, F. d. Pozo, and S. Boccaletti, "Emergence of network features from multiplexity," *Scientific reports*, vol. 3, no. 1, pp. 1–6, 2013.

[62] C. D. Brummitt, R. M. D'Souza, and E. A. Leicht, "Suppressing cascades of load in interdependent networks," *Proceedings of the national academy of sciences*, vol. 109, no. 12, pp. E680–E689, 2012.

[63] M. De Domenico, A. Solé-Ribalta, S. Gómez, and A. Arenas, "Navigability of interconnected networks under random failures," *Proceedings of the National Academy of Sciences*, vol. 111, no. 23, pp. 8351–8356, 2014.

[64] R. Hausmann, C. A. Hidalgo, S. Bustos, M. Coscia, and A. Simoes, *The atlas of economic complexity: Mapping paths to prosperity.* Mit Press, 2014.

[65] A. Tacchella, M. Cristelli, G. Caldarelli, A. Gabrielli, and L. Pietronero, "A new metrics for countries' fitness and products' complexity," *Scientific reports*, vol. 2, no. 1, p. 723, 2012.

[66] L. Bennett, A. Kittas, G. Muirhead, L. G. Papageorgiou, and S. Tsoka, "Detection of composite communities in multiplex biological networks," *Scientific reports*, vol. 5, no. 1, p. 10345, 2015.

[67] E. Bullmore and O. Sporns, "Complex brain networks: graph theoretical analysis of structural and functional systems," *Nature reviews neuroscience*, vol. 10, no. 3, pp. 186–198, 2009.

[68] J. A. Dunne, R. J. Williams, and N. D. Martinez, "Network structure and biodiversity loss in food webs: robustness increases with connectance," *Ecology letters*, vol. 5, no. 4, pp. 558–567, 2002.

[69] C. J. Melián, J. Bascompte, P. Jordano, and V. Krivan, "Diversity in a complex ecological network with two interaction types," *Oikos*, vol. 118, no. 1, pp. 122–130, 2009.

[70] S. Pilosof, M. A. Porter, M. Pascual, and S. Kéfi, "The multilayer nature of ecological networks," *Nature Ecology & Evolution*, vol. 1, no. 4, p. 0101, 2017.

[71] R. J. Williams and N. D. Martinez, "Simple rules yield complex food webs," *Nature*, vol. 404, no. 6774, pp. 180–183, 2000.

[72] J. F. Donges, Y. Zou, N. Marwan, and J. Kurths, "The backbone of the climate network," *Europhysics Letters*, vol. 87, no. 4, p. 48007, 2009.

[73] ——, "Complex networks in climate dynamics: Comparing linear and nonlinear network construction methods," *The European Physical Journal Special Topics*, vol. 174, no. 1, pp. 157–179, 2009.

[74] F. Battiston, E. Amico, A. Barrat, G. Bianconi, G. Ferraz de Arruda, B. Franceschiello, I. Iacopini, S. Kéfi, V. Latora, Y. Moreno *et al.*, "The physics of higher-order interactions in complex systems," *Nature Physics*, vol. 17, no. 10, pp. 1093–1098, 2021.

[75] F. Battiston, G. Cencetti, I. Iacopini, V. Latora, M. Lucas, A. Patania, J.-G. Young, and G. Petri, "Networks beyond pairwise interactions: Structure and dynamics," *Phys. Rep.*, vol. 874, pp. 1–92, 2020.

[76] H. Sun and G. Bianconi, "Higher-order percolation processes on multiplex hypergraphs," *Physical Review E*, vol. 104, no. 3, p. 034306, 2021.

[77] I. Kryven, R. M. Ziff, and G. Bianconi, "Renormalization group for link percolation on planar hyperbolic manifolds," *Physical Review E*, vol. 100, no. 2, p. 022306, 2019.

[78] G. St-Onge, H. Sun, A. Allard, L. Hébert-Dufresne, and G. Bianconi, "Universal nonlinear infection kernel from heterogeneous exposure on higher-order networks," *Physical review letters*, vol. 127, no. 15, p. 158301, 2021.

[79] G. St-Onge, V. Thibeault, A. Allard, L. J. Dubé, and L. Hébert-Dufresne, "Master equation analysis of mesoscopic localization in contagion dynamics on higher-order networks," *Phys. Rev. E*, vol. 103, p. 032301, 2021. [Online]. Available: https://link.aps.org/doi/10.1103/PhysRevE.103.032301

[80] P. S. Skardal and A. Arenas, "Abrupt desynchronization and extensive multistability in globally coupled oscillator simplexes," *Physical review letters*, vol. 122,

no. 24, p. 248301, 2019.

[81] A. P. Millán, J. J. Torres, and G. Bianconi, "Complex network geometry and frustrated synchronization," *Scientific reports*, vol. 8, no. 1, pp. 1–10, 2018.

[82] A. P. Millán, R. Ghorbanchian, N. Defenu, F. Battiston, and G. Bianconi, "Local topological moves determine global diffusion properties of hyperbolic higher-order networks," *Physical Review E*, vol. 104, no. 5, p. 054302, 2021.

[83] G. Bianconi, *Higher-order networks*. Cambridge University Press, 2021.

[84] A. Patania, F. Vaccarino, and G. Petri, "Topological analysis of data," *EPJ Data Science*, vol. 6, no. 1, pp. 1–6, 2017.

[85] F. Baccini, F. Geraci, and G. Bianconi, "Weighted simplicial complexes and their representation power of higher-order network data and topology," *Physical Review E*, vol. 106, no. 3, p. 034319, 2022.

[86] Y. Zhang, M. Lucas, and F. Battiston, "Higher-order interactions shape collective dynamics differently in hypergraphs and simplicial complexes," *Nature Communications*, vol. 14, no. 1, p. 1605, 2023.

[87] H. Sun, F. Radicchi, J. Kurths, and G. Bianconi, "The dynamic nature of percolation on networks with triadic interactions," *Nature Communications*, vol. 14, no. 1, p. 1308, 2023.

[88] S. N. Dorogovtsev, A. V. Goltsev, and J. F. Mendes, "Critical phenomena in complex networks," *Reviews of Modern Physics*, vol. 80, no. 4, p. 1275, 2008.

[89] M. Li, R.-R. Liu, L. Lü, M.-B. Hu, S. Xu, and Y.-C. Zhang, "Percolation on complex networks: Theory and application," *Physics Reports*, vol. 907, pp. 1–68, 2021.

[90] N. Araújo, P. Grassberger, B. Kahng, K. Schrenk, and R. M. Ziff, "Recent advances and open challenges in percolation," *The European Physical Journal Special Topics*, vol. 223, pp. 2307–2321, 2014.

[91] R. Cohen, K. Erez, D. Ben-Avraham, and S. Havlin, "Breakdown of the internet under intentional attack," *Physical review letters*, vol. 86, no. 16, p. 3682, 2001.

[92] D. Stauffer and A. Aharony, *Introduction to percolation theory*. CRC press, 2018.

[93] M. Ohzeki, "Duality with real-space renormalization and its application to bond

percolation," *Physical Review E*, vol. 87, no. 1, p. 012137, 2013.

[94] H. Duminil-Copin, "Sixty years of percolation," in *Proceedings of the International Congress of Mathematicians: Rio de Janeiro 2018*. World Scientific, 2018, pp. 2829–2856.

[95] M. Newman and R. M. Ziff, "Efficient monte carlo algorithm and high-precision results for percolation," *Physical Review Letters*, vol. 85, no. 19, p. 4104, 2000.

[96] Y. Deng and H. W. Blöte, "Monte carlo study of the site-percolation model in two and three dimensions," *Physical Review E*, vol. 72, no. 1, p. 016126, 2005.

[97] J. Hammersley, "Bornes supérieures de la probabilité critique dans un processus de filtration," *Le Calcul des Probabilités et ses Applications, CNRS, Paris*, pp. 17–37, 1959.

[98] M. Mensikov, "Coincidence of critical points in percolation problems," in *Soviet Mathematics Doklady*, vol. 33, 1986, pp. 856–859.

[99] M. Aizenman and D. J. Barsky, "Sharpness of the phase transition in percolation models," *Communications in Mathematical Physics*, vol. 108, no. 3, pp. 489–526, 1987.

[100] M. Aizenman, H. Kesten, and C. M. Newman, "Uniqueness of the infinite cluster and continuity of connectivity functions for short and long range percolation," *Communications in Mathematical Physics*, vol. 111, no. 4, pp. 505–531, 1987.

[101] R. M. Burton and M. Keane, "Density and uniqueness in percolation," *Communications in mathematical physics*, vol. 121, pp. 501–505, 1989.

[102] M. Molloy and B. Reed, "A critical point for random graphs with a given degree sequence," *Random structures & algorithms*, vol. 6, no. 2-3, pp. 161–180, 1995.

[103] ——, "The size of the giant component of a random graph with a given degree sequence," *Combinatorics, probability and computing*, vol. 7, no. 3, pp. 295–305, 1998.

[104] N. Schwartz, R. Cohen, D. Ben-Avraham, A.-L. Barabási, and S. Havlin, "Percolation in directed scale-free networks," *Physical Review E*, vol. 66, no. 1, p. 015104, 2002.

[105] M. M. Danziger, A. Bashan, Y. Berezin, and S. Havlin, "Percolation and cas-

cade dynamics of spatial networks with partial dependency," *Journal of Complex Networks*, vol. 2, no. 4, pp. 460–474, 2014.

[106] B. Gross and S. Havlin, "Percolation in spatial networks: Spatial network models beyond nearest neighbours structures," *Elements in Structure and Dynamics of Complex Networks*, 2022.

[107] R. Parshani, C. Rozenblat, D. Ietri, C. Ducruet, and S. Havlin, "Inter-similarity between coupled networks," *Europhysics Letters*, vol. 92, no. 6, p. 68002, 2011.

[108] G. Baxter, S. Dorogovtsev, A. Goltsev, and J. Mendes, "Avalanche collapse of interdependent networks," *Physical review letters*, vol. 109, no. 24, p. 248701, 2012.

[109] S. V. Buldyrev, N. W. Shere, and G. A. Cwilich, "Interdependent networks with identical degrees of mutually dependent nodes," *Physical Review E*, vol. 83, no. 1, p. 016112, 2011.

[110] S. Boccaletti, G. Bianconi, R. Criado, C. I. Del Genio, J. Gómez-Gardenes, M. Romance, I. Sendina-Nadal, Z. Wang, and M. Zanin, "The structure and dynamics of multilayer networks," *Physics reports*, vol. 544, no. 1, pp. 1–122, 2014.

[111] M. Kivelä, A. Arenas, M. Barthelemy, J. P. Gleeson, Y. Moreno, and M. A. Porter, "Multilayer networks," *Journal of complex networks*, vol. 2, no. 3, pp. 203–271, 2014.

[112] S. N. Dorogovtsev, A. V. Goltsev, and J. F. F. Mendes, "K-core organization of complex networks," *Physical review letters*, vol. 96, no. 4, p. 040601, 2006.

[113] A. V. Goltsev, S. N. Dorogovtsev, and J. F. F. Mendes, "k-core (bootstrap) percolation on complex networks: Critical phenomena and nonlocal effects," *Physical Review E*, vol. 73, no. 5, p. 056101, 2006.

[114] D. Lee, M. Jo, and B. Kahng, "Critical behavior of k-core percolation: Numerical studies," *Physical Review E*, vol. 94, no. 6, p. 062307, 2016.

[115] R. M. D'Souza, J. Gómez-Gardenes, J. Nagler, and A. Arenas, "Explosive phenomena in complex networks," *Advances in Physics*, vol. 68, no. 3, pp. 123–223, 2019.

[116] R. A. da Costa, S. N. Dorogovtsev, A. V. Goltsev, and J. F. F. Mendes, "Explosive

percolation transition is actually continuous," *Physical review letters*, vol. 105, no. 25, p. 255701, 2010.

[117] D. Achlioptas, R. M. D'Souza, and J. Spencer, "Explosive percolation in random networks," *science*, vol. 323, no. 5920, pp. 1453–1455, 2009.

[118] O. Riordan and L. Warnke, "Explosive percolation is continuous," *Science*, vol. 333, no. 6040, pp. 322–324, 2011.

[119] G. J. Baxter, R. A. Da Costa, S. N. Dorogovtsev, and J. F. Mendes, *Weak multiplex percolation*. Cambridge University Press, 2021.

[120] O. Bobrowski and P. Skraba, "Homological percolation and the euler characteristic," *Physical Review E*, vol. 101, no. 3, p. 032304, 2020.

[121] Y. Lee, J. Lee, S. M. Oh, D. Lee, and B. Kahng, "Homological percolation transitions in growing simplicial complexes," *Chaos: An Interdisciplinary Journal of Nonlinear Science*, vol. 31, no. 4, p. 041102, 2021.

[122] S.-W. Son, G. Bizhani, C. Christensen, P. Grassberger, and M. Paczuski, "Percolation theory on interdependent networks based on epidemic spreading," *EPL (Europhysics Letters)*, vol. 97, no. 1, p. 16006, 2012.

[123] D. Zhou, J. Gao, H. E. Stanley, and S. Havlin, "Percolation of partially interdependent scale-free networks," *Physical Review E*, vol. 87, no. 5, p. 052812, 2013.

[124] G. Bianconi and A. Capocci, "Number of loops of size h in growing scale-free networks," *Physical review letters*, vol. 90, no. 7, p. 078701, 2003.

[125] G. Parisi and T. Rizzo, "k-core percolation in four dimensions," *Physical Review E*, vol. 78, no. 2, p. 022101, 2008.

[126] J. M. Schwarz, A. J. Liu, and L. Chayes, "The onset of jamming as the sudden emergence of an infinite k-core cluster," *Europhysics Letters*, vol. 73, no. 4, p. 560, 2006.

[127] J. Gao, S. V. Buldyrev, H. E. Stanley, and S. Havlin, "Networks formed from interdependent networks," *Nature physics*, vol. 8, no. 1, pp. 40–48, 2012.

[128] M. Plischke and B. Bergersen, *Equilibrium statistical physics*. World scientific, 1994.

[129] H. Sun, D. Saad, and A. Y. Lokhov, "Competition, collaboration, and optimization

in multiple interacting spreading processes," *Physical Review X*, vol. 11, no. 1, p. 011048, 2021.

[130] R. Cohen, S. Havlin, and D. Ben-Avraham, "Efficient immunization strategies for computer networks and populations," *Phys. Rev. Lett.*, vol. 91, no. 24, p. 247901, 2003.

[131] W. O. Kermack and A. G. McKendrick, "A Contribution to the Mathematical Theory of Epidemics," *Proc. R. Soc. A*, vol. 115, pp. 700–721, 1927.

[132] M. Mézard, G. Parisi, and M. A. Virasoro, *Spin glass theory and beyond: An Introduction to the Replica Method and Its Applications.* World Scientific Publishing Company, 1987, vol. 9.

[133] M. Mezard and A. Montanari, *Information, physics, and computation.* Oxford University Press, 2009.

[134] J. S. Yedidia, W. Freeman, and Y. Weiss, "Generalized belief propagation," *Advances in neural information processing systems*, vol. 13, 2000.

[135] A. Y. Lokhov, M. Mézard, H. Ohta, and L. Zdeborová, "Inferring the origin of an epidemic with a dynamic message-passing algorithm," *Physical Review E*, vol. 90, no. 1, p. 012801, 2014.

[136] A. Y. Lokhov, M. Mézard, and L. Zdeborová, "Dynamic message-passing equations for models with unidirectional dynamics," *Physical Review E*, vol. 91, no. 1, p. 012811, 2015.

[137] A. Y. Lokhov and D. Saad, "Optimal deployment of resources for maximizing impact in spreading processes," *Proceedings of the National Academy of Sciences*, vol. 114, no. 39, pp. E8138–E8146, 2017.

[138] G. Bianconi, H. Sun, G. Rapisardi, and A. Arenas, "Message-passing approach to epidemic tracing and mitigation with apps," *Physical Review Research*, vol. 3, no. 1, p. L012014, 2021.

[139] F. Altarelli, A. Braunstein, L. Dall'Asta, J. R. Wakeling, and R. Zecchina, "Containing epidemic outbreaks by message-passing techniques," *Physical Review X*, vol. 4, no. 2, p. 021024, 2014.

[140] B. Karrer, M. E. Newman, and L. Zdeborová, "Percolation on sparse networks,"

Physical review letters, vol. 113, no. 20, p. 208702, 2014.

[141] B. Karrer and M. E. Newman, "Message passing approach for general epidemic models," *Physical Review E*, vol. 82, no. 1, p. 016101, 2010.

[142] S. Melnik, A. Hackett, M. A. Porter, P. J. Mucha, and J. P. Gleeson, "The unreasonable effectiveness of tree-based theory for networks with clustering," *Physical Review E*, vol. 83, no. 3, p. 036112, 2011.

[143] A. Kirkley, G. T. Cantwell, and M. Newman, "Belief propagation for networks with loops," *Science Advances*, vol. 7, no. 17, p. eabf1211, 2021.

[144] G. T. Cantwell and M. E. Newman, "Message passing on networks with loops," *Proceedings of the National Academy of Sciences*, vol. 116, no. 47, pp. 23 398–23 403, 2019.

[145] K.-i. Hashimoto, "Zeta functions of finite graphs and representations of p-adic groups," in *Automorphic forms and geometry of arithmetic varieties*. Elsevier, 1989, pp. 211–280.

[146] G. Bianconi, "Fluctuations in percolation of sparse complex networks," *Physical Review E*, vol. 96, no. 1, p. 012302, 2017.

[147] M. J. Feigenbaum, "Quantitative universality for a class of nonlinear transformations," *Journal of statistical physics*, vol. 19, no. 1, pp. 25–52, 1978.

[148] D. d'Humieres, M. Beasley, B. Huberman, and A. Libchaber, "Chaotic states and routes to chaos in the forced pendulum," *Physical Review A*, vol. 26, no. 6, p. 3483, 1982.

[149] F. Radicchi, "Percolation in real interdependent networks," *Nature Physics*, vol. 11, no. 7, pp. 597–602, 2015.

[150] K. Zhao and G. Bianconi, "Percolation on interacting, antagonistic networks," *Journal of Statistical Mechanics: Theory and Experiment*, vol. 2013, no. 05, p. P05005, 2013.

[151] A. Majdandzic, L. A. Braunstein, C. Curme, I. Vodenska, S. Levy-Carciente, H. Eugene Stanley, and S. Havlin, "Multiple tipping points and optimal repairing in interacting networks," *Nature communications*, vol. 7, no. 1, p. 10850, 2016.

[152] M. M. Danziger and A.-L. Barabási, "Recovery coupling in multilayer networks,"

Nature communications, vol. 13, no. 1, p. 955, 2022.

[153] W.-H. Cho, E. Barcelon, and S. J. Lee, "Optogenetic glia manipulation: possibilities and future prospects," *Experimental neurobiology*, vol. 25, no. 5, pp. 197–204, 2016.

[154] R. Rossi and N. Ahmed, "The network data repository with interactive graph analytics and visualization," in *Proceedings of the AAAI conference on artificial intelligence*, vol. 29, no. 1, 2015.

[155] R. C. Hilborn *et al.*, *Chaos and nonlinear dynamics: an introduction for scientists and engineers*. Oxford University Press on Demand, 2000.

[156] A. E. Motter and M. Timme, "Antagonistic phenomena in network dynamics," *Annual review of condensed matter physics*, vol. 9, pp. 463–484, 2018.

[157] P. Grassberger, "Chaos and diffusion in deterministic cellular automata," *Physica D: Nonlinear Phenomena*, vol. 10, no. 1-2, pp. 52–58, 1984.

[158] M. ANDRECUT and M. Ali, "Chaos in a simple boolean network," *International Journal of Modern Physics B*, vol. 15, no. 01, pp. 17–23, 2001.

[159] I. Shmulevich and S. A. Kauffman, "Activities and sensitivities in boolean network models," *Physical review letters*, vol. 93, no. 4, p. 048701, 2004.

[160] K. Zhao, J. Stehlé, G. Bianconi, and A. Barrat, "Social network dynamics of face-to-face interactions," *Physical review E*, vol. 83, no. 5, p. 056109, 2011.

[161] N. A. Kiani, D. Gomez-Cabrero, and G. Bianconi, *Networks of Networks in Biology: Concepts, Tools and Applications*. Cambridge University Press, 2021.

[162] L. Calmon, J. G. Restrepo, J. J. Torres, and G. Bianconi, "Dirac synchronization is rhythmic and explosive," *Communications Physics*, vol. 5, no. 1, pp. 1–17, 2022.

[163] L. Giambagli, L. Calmon, R. Muolo, T. Carletti, and G. Bianconi, "Diffusion-driven instability of topological signals coupled by the dirac operator," *Physical Review E*, vol. 106, no. 6, p. 064314, 2022.

[164] O. T. Courtney and G. Bianconi, "Generalized network structures: The configuration model and the canonical ensemble of simplicial complexes," *Physical Review E*, vol. 93, no. 6, p. 062311, 2016.

[165] V. Nicosia, P. S. Skardal, A. Arenas, and V. Latora, "Collective phenomena emerg-

ing from the interactions between dynamical processes in multiplex networks," *Physical review letters*, vol. 118, no. 13, p. 138302, 2017.

[166] K. Zhao, M. Karsai, and G. Bianconi, "Entropy of dynamical social networks," *PloS one*, vol. 6, no. 12, p. e28116, 2011.

[167] M. E. Newman, A.-L. E. Barabási, and D. J. Watts, *The structure and dynamics of networks.* Princeton university press, 2006.

[168] D. Centola, "The spread of behavior in an online social network experiment," *science*, vol. 329, no. 5996, pp. 1194–1197, 2010.

[169] C. Rivers, J.-P. Chretien, S. Riley, J. A. Pavlin, A. Woodward, D. Brett-Major, I. Maljkovic Berry, L. Morton, R. G. Jarman, M. Biggerstaff *et al.*, "Using "outbreak science" to strengthen the use of models during epidemics," *Nature communications*, vol. 10, no. 1, p. 3102, 2019.

[170] J. M. Epstein, "Why model?" *Journal of artificial societies and social simulation*, vol. 11, no. 4, p. 12, 2008.

[171] M. Biggerstaff, M. Johansson, D. Alper, L. C. Brooks, P. Chakraborty, D. C. Farrow, S. Hyun, S. Kandula, C. McGowan, N. Ramakrishnan, R. Rosenfeld, J. Shaman, R. Tibshirani, R. J. Tibshirani, A. Vespignani, W. Yang, Q. Zhang, and C. Reed, "Results from the second year of a collaborative effort to forecast influenza seasons in the United States," *Epidemics*, vol. 24, p. 26, 2018.

[172] S. N. Busenberg, M. Iannelli, and H. R. Thieme, "Global Behavior of an Age-Structured Epidemic Model," *SIAM J. Math. Anal.*, vol. 22, pp. 1065–1080, 1991.

[173] Z. Feng and H. R. Thieme, "Endemic Models with Arbitrarily Distributed Periods of Infection I: Fundamental Properties of the Model," *SIAM J. Appl. Math.*, vol. 61, pp. 803–833, 2000.

[174] R. Pastor-Satorras and A. Vespignani, "Epidemic spreading in scale-free networks," *Physical review letters*, vol. 86, no. 14, p. 3200, 2001.

[175] W.-m. Liu, S. A. Levin, and Y. Iwasa, "Influence of nonlinear incidence rates upon the behavior of SIRS epidemiological models," *J. Math. Biol.*, vol. 23, pp. 187–204, 1986.

[176] H. W. Hethcote and P. van den Driessche, "Some epidemiological models with

nonlinear incidence," *J. Math. Biol.*, vol. 29, pp. 271–287, 1991.

[177] V. Balasubramanian, E. H. Wiegeshaus, B. T. Taylor, and D. W. Smith, "Pathogenesis of tuberculosis: Pathway to apical localization," *Tuber. Lung Dis.*, vol. 75, pp. 168–178, 1994.

[178] R. C. LaRocque and S. B. Calderwood, "Syndromes of enteric infection," in *Mandell, Douglas, and Bennett's Principles and Practice of Infectious Diseases*. Elsevier, 2015, pp. 1238–1247.

[179] T. P. Weber and N. I. Stilianakis, "Inactivation of influenza A viruses in the environment and modes of transmission: A critical review," *J. Infect.*, vol. 57, pp. 361–373, 2008.

[180] J. A. Gama, S. S. Abby, S. Vieira-Silva, F. Dionisio, and E. P. C. Rocha, "Immune subversion and quorum-sensing shape the variation in infectious dose among bacterial pathogens," *PLOS Pathog.*, vol. 8, no. 2, p. e1002503, 2012.

[181] B. B. Finlay and S. Falkow, "Common themes in microbial pathogenicity revisited." *Microbiol. Mol. Biol. Rev.*, vol. 61, no. 2, p. 136, 1997. [Online]. Available: https://mmbr.asm.org/content/61/2/136

[182] M. W. Hornef, M. J. Wick, M. Rhen, and S. Normark, "Bacterial strategies for overcoming host innate and adaptive immune responses," *Nat. immunol.*, vol. 3, no. 11, p. 1033, 2002.

[183] M. Lipsitch and J. J. O'Hagan, "Patterns of antigenic diversity and the mechanisms that maintain them," *J. R. Soc. Interface*, vol. 4, no. 16, p. 787, 2007.

[184] A. Casadevall, "Evolution of intracellular pathogens," *Annu. Rev. Microbiol.*, vol. 62, p. 19, 2008.

[185] S. Q. Du and W. Yuan, "Mathematical modeling of interaction between innate and adaptive immune responses in COVID-19 and implications for viral pathogenesis," *J. Med. Virol.*, vol. 92, no. 9, p. 1615, 2020.

[186] C. A. Beauchemin and A. Handel, "A review of mathematical models of influenza A infections within a host or cell culture: lessons learned and challenges ahead," *BMC Public Health*, vol. 11, no. 1, p. S7, 2011.

[187] Y. Liu, R. M. Eggo, and A. J. Kucharski, "Secondary attack rate and

superspreading events for sars-cov-2," *Lancet*, vol. 395, no. 10227, p. e47, 2020. [Online]. Available: https://www.sciencedirect.com/science/article/pii/S0140673620304621

[188] F. Wong and J. J. Collins, "Evidence that coronavirus superspreading is fat-tailed," *Proc. Natl. Acad. Sci. U.S.A.*, vol. 117, pp. 29 416–29 418, 2020.

[189] B. M. Althouse, E. A. Wenger, J. C. Miller, S. V. Scarpino, A. Allard, L. Hébert-Dufresne, and H. Hu, "Superspreading events in the transmission dynamics of SARS-CoV-2: Opportunities for interventions and control," *PLOS Biol.*, vol. 18, p. e3000897, 2020.

[190] A. Endo, S. Abbott, A. J. Kucharski, and S. Funk, "Estimating the overdispersion in COVID-19 transmission using outbreak sizes outside china," *Wellcome Open Res.*, vol. 5, p. 67, 2020.

[191] Q. Bi *et al.*, "Epidemiology and transmission of COVID-19 in 391 cases and 1286 of their close contacts in shenzhen, china: a retrospective cohort study," *Lancet Infect. Dis.*, vol. 20, no. 8, p. 911, 2020.

[192] D. Miller, M. A. Martin, N. Harel, O. Tirosh, T. Kustin, M. Meir, N. Sorek, S. Gefen-Halevi, S. Amit, O. Vorontsov *et al.*, "Full genome viral sequences inform patterns of SARS-CoV-2 spread into and within israel," *Nat. Commun.*, vol. 11, p. 5518, 2020.

[193] M. S. Y. Lau, B. Grenfell, M. Thomas, M. Bryan, K. Nelson, and B. Lopman, "Characterizing superspreading events and age-specific infectiousness of SARS-CoV-2 transmission in Georgia, USA," *Proc. Natl. Acad. Sci. U.S.A.*, vol. 117, no. 36, p. 22430, 2020. [Online]. Available: https://www.pnas.org/content/117/36/22430

[194] B. F. Nielsen, L. Simonsen, and K. Sneppen, "Covid-19 superspreading suggests mitigation by social network modulation," *Phys. Rev. Lett.*, vol. 126, p. 118301, 2021. [Online]. Available: https://link.aps.org/doi/10.1103/PhysRevLett.126.118301

[195] J. O. Lloyd-Smith, S. J. Schreiber, P. E. Kopp, and W. M. Getz, "Superspreading and the effect of individual variation on disease emergence," *Nature*, vol. 438, no.

7066, p. 355, 2005.

[196] M. Karsai, H.-H. Jo, and K. Kaski, *Bursty Human Dynamics*. Springer International Publishing, 2018.

[197] M. Karsai, K. Kaski, A.-L. Barabási, and J. Kertész, "Universal features of correlated bursty behaviour," *Sci. Rep.*, vol. 2, p. 397, 2012.

[198] C. Cattuto, W. Van den Broeck, A. Barrat, V. Colizza, J.-F. Pinton, and A. Vespignani, "Dynamics of person-to-person interactions from distributed rfid sensor networks," *PLOS ONE*, vol. 5, p. e11596, 2010.

[199] J. Stehlé, A. Barrat, and G. Bianconi, "Dynamical and bursty interactions in social networks," *Phys. Rev. E*, vol. 81, p. 035101(R), 2010.

[200] G. Cencetti, F. Battiston, B. Lepri, and M. Karsai, "Temporal properties of higher-order interactions in social networks," *Scientific reports*, vol. 11, no. 1, p. 7028, 2021.

[201] K. Swinkels, "SARS-CoV-2 superspreading events from around the world," 2020, accessed: 2020-07-02. [Online]. Available: http://www.superspreadingdatabase.com/

[202] Q. J. Leclerc, N. M. Fuller, L. E. Knight, S. Funk, G. M. Knight, and C. C.-. W. Group, "What settings have been linked to sars-cov-2 transmission clusters?" *Wellcome Open Research*, vol. 5, 2020. [Online]. Available: https://doi.org/10.12688/wellcomeopenres.15889.2

[203] Icons made by Freepik from www.flaticon.com.

[204] C. Berge, *Hypergraphs: Combinatorics of Finite Sets*. North Holland, 1989. [Online]. Available: https://www.elsevier.com/books/hypergraphs/berge/978-0-444-87489-4

[205] L. Torres, A. S. Blevins, D. Bassett, and T. Eliassi-Rad, "The why, how, and when of representations for complex systems," *SIAM Review*, vol. 63, no. 3, pp. 435–485, 2021.

[206] M. Granovetter, "Threshold Models of Collective Behavior," *Am. J. Sociol.*, vol. 83, pp. 1420–1443, 1978.

[207] D. J. Watts, "A simple model of global cascades on random networks," *Proc. Natl.*

Acad. Sci. U.S.A., vol. 99, pp. 5766–5771, 2002.

[208] P. S. Dodds and D. J. Watts, "Universal Behavior in a Generalized Model of Contagion," *Phys. Rev. Lett.*, vol. 92, p. 218701, 2004.

[209] J. Anttila, L. Mikonranta, T. Ketola, V. Kaitala, J. Laakso, and L. Ruokolainen, "A mechanistic underpinning for sigmoid dose-dependent infection," *Oikos*, vol. 126, pp. 910–916, 2017.

[210] W.-m. Liu, H. W. Hethcote, and S. A. Levin, "Dynamical behavior of epidemiological models with nonlinear incidence rates," *J. Math. Biol.*, vol. 25, no. 4, pp. 359–380, sep 1987. [Online]. Available: http://link.springer.com/10.1007/BF00277162

[211] S. V. Scarpino, A. Allard, and L. Hébert-Dufresne, "The effect of a prudent adaptive behaviour on disease transmission," *Nat. Phys.*, vol. 12, no. 11, p. 1042, 2016.

[212] G. F. de Arruda, E. Cozzo, T. P. Peixoto, F. A. Rodrigues, and Y. Moreno, "Disease localization in multilayer networks," *Phys. Rev. X*, vol. 7, no. 1, p. 011014, feb 2017. [Online]. Available: https://link.aps.org/doi/10.1103/PhysRevX.7.011014

[213] C. Fraser, S. Riley, R. M. Anderson, and N. M. Ferguson, "Factors that make an infectious disease outbreak controllable," *Proceedings of the National Academy of Sciences*, vol. 101, no. 16, pp. 6146–6151, 2004.

[214] L. Ferretti, C. Wymant, M. Kendall, L. Zhao, A. Nurtay, L. Abeler-Dörner, M. Parker, D. Bonsall, and C. Fraser, "Quantifying sars-cov-2 transmission suggests epidemic control with digital contact tracing," *Science*, vol. 368, no. 6491, p. eabb6936, 2020.

[215] S. Kojaku, L. Hébert-Dufresne, E. Mones, S. Lehmann, and Y.-Y. Ahn, "The effectiveness of backward contact tracing in networks," *Nature physics*, vol. 17, no. 5, pp. 652–658, 2021.

[216] C. Granell, S. Gómez, and A. Arenas, "Competing spreading processes on multiplex networks: awareness and epidemics," *Physical review E*, vol. 90, no. 1, p. 012808, 2014.

[217] B. Rozemberczki, R. Davies, R. Sarkar, and C. Sutton, "Gemsec: graph embedding

with self clustering," *Proceedings of the 2019 IEEE/ACM International Conference on Advances in Social Networks Analysis and Mining*, Aug 2019. [Online]. Available: http://dx.doi.org/10.1145/3341161.3342890

[218] R. Zafarani and H. Liu, "Social computing data repository at ASU," 2009. [Online]. Available: http://socialcomputing.asu.edu

[219] T. Rogers, "Assessing node risk and vulnerability in epidemics on networks," *EPL (Europhysics Letters)*, vol. 109, no. 2, p. 28005, 2015.

[220] S. Moore and T. Rogers, "Predicting the speed of epidemics spreading in networks," *Physical review letters*, vol. 124, no. 6, p. 068301, 2020.

[221] B. Min and M. San Miguel, "Competing contagion processes: Complex contagion triggered by simple contagion," *Scientific reports*, vol. 8, no. 1, p. 10422, 2018.

[222] W. Cai, L. Chen, F. Ghanbarnejad, and P. Grassberger, "Avalanche outbreaks emerging in cooperative contagions," *Nature physics*, vol. 11, no. 11, pp. 936–940, 2015.

[223] P. Rodríguez, S. Graña, E. E. Alvarez-León, M. Battaglini, F. J. Darias, M. A. Hernán, R. López, P. Llaneza, M. C. Martín, R. Group *et al.*, "A population-based controlled experiment assessing the epidemiological impact of digital contact tracing," *Nature communications*, vol. 12, no. 1, p. 587, 2021.

[224] A. Barrat, C. Cattuto, M. Kivelä, S. Lehmann, and J. Saramäki, "Effect of manual and digital contact tracing on covid-19 outbreaks: a study on empirical contact data," *Journal of the Royal Society Interface*, vol. 18, no. 178, p. 20201000, 2021.

[225] D. H. Silva, C. Anteneodo, and S. C. Ferreira, "Epidemic outbreaks with adaptive prevention on complex networks," *Communications in Nonlinear Science and Numerical Simulation*, vol. 116, p. 106877, 2023.

[226] G. Burgio, B. Steinegger, G. Rapisardi, and A. Arenas, "Homophily in the adoption of digital proximity tracing apps shapes the evolution of epidemics," *Physical Review Research*, vol. 3, no. 3, p. 033128, 2021.